Received: 5 December 2022 | Revised: 14 March 2023 | Accepted: 16 March 2023

DOI: 10.1111/acel.13838

Aging Cell WILEY

RESEARCH ARTICLE

Age-mediated gut microbiota dysbiosis promotes the loss of dendritic cells tolerance

Hilal Bashir[1] | Sanpreet Singh[1] | Raghwendra Pratap Singh[1,2] | Javed N. Agrewala[1,3] | Rashmi Kumar[1,2]

[1]Immunology Laboratory, CSIR-Institute of Microbial Technology, Sector 39A, Chandigarh, 160036, India

[2]Academy of Scientific and Innovative Research (AcSIR), Ghaziabad, 201002, India

[3]Immunology Laboratory, Department of Biomedical Engineering, Indian Institute of Technology, Ropar, Rupnagar, 140001, Punjab, India

Correspondence
Javed N. Agrewala, Indian Institute of Technology, Ropar, Rupnagar 140001, Punjab, India.
Email: jagrewala@iitrpr.ac.in

Rashmi Kumar, CSIR-Institute of Microbial Technology, Sector-39A, Chandigarh 160036, India.
Email: rashmi@imtech.res.in

Funding information
Council of Scientific and Industrial Research, India, Grant/Award Number: MLP062, BSC0119 and OLP134

Abstract

The old age-related loss of immune tolerance inflicts a person with a wide range of autoimmune and inflammatory diseases. Dendritic cells (DCs) are the sentinels of the immune system that maintain immune tolerance through cytokines and regulatory T-cells generation. Aging disturbs the microbial composition of the gut, causing immune system dysregulation. However, the *vis-à-vis* role of gut dysbiosis on DCs tolerance remains highly elusive. Consequently, we studied the influence of aging on gut dysbiosis and its impact on the loss of DC tolerance. We show that DCs generated from either the aged (DC^{Old}) or gut-dysbiotic young ($DC^{Dysbiotic}$) but not young (DC^{Young}) mice exhibited loss of tolerance, as evidenced by their failure to optimally induce the generation of Tregs and control the overactivation of $CD4^+$ T cells. The mechanism deciphered for the loss of DC^{Old} and $DC^{Dysbiotic}$ tolerance was chiefly through the overactivation of NF-κB, impaired frequency of Tregs, upregulation in the level of pro-inflammatory molecules (IL-6, IL-1β, TNF-α, IL-12, IFN-γ), and decline in the anti-inflammatory moieties (IL-10, TGF-β, IL-4, IDO, arginase, NO, IRF-4, IRF-8, PDL1, BTLA4, ALDH2). Importantly, a significant decline in the frequency of the *Lactobacillus* genus was noticed in the gut. Replenishing the gut of old mice with the *Lactobacillus plantarum* reinvigorated the tolerogenic function of DCs through the rewiring of inflammatory and metabolic pathways. Thus, for the first time, we demonstrate the impact of age-related gut dysbiosis on the loss of DC tolerance. This finding may open avenues for therapeutic intervention for treating age-associated disorders with the *Lactobacillus plantarum*.

KEYWORDS
aging, dendritic cells, dysbiosis, gut microbiota, immune response, tolerance

Abbreviations: 2-NBDG, 2-(N-(7-nitrobenz-2-oxa-1,3-diazol-4-yl) amino)-2-deoxyglucose; Abx, Antibiotic; ACK, Ammonium-chloride-potassium bicarbonate lysis buffer; ALDH, Aldehyde dehydrogenase; ANOVA, Analysis of variance; APCs, Antigen-presenting cells; BHI, Brain heart infusion agar; BMDC, Bone marrow-derived dendritic cells; BTLA, B and T lymphocyte attenuator; CD, Cluster of differentiation; CFSE, Carboxyfluorescein succinimidyl ester; CFU, Colony-forming unit; DCs, Dendritic cells; ELISA, Enzyme linked immuno sorbent assay; FBS, Fetal bovine serum; GM-CSF, Granulocyte-macrophage colony-stimulating factor; HRP, Horse radish peroxidase; IDO, Indoleamine 2,3-dioxygenase; IL, Interleukin; iNOS, Inducible nitric oxide synthase; LP, *Lactobacillus plantarum*; LPS, Lipopolysaccharide; MHC, Major histocompatibility complex; MLN, Mesenteric lymph node; NO, Nitric oxide; PDL, Programmed death-ligand; PP, Peyer's patches; RIPA, Radioimmunoprecipitation assay; TMB, 5,5′-Tetramethylbenzidine; Tregs, Regulatory T cells.

1 | INTRODUCTION

Age-inflicted inflamed microenvironment favors inflammatory and autoimmune responses with a concurrent decline in the protective immunity (Kim et al., 2017). Both Innate and adaptive arms of the immune system show age-related changes in their functional capacity, manifested by diminished antigen uptake and presentation capacity, phagocytic activity, thymic involution, antibody production, and reduced response to vaccination and infection. A gain of non-specific innate immunity with a loss of adaptive immunity is linked with the advancement of age (Lee et al., 2022).

Dendritic cells (DCs) are professional antigen-presenting cells (APCs) and multifaceted regulators of immunity against pathogens (Banchereau & Steinman, 1998). Furthermore, they also induce tolerance to self and innocuous antigens (Coquerelle & Moser, 2010). Recognition of pathogen's danger signals, uptake of antigens, and their processing provides developmental cues to DCs for their maturation and activation. DCs are the only APCs with the capacity to activate and differentiate naive T cells (Trombetta & Mellman, 2005). Immunogenic DCs express a higher level of MHCII and co-stimulatory molecules CD40, CD80 and CD86, and release an elevated amount of pro-inflammatory cytokines like IL-12, IL-6, IL1-β, and TNF-α (Hackstein & Thomson, 2004). In contrast, tolerogenic DCs display comparatively lower levels of MHCII and co-stimulatory molecules and higher expression of inhibitory receptors such as Tim-3 and PDL-1 (Iberg & Hawiger, 2020). Tolerogenic DCs produce augmented quantities of anti-inflammatory cytokines like IL-10 and TGF-β (Vogel et al., 2022) and reduced production of IL-12 (Steinman et al., 2003). DCs maintain immunological tolerance by clonal deletion of T cells, induction of anergy, and generation of Tregs (Horton et al., 2017). In addition, they maintain peripheral tolerance against self-antigens and presentation to autoreactive T cells (Hawiger et al., 2001). This heterogeneity in the functionality of DCs establishes a fine balance between the activation and suppression of the immune system. The loss of DC tolerance is a gradual process connected with aging, as observed by the increased production of pro-inflammatory cytokines, reduced phagocytic capacity (Agrawal et al., 2017), deficient Tregs-inducing capacity, and failure to curb autoimmune and inflammatory responses. Although enhanced activation of NF-κB and pro-inflammatory responses are considered responsible for this phenomenon (Agrawal et al., 2007), the mechanism connected with age-associated DCs dysfunction remains extensively elusive.

Recently, the role of gut microbiota is increasingly being recognized in the development, maturation, and maintenance of homeostasis of the immune system through elegant experiments conducted on germ-free mice models (Honda & Littman, 2016). Gut microbiota induces peripheral tolerance through the induction of Tregs, IgA-secreting B cells, Th17 cells, and through the DC modulation (Zheng, Liwinski, & Elinav, 2020). An alteration in gut microbiota composition and function has been reported with age, and concomitantly, it is associated with various autoimmune diseases (Bosco & Noti, 2021). Gut dysbiosis with age results in a loss of mainly Firmicutes and Bacteroides and the predominance of Proteobacteria and therefore predisposes to increased risk of immune dysregulation and persistence of chronic inflammation (Ragonnaud & Biragyn, 2021). However, it is still largely unknown how aging provokes gut dysbiosis and loss of DC tolerance.

Taking into consideration the aforesaid facts, we studied the influence of aging on gut microbiota and its implication on the activation, differentiation, and function of DCs. Through comparison of DCs derived from young (DC^{Young}), old (DC^{Old}), and antibiotic-treated young animals ($DC^{Dysbiotic}$). We show the correlation between gut dysbiosis and loss of DC tolerance. Our study revealed that aging incited gut disruptions linked with the failure in the expansion of Tregs and downregulation of tolerance-associated gene network and signaling pathways that resulted in the loss of DC tolerance. Importantly, the loss of DC tolerance was connected with the disappearance of the beneficial bacteria Lactobacillus. Interestingly, replenishing the gut of aged mice with *Lactobacillus plantarum*, restored the age-associated loss of tolerance in DCs ($DC^{Old\text{-}LP}$). The study suggests the therapeutic role of *Lactobacillus plantarum* in the maintenance of DC tolerance and its use as a remedial measure for alleviating age-associated immune system defects.

2 | RESULTS

2.1 | Bone marrow-derived hematopoietic cells exhibit declined differentiation potential with age and gut dysbiosis to DCs

Aged hematopoietic stem cells (HSCs) generate a dysfunctional immune system that contributes to immunosenescence (Geiger et al., 2013). Additionally, dysbiosis of the microbial population with antibiotic treatment adversely affects the bone marrow cells

FIGURE 1 Aging and Abx treatment of young animals disrupts gut microbiota and impairs the differentiation of BMCs to DCs. Young control, young dysbiotic (21 days of antibiotics treated) and old, groups of animals were compared; (a) quantification of facultative anaerobes and aerobes bacteria from fecal matter; (b) quantification of total BMCs; (c) comparative analysis of the total number of BMCs and DCs differentiated from BMCs; (d) phenotypic ($CD11c^+CD80^+$ population (top), $CD11c^+CD86^+$(middle) and $CD11c^+MHCII^+$ (bottom) analysis of differentiated (-LPS) DC^{Young}, $DC^{dysbiotic}$ and DC^{Old}; (e) representative FACS plot and bar graph of syngeneic and allogeneic $CD4^+$ T-cell proliferation induced by DC^{Young}, $DC^{Dysbiotic}$ and DC^{Old}; (f) representative FACS plot and bar graph of $CD4^+FoxP3^+$Tregs differentiation by DC^{Young}, $DC^{Dysbiotic}$ and DC^{Old}. The data (mean ± SD) are from three independent experiments, with each point representing a pool of three animals for one independent experiment ($n = 3$ mice/group). Statistical analysis was done by one-way ANOVA followed by Tukey's multiple comparison tests except (c, d), where two-way ANOVA followed by Sidak's multiple comparisons test was done. $^*p < 0.05$, $^{**}p < 0.01$, $^{***}p < 0.001$, $^{****}p < 0.0001$.

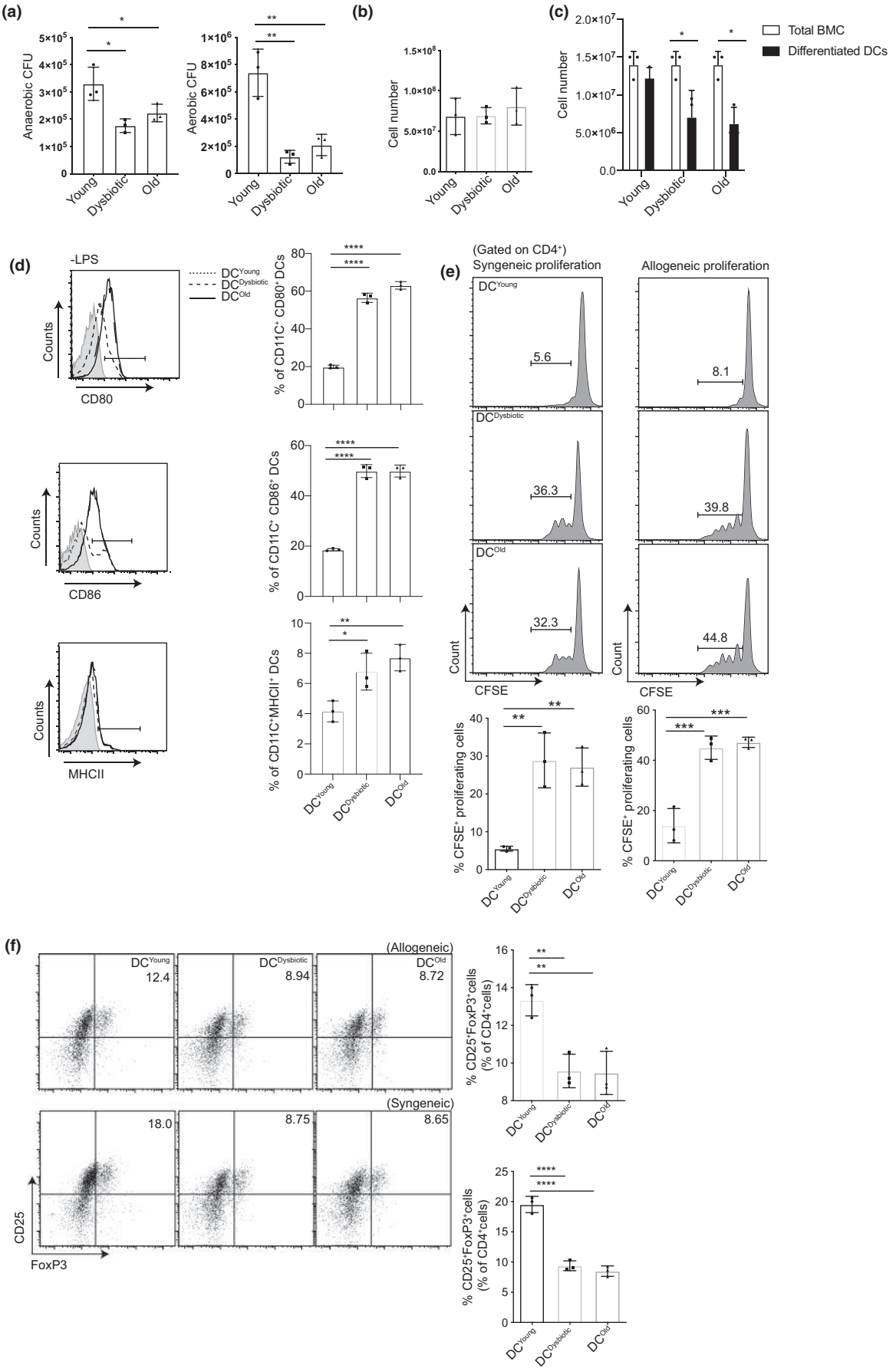

(Josefsdottir et al., 2017). These observations led us to evaluate the number and differentiation potential of HSCs in aged (20–22 months) and young dysbiotic mice (young mice treated with an antibiotic cocktail for 21 days) compared to young mice (2–4 months). Gut bacterial colony-forming units (CFUs) were enumerated and compared in all three groups under anaerobic and aerobic conditions from their fecal homogenate. We observed a significant decrease in the gut bacterial load in both facultative anaerobes and aerobes in old and young dysbiotic mice in comparison with young mice (Figure 1a). Next, an absolute number of bone marrow cells (BMCs) and their differentiation potential towards dendritic cells were compared. No significant alteration was observed in the absolute cell counts among the three groups (Figure 1b) but a significant decrease in the differentiation of BMCs to DCs in both old and young dysbiotic groups (Figure 1c) compared to the young group was noticed. We conclude that gut dysbiosis, either due to old age or antibiotic treatment, impairs the differentiation potential of bone marrow/myeloid progenitor cells.

2.2 | Age and gut dysbiosis affects the maturation and function of DCs

DCs play an important role in both, orchestrating antigen-specific T-cell responses and maintenance of the peripheral tolerance (Coquerelle & Moser, 2010). However, their functional capacity gets curtailed with chronological aging (Agrawal et al., 2007), and with gut microbiota modulation (Uribe-Herranz et al., 2020). The phenotype of the DCs can ascertain their activation or tolerization function. A significant upregulation in the expression of co-stimulatory molecules CD80, CD86, and MHCII molecules (Figure 1d), and CD40 (Figure S1c) molecules was observed on the $DC^{Dysbiotic}$ and DC^{Old}, as compared to DC^{Young} upon differentiation.

One of the mechanisms for the induction of peripheral T-cell tolerance by dendritic cells is attributed to their capacity to phagocytose foreign pathogens, cancer cells, and self-apoptotic cells. A defect in this capacity leads to a breach of tolerance (Savill et al., 2002). Given that we observed the mature phenotype of DCs in our experimental setup, we checked their ability for phagocytosis. We observed a significant decline in phagocytosis of the antigen (Dextran-FITC) by both $DC^{Dysbiotic}$ and DC^{Old} compared to DC^{Young} (Figure S1d). Additionally, we noticed a notable decrease in the engulfment of apoptotic bodies (Figure S1e). These results indicate reduced phagocytosis by DCs on aging and gut dysbiosis.

DCs induce immunogenic or tolerogenic T-cell stimulation based on their maturation state (de Heusch et al., 2004). We next examined the effect of gut dysbiosis on the ability of DCs to activate $CD4^+$ T cells. $DC^{Dysbiotic}$ and DC^{Old} induced rigorous proliferation of syngeneic $CD4^+$ T cells in comparison with DC^{Young}.This was further authenticated using allogeneic $CD4^+$ T cells (Figure 1e). These data suggest that $DC^{Dysbiotic}$ and DC^{Old} exhibit hyperactivation of $CD4^+$ T cells. Further to confirm this, we examined the Tregs-inducing potential of all three DCs, as the regulatory function of DCs is well recognized for the maintenance of central and peripheral tolerance by driving naive T cells to differentiate towards Tregs (Raker et al., 2015). A significant loss of the Tregs-inducing potential of $DC^{Dysbiotic}$ and DC^{Old} was noted (Figure 1f). These results indicate loss of tolerogenic and acquisition of immunogenic properties in old and young dysbiotic DCs, suggesting a substantial role of gut dysbiosis in the modulation of DCs function. Next, we focused our studies on understanding the possible mechanism of action for the loss of tolerogenic effect of BMDCs with Abx treatment and old age.

2.3 | Loss of tolerogenic potential of DCs with gut dysbiosis is primarily mediated through secreted factors and modulation of regulatory and metabolic gene expression

In both proliferation and Tregs induction experiments, total $CD4^+$ T cells were stimulated through plate-bound anti-CD3 and soluble anti-CD28 antibodies while co-culturing with DCs for optimal activation of T cells. This approach nullifies the effect of phenotypic difference among DCs for the observed effect; hence, we hypothesized that gut dysbiosis with old age and antibiotic treatment instigate cell-intrinsic properties of myeloid precursors and turn them towards immunogenic rather than tolerogenic, and this effect is mediated through secreted factors in the microenvironment of DC and T-cell co-culture.

FIGURE 2 Mechanism of gut dysbiosis-mediated loss of tolerogenic potential in DCs. Co-culture supernatants of LPS-stimulated DC^{Young}, $DC^{Dysbiotic}$, and DC^{Old} with syngeneic $CD4^+$ T cells were analyzed with ELISA for cytokines secretion; (a) bar graph representation of pro-inflammatory cytokines IL-6, IL1-β, TNF-α, IL-12, and IFN-γ; (b) bar graph representation of anti-inflammatory cytokines IL-2, IL-10, TGF-β, and IL-4. qRT-PCR based quantification of gene expression in DC^{Young}, $DC^{Dysbiotic}$, and DC^{Old}. Bar graph representation of (c) relative gene expression of pro-inflammatory cytokine genes; (d) relative gene expression of anti-inflammatory cytokine genes; (e) relative gene expression of tolerogenic genes *Irf4*, *Irf8*, *Pdl1*, *Btla*, and *Aldh2*. LPS-stimulated DC SNs were estimated for NO secretion, and the same cells were examined for the expression of tolerogenic metabolic enzymes and phosphorylation status of the p65 subunit of NF-kB; (f) representative Western blots and protein level quantification of iNOS, IDO, and arginase; (g) relative expression of metabolic genes *iNOS*, *Ido*, and arginase-1 by qRT-PCR; (h) bar graph representation of NO secretion by Griess method; (i) representative Western blot and protein level quantification of phospho-p65 in DCs lysate (left panel), bar graph representation of the percentage of phospho-$p65^+$ DCs through flow cytometry and relative expression of p65 encoding gene *RelA* through qRT-PCR. Data (mean ± SD) representing RT-PCR and flow cytometry are of three independent experiments, with each point representing a pool of three animals for one independent experiment, $n = 3$ mice/group, and Western blot data representing two independent experiments. $^*p < 0.05$, $^{**}p < 0.01$, $^{***}p < 0.001$, $^{****}p < 0.0001$. Statistical analysis was done by one-way ANOVA followed by Tukey's multiple comparison test.

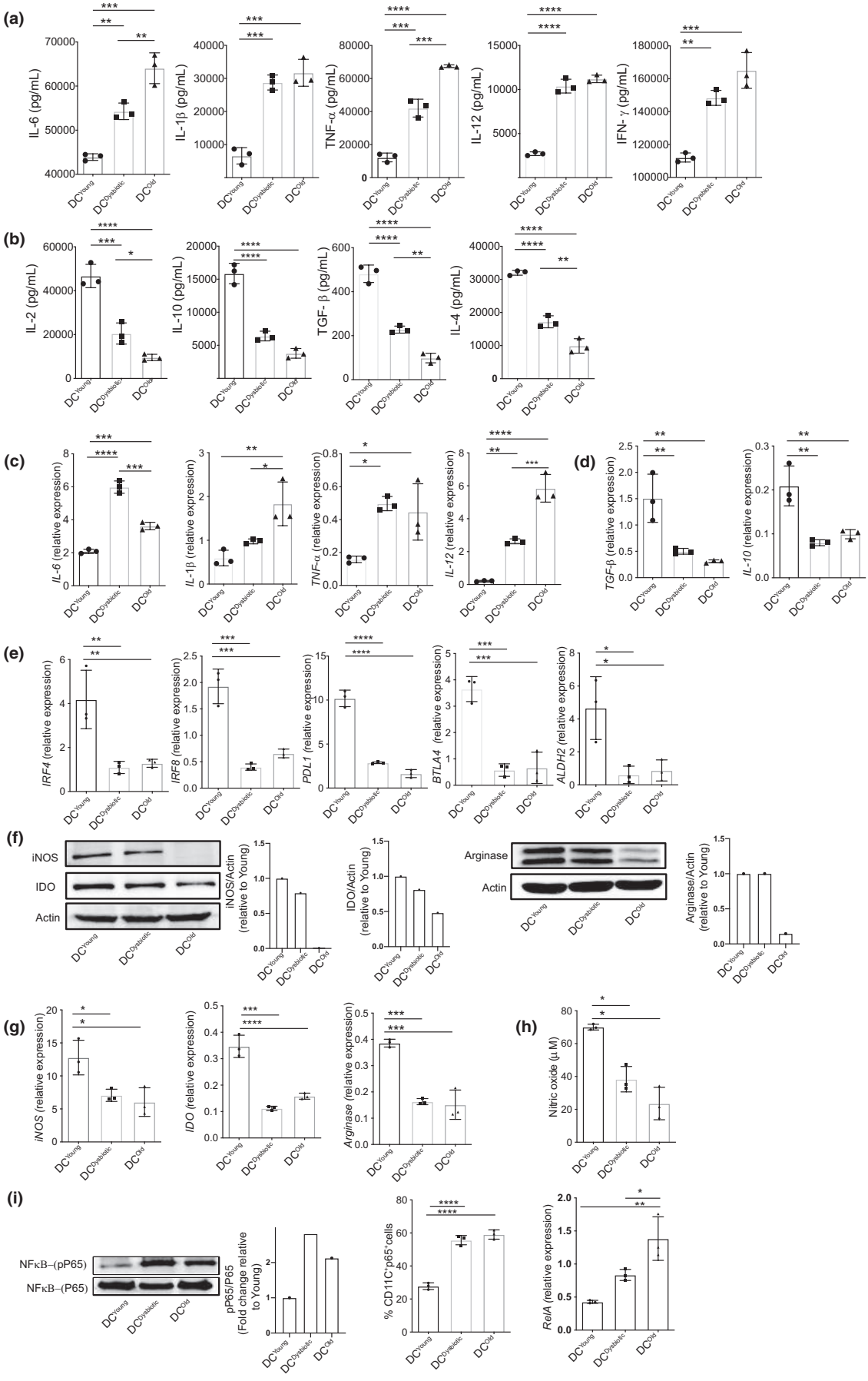

We analyzed the supernatant of DC:CD4$^+$ T-cell co-culture for estimation of pro-inflammatory and anti-inflammatory cytokines concentration. A significant increase in pro-inflammatory cytokines IL-6, IL1-β, TNF-α, IL-12, and IFN-γ was noticed when CD4$^+$ T cells were co-cultured with DC^{Dysbiotic} and DC^{Old} compared to DC^{Young}, which corroborates with a significant reduction in the anti-inflammatory cytokines IL-2, IL-10, TGF-β, and IL-4 release (Figure 2a, b). These results were further validated at the transcript level. We found significantly increased expression of pro-inflammatory cytokines (*Il-6*, *Il1b*, *Tnfa*, and *Il-12*) while reduced transcripts were observed for anti-inflammatory cytokines *Il-10*, and *Tgfb* (Figure 2c, d) in DC^{Dysbiotic} and DC^{Old} compared to DC^{Young}. Reduced induction of Tregs and decreased production of anti-inflammatory cytokines strongly supported the curtailed tolerogenic immune responses of DC^{Dysbiotic} and DC^{Old} compared to DC^{Young}. These results agree with the studies demonstrating the role of DCs in the induction of peripheral tolerance (Domogalla et al., 2017).

Several studies have demonstrated the role of tolerogenic genes *Irf4*, *Irf8* (McDaniel et al., 2020), *Pdl1* (Oh et al., 2020), *Btla* (Li et al., 2011), and *Aldh2* in regulating the function of DCs (Zhu et al., 2013). To further confirm the tolerogenic dysfunction of young dysbiotic and old DCs, we checked the expression of these genes on matured DCs. A significant decline in the expression of *Irf4*, *Irf8*, *Pdl1*, *Btla4*, and *Aldh2* was noticed in the DC^{Dysbiotic} and DC^{Old} in comparison with DC^{Young} (Figure 2e). In addition, we checked the expression of *Tim3*, an inhibitory receptor (Anderson et al., 2016) on BMDCs through flow cytometry and observed a reduced expression (Figure S2).

Cellular metabolism plays a key role in determining the immunogenic or tolerogenic fate of DCs (Sim et al., 2016). Tryptophan and L-arginine catabolizing enzymes Indoleamine 2,3-dioxygenase (IDO) and Arginase I (Arg 1), respectively, cooperate with DCs to confer their immunosuppressive effect (Mondanelli et al., 2017). These catabolizing enzymes deprive T cells of amino acids and lead to their suppression (Grohmann et al., 2003). IDO1 suppresses the allogeneic T-cell proliferation (Funeshima et al., 2005) and is implicated in the Tregs generation (Fallarino et al., 2006). On the contrary, DC-derived nitric oxide (NO) determines either the regulatory or effector DC differentiation (Si et al., 2016). NO is synthesized from the metabolism of L-arginine by inducible NO synthase (iNOS) and induces tolerance in allograft models (Peche et al., 2005). Hence, it was of our interest to determine their role in gut dysbiosis-mediated DC modulation. We evaluated the protein, and transcript levels of IDO, iNOS, and Arginase1 in DC^{Young}, DC^{Dysbiotic}, and DC^{Old} stimulated with LPS. A reduction in iNOS, arginase, and IDO at the protein level was observed in DC^{Dysbiotic} and DC^{Old} compared to DC^{Young} through Western blot (Figure 2f); concurrently, their transcript levels were also significantly reduced (Figure 2g). Next, NO was measured in the culture supernatants, and a significant decrease in the production of NO was observed in both DC^{Dysbiotic} and DC^{Old} compared to DC^{Young} (Figure 2h) complementing the decreased NO metabolizing enzyme, iNOS.

2.4 | Gut dysbiosis due to aging and antibiotic treatment of young mice induces the NF-κB pathway in DCs to regulate their immunogenic/inflammatory phenotype

To decipher the molecular mechanism that plays a role in influencing the tolerogenic properties of DCs upon gut dysbiosis, we investigated NF-κB signaling pathway. This pathway has a quintessential role in regulating DC tolerance as it is the master regulator of various genes involved in the DC maturation (Ade et al., 2007). Inhibiting NF-κB signaling has been reported to differentiate and maintain tolerogenic DCs in the context of cancer, autoimmune disorders, and aging (Carreno et al., 2011). First, to quantify NF-κB activation, we checked the phosphorylation status of p65, a DNA binding subunit through Western blot and flow cytometry. An increase in phosphorylation of p65 was observed in DC^{Dysbiotic} and DC^{Old} compared to DC^{Young} (Figure 2i, left and middle panel). Furthermore, the mRNA expression of *RelA* encoding for RelA/P65 in total DC extract was observed significantly augmented in young dysbiotic and aged DCs compared to DC^{Young} (Figure 2i, right panel). These results suggested an activated NF-κB phenotype of DCs and the possible role of gut microbiota in the functional modulation of DCs.

2.5 | Gut dysbiosis influenced by aging alters the abundance of the genus *Lactobacillus* in the gut, and its replenishment with *Lactobacillus plantarum* restores dysbiosis and DC phenotype

Next, we were curious to decode the involvement of the gut microbiota in age-predisposed dysbiosis and loss of DC tolerance. We observed a significant difference in the overall microbiota composition of young dysbiotic and old mice compared to young mice. The beta diversity plot which measures the phylogenetic relationship of bacterial communities between groups through both weighted and unweighted principal coordinate analysis indicated separate clustering among all three groups, suggesting a difference in microbial communities (Figure 3a). Alpha diversity analysis which measures the species richness and evenness within an ecological community through Chao1 (community richness) and Shannon index (evenness) (Hughes et al., 2001) showed distinct measures among the group. Both indices indicated a gradual decrease in diversity and evenness of microbiota in young dysbiotic and old mice groups. The Chao1 diversity index revealed a decreased species richness in young dysbiotic and old groups of mice compared to the young group, but the difference was not significant (Figure S3a). However, a significant decrease was noted in the Shannon diversity index (Figure 3b), indicating a biased microbial community structure in old and young dysbiotic mice. Further, phylum and genus level comparisons for relative abundance among all three groups were done. Phylum, like Firmicutes showed a substantial decrease in young dysbiotic and old mice with a concurrent increase in phylum Bacteroidetes with respect to the young group (Figure 3c). At the genus level within

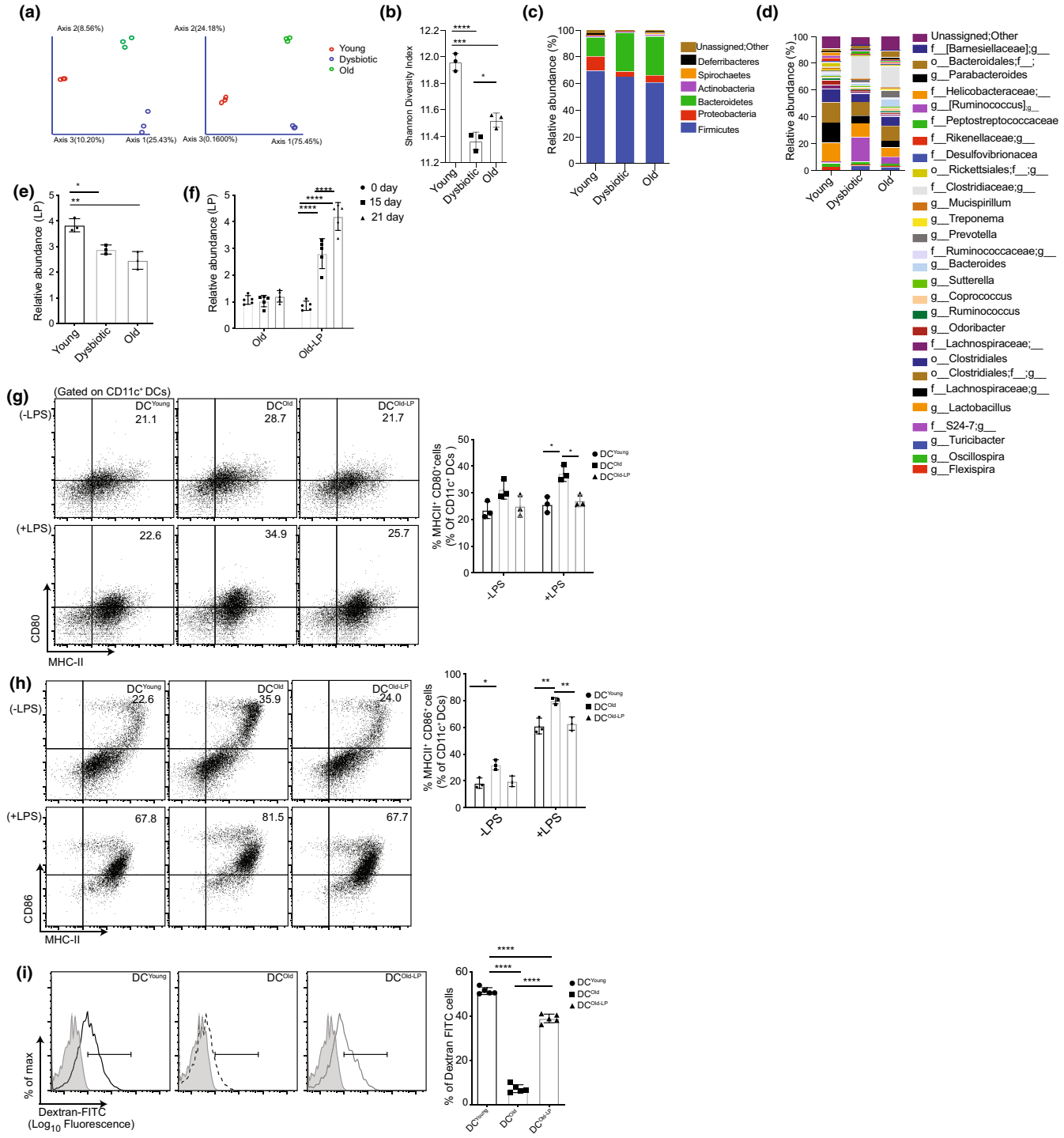

FIGURE 3 Gut microbiota alteration with aging and antibiotics exposure and evaluation of the immunomodulatory role of *Lactobacillus plantarum*. The fecal DNA of young control, young dysbiotic (21 days of antibiotics treated), and old mice were analyzed with 16S rRNA sequencing and qRT-PCR; (a) adapted weighted and unweighted unifrac PCoA plots indicating differential beta diversity; (b) Shannon diversity index depicting alpha diversity; (c) bar graphs represent relative abundance at the phylum level; (d) bar graphs represent relative abundance at the genus level; (e) bar graph represents qRT-PCR data for the indigenous relative abundance of species *L. plantarum*; (f) bar graph represents qRT-PCR based quantification of relative accumulation of *L. plantarum*on the day 0, 15 and 21 of administration through oral gavage with (10^8 CFU/mL) in old mice; (g) dot plot and bar graph depicting percentage population of $MHCII^+CD80^+$ DCs; (h) $MHCII^+CD86^+$ DCs gated on $CD11c^+$ cells and (i) Representative histogram and frequency of dextran-FITC uptake, as assessed by flow cytometry in DC^{Young}, DC^{Old} and $DC^{old\text{-}LP}$. All the data (mean ± SD) are from three independent experiments, with each point representing a pool of three animals for one independent experiment, $n = 3$ mice/group except (f, i), with each point in the bar graph indicating one animal, $n = 5$. The statistical analysis done for RT-PCR (f) and flow cytometry data (g, h) is by two-way ANOVA followed by Sidak's multiple comparisons test, and the rest is by one-way ANOVA followed by Tukey's multiple comparison test. $^*p < 0.05$, $^{**}p < 0.01$, $^{***}p < 0.001$, $^{****}p < 0.0001$.

phylum Firmicutes, beneficial genera like *Lactobacillus* and the genus of the family Lachnospiraceae expressed a significant drop while harmful bacterial genera like *Turicibacter* and the genus of the family Clostridiaceae showed a substantial increase in abundance with the age and Abx treatment of young mice (Figure 3d). The differential abundance in young dysbiotic and old mice in comparison with young was also confirmed by linear discriminant analysis, as depicted in LEfSe plots (Figure S3b).

In our analysis, the diversity plot showed significant downregulation of the genus *Lactobacillus* in both old and young dysbiotic groups. *Lactobacillus* strains maintain immune tolerance by inhibiting inflammatory immune responses (Esmaeili et al., 2018; Macho Fernandez et al., 2011) of macrophages and epithelial cells (Ferreira Dos Santos et al., 2016) and by induction of Tregs (Bermudez-Brito et al., 2018). Consequently, we were intrigued to explore the role of *Lactobacillus* in restoring the function of DCs. First, we measured the abundance of *Lactobacillus plantarum* (LP) in fecal samples of all three groups of mice and observed a significant reduction in LP abundance with age and antibiotic treatment of young mice compared to young mice (Figure 3e). Next, we obtained *Lactobacillus plantarum* (LP) (MTCC-2621 corresponding to ATCC-8014) from MTCC-CSIR-IMTECH and replenished the old mice group. We observed a gradual accumulation of LP in the gut of inoculated mice (Old-LP) from Days 15 to 21 (Figure 3f). Age-associated microbial dysbiosis promotes increased intestinal permeability leading to systemic inflammation and innate immune system dysfunction (Thevaranjan et al., 2017). Therefore, we first measured the effect of LP on the restoration of intestinal permeability. LP-inoculated old mice showed a significant decrease in gut permeability compared to young dysbiotic and old mice as evidenced by a lower level of dextran FITC in blood plasma (Figure S3c). As LP was able to recover the intestinal permeability, we hypothesized that LP inoculation and establishment in the gut can circumvent the systemic inflammatory condition, by modulating bone marrow myeloid progenitors to acquire tolerogenic properties. Hence, we investigated the effect of LP administration on the phenotype and functional properties of the DCs of LP-inoculated old mice ($DC^{Old\text{-}LP}$). We observed a significant decline in the display of the MHCII and co-stimulatory molecules CD80, CD86, and CD40 (Figure 3g, h and Figure S3d) and an increase in co-inhibitory molecule Tim-3 (Figure S3d, lower panel) on $DC^{Old\text{-}LP}$ compared to DC^{Old}. LP plays a critical role in regulating immune response by modulating the expression of anti-inflammatory cytokines such as IL-10 and TGF-β (Lamubol et al., 2021). Once we had the evidence of phenotypic restoration, we intended to investigate the LP modulation on secretory components of old DCs. We detected a significant reduction in pro-inflammatory cytokines (IL-6, TNF-α, IL-12, IFN-γ, IL1-β, and IL-17) and an increase in anti-inflammatory cytokines (IL-2, IL-10, TGF-β, IL-4) in the $CD4^+$ T cell: $DC^{Old\text{-}LP}$ co-culture in comparison with DC^{Old} (Figure S3e). These results were further validated by transcript-level analysis. Concurrently, significantly decreased transcript levels of pro-inflammatory cytokines (*Il-6*, *Il-12*, *Il-23*, *Il1b*, *Tnfa*) and increased transcripts of anti-inflammatory cytokines (*Il-10* and *Tgfb*) (Figure S3f) genes were observed in $DC^{Old\text{-}LP}$. Intriguingly, our observation further got strengthened with the results showing upregulation in the transcript levels of *Irf4*, *Irf8*, *Pdl1*, *Pdl2*, *Btla4*, and *Aldh2* tolerogenic genes in $DC^{Old\text{-}LP}$ (Figure S3g). Next, we checked the effect of LP on functional properties of DCs and assessed the phagocytic capacity of replenished $DC^{Old\text{-}LP}$, an increase in phagocytosis of dextran-FITC and apoptotic Jurkat cells in old-LP BMDCs was observed (Figure 3i and Figure S3h).

2.6 | *Lactobacillus plantarum* modulates the tolerogenic regulatory program of old DCs by metabolic rewiring and downregulation of NF-κB pathway

Lactobacillus plantarum has been shown to modulate NF-κB mediated inflammatory pathway in the model of colitis (Yu et al., 2020) and bacterial pathogenesis (K. Li et al., 2022). Hence, we revisited NF-κB signaling and metabolic pathways involved in the loss of tolerogenic properties of old-DCs to evaluate the potential of LP for restoration of tolerance. Replenishing the gut of old mice with LP significantly reduced the phosphorylation of p65 in $DC^{Old\text{-}LP}$ as evident from the Western blot and flow cytometry compared to DC^{Old} (Figure 4a, b), with a concomitant decline in *RelA* expression in LPS-stimulated $DC^{Old\text{-}LP}$ compared to DC^{Old} while their level was comparable with DC^{Young} (Figure 4b, right panel). Next, we intended to examine the impact of LP replenishment in regulating DC-mediated T-cell proliferation through attenuation of NF-κB signaling. We used NF-κB inhibitor JSH-23 (Wu & Li, 2012) to block its translocation in the nucleus, and parallelly supernatant of DC^{Young} with attenuated NF-κB signaling was used (shown in Figure 2i) in further experiments. We observed significant inhibition of both syngeneic and allogeneic $CD4^+$ T-cell proliferation in $DC^{old\text{-}LP}$, DC^{Old} with JSH-23, and DC^{Old} co-culture suspended in DC^{Young} cell-free supernatant compared to DC^{Old} (Figure 4c). Additionally, a significant alleviation in Tregs conversion with NF-κB attenuation was noticed (Figure 4d). These results confirmed our led hypothesis that the age-mediated tolerogenic defect of old DCs emanates from secretory factors in the microenvironment. Our experimental evidence shows that the pro-inflammatory microenvironment is the driving factor of deregulated NF-κB pathway in old DCs. Upon correction of the microenvironment with young DCs supernatant, tolerogenic properties can be restored.

We further substantiated our results by examining metabolic moieties responsible for tolerogenic behavior of DCs. $DC^{old\text{-}LP}$ exhibited a significant increase in the secretion of NO (Figure 4e) with elevated expression of *iNOS*, *arginase1*, and *Ido* genes as compared to DC^{old} (Figure 4f). We further confirm their increase at protein levels by Western blotting (Figure 4g). Dendritic cells that exhibit tolerogenic behavior normally engage in the mitochondrial OXPHOS for energy. After activation, they become immunogenic and switch towards glycolysis, akin to Warburg metabolism (Krawczyk et al., 2010). Accordingly, we found it a factor of relevance whether LP replenishment is also modulating the same. Additionally, glucose

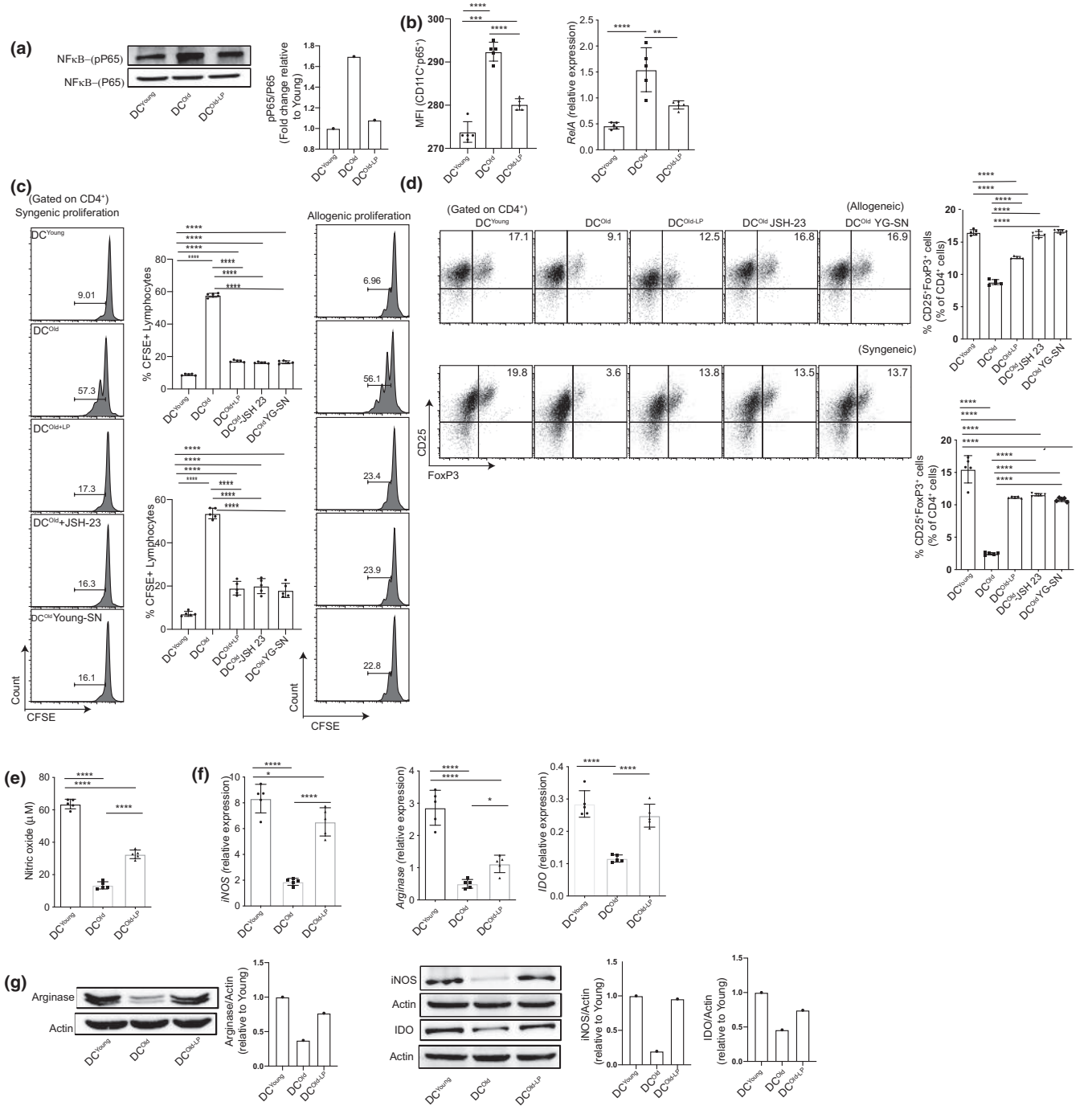

FIGURE 4 Replenishment of the gut of old mice with *Lactobacillus plantarum* reinstates the tolerogenic and metabolic function of old DCs with downregulation of the NF-kB pathway. Evaluation of LPS-stimulated DC^{Young}, DC^{Old}, and $DC^{Old\text{-}LP}$ for NF-kB pathway activation, metabolic gene modulation and their functional properties; (a) representative Western blot and protein level quantification of phospho-p65 in DCs lysate; (b) bar graph representation of the frequency of phospho-$p65^+$ DCs through flow cytometry and relative expression of p65 encoding gene *RelA* through qRT-PCR; (c) representative histogram and frequency of proliferative $CD4^+$ T cells in syngeneic and allogeneic setup; (d) representative dot plots and frequency of Tregs ($CD25^+FoxP3^+$) gated on $CD4^+$ T cells in different groups with allogeneic and syngeneic setup; (e) quantification for the concentration of NO released by LPS-stimulated DCs in SN as determined by the Griess method; (f) relative gene expression of *iNOS*, *arginase1*, and *Ido1* evaluated by qRT-PCR; (g) representative Western blot and quantification of iNOS, IDO, and arginase1 at the protein level. Data (mean ± SD) are of 5 animals, with each point in the bar graph representing one animal, $n = 5$ except (a, g) data representing one independent experiment. $^*p < 0.05$, $^{**}p < 0.01$, $^{***}p < 0.001$, $^{****}p < 0.0001$. One-way ANOVA followed by Tukey's multiple comparison test was performed for statistical analysis.

uptake and associated transporter molecules could be the related factors, that directly regulate this process (Cho et al., 2017). Hence, we monitored 2-NBDG (2-(N-(7-Nitrobenz-2-oxa-1,3-diazol-4-yl) Amino)-2-Deoxyglucose) uptake in both BMCs and BMDCs by flow cytometry. A significant reduction in 2-NBDG uptake was observed in both DC^{Young} and $DC^{Old\text{-}LP}$ in comparison with DC^{Old} and $DC^{Dysbiotic}$

(Figure S4). Further, we evaluated the expression of the *Slc2a1* gene, encoding GLUT1, a known glucose transporter, and observed lesser expression in $DC^{Old\text{-}LP}$ (Figure S4c). These results suggest that LP fixes the metabolic network to promote tolerance in $DC^{Old\text{-}LP}$. These results suggest that administration of LP in the gut not only restores the phenotype and the features of DC^{Old} but also reinvigorates their functional properties to the level of DC^{Young}.

2.7 | *Lactobacillus plantarum* modulates aged DCs by enhancing their migratory and regulatory function

The regulatory role of DCs depends on their ability to migrate to the draining lymph nodes to activate T cells (Hadeiba et al., 2008). CCR7 and CCR9 are important migratory molecules present on the DC surface, driving their trafficking in the skin and gut, respectively, to induce tolerance (Ohl et al., 2004; Pathak et al., 2020). Therefore, we studied the expression of these molecules and DC migration in vivo. A significant decline in the expression of both CCR7 and CCR9 was observed on $DC^{Dysbiotic}$ and DC^{Old} compared to DC^{Young}; however, their expression was restored significantly upon LP administration on $DC^{Old\text{-}LP}$ (Figure 5a, b). Next, we checked the migratory capacities of adoptively transferred DCs from all four groups in old mice in the spleen, mesenteric lymph nodes (mLN), and Peyer's patches (PP). In the same group of mice, the regulatory functions of these migrated DCs were evaluated by analyzing the Tregs induction. We observed a significant decrease in the migratory ability of DC^{Old} and $DC^{Dysbiotic}$ compared to DC^{Young}, while restoration of migration was observed upon LP administration in all three examined organs: spleen, mLN, and PP (Figure 5c). Likewise, shrinkage in the pool of Tregs was detected which was reinvigorated in the LP-inoculated old animals (Figure 5d). Our results showed that DC^{Young} is a potent inducer of Tregs in all three organs (spleen, mLN, and PP) under inflammatory conditions (old recipient), whereas $DC^{Dysbiotic}$ and DC^{Old} significantly lose their Tregs induction potential compared to young DCs. These experiments suggest that due to the enhanced migratory ability, DC^{Young} and $DC^{Old\text{-}LP}$ induced Tregs differentiation and thereby induced tolerance.

2.8 | *Lactobacillus plantarum* modulates the age-associated gene expression profile of DC^{Old} and directs them towards a tolerogenic phenotype

Lactobacillus influence the physiology of their hosts by diverse mechanisms, specifically by interacting with the immune system and play an imperative role in the development and maintenance of the same (Kemgang et al., 2014; van Baarlen et al., 2009). To unravel the molecular mechanism of LP-mediated immunomodulation, we performed the global transcriptomic profiling of DC^{Young}, DC^{Old}, $DC^{Dysbiotic}$, and $DC^{Old\text{-}LP}$ groups. The differential gene expression analysis was filtered by logFC cutoff of 0.5 and a significant *p* value cutoff threshold of <0.05. Our data revealed a contrasting similarity between $DC^{Dysbiotic}$ with DC^{Old} and DC^{Young} with $DC^{Old\text{-}LP}$ as depicted in volcano plots (Figure S5a). Maximum significantly differentially expressed (DE) features were observed between DC^{Young} and DC^{Old} pair (1673), and importantly least DE features were obtained among DC^{Young} and $DC^{Old\text{-}LP}$pair (19), $DC^{Old\text{-}LP}$ exhibit intermediate significant DE features when compared with DC^{Old} (1478) and $DC^{Dysbiotic}$(839), which suggests that LP replenishment rewires the transcriptome profile of old-LP DCs. The intersection of differentially expressed gene sets is represented as an UpSet plot (Marwah et al., 2019) which infers overall larger variation among DC^{Young} with DC^{Old} and $DC^{Dysbiotic}$ groups while there was little variation with $DC^{Old\text{-}LP}$. Similar observations were made for the comparison of DC^{Old} with $DC^{Dysbiotic}$ (Figure 6a). On further analysis differentially expressed genes were grouped under three broad categories of immune response, metabolism, and cell cycle-DNA repair pathways (Figure 6b and Figure S5b). Tolerogenic genes such as *Tgfb*, *Lag3*, *Irf4*, *Irf8*, and *Aldh1a2* were found upregulated in $DC^{Old\text{-}LP}$, and similar patterns were observed for metabolic genes with significant fold change in DC^{Old} versus $DC^{Old\text{-}LP}$ with upregulation of genes encoding immune tolerance enzymes as Ido1, *CD38*, and *NOS2* with least fold difference in DC^{Young} versus $DC^{Old\text{-}LP}$ (Figure 6b). Furthermore, in the case of DNA damage-associated genes, most of them showed increased fold change expression in DC^{Young} and $DC^{Old\text{-}LP}$ compared to DC^{Old} such as *Cdc20*, *Cdk2*, *Pik4*, *Pik2*, and *Parp* group of genes 1, 3, 4, and 11 having an important role in the recovery of cells from DNA damage (Figure S5). All these findings indicate the substantial role of aging and antibiotic-mediated gut dysbiosis towards the generation of inflammatory phenotype, which interestingly resorted towards tolerogenic mode by replenishment of gut of old mice with LP.

3 | DISCUSSION

Aging is an incessant and irrevocable physiological process accompanied by the phenotypic and functional changes of senescence. It results in chronic inflammation, the decline in functional immunity, and altered gut microbial composition. The gut microbiome profoundly influences human health and disease, and recently, gut dysbiosis has been connected with several chronic diseases viz.

FIGURE 5 *Lactobacillus plantarum* reinvigorates the migratory and regulatory function of Old- DCs. LPS-stimulated DC^{Young}, $DC^{Dysbiotic}$, DC^{Old}, and $DC^{Old\text{-}LP}$ were estimated for in-vitro estimation of migratory markers. Representative histogram and frequency of (a) $CCR7^{+}$ $CD11c^{+}$ cells; (b) $CCR9^{+}$ $CD11c^{+}$ cells through flow cytometry. Estimation of in vivo migration and Tregs inducing capacity of adoptively transferred LPS-stimulated DC^{Young}, $DC^{Dysbiotic}$, DC^{Old}, and $DC^{Old\text{-}LP}$; (c) bar graph representation of the frequency of $CFSE^{+}$ $CD11c^{+}$ (R: Recipient, D: donor), and (d) representative dot plot and bar graph representation of $CD25^{+}Fox\ P3^{+}$Tregs (gated on CD4 cells) in the spleen, MLN and Peyer's patches. Data (mean ± SD) are of 3 animals, with each point in the bar graph representing one mouse ($n = 3$/group). $^{*}p < 0.05$, $^{**}p < 0.01$, $^{***}p < 0.001$, $^{****}p < 0.0001$. Statistical analysis was done by one-way ANOVA and Tukey's multiple comparison test.

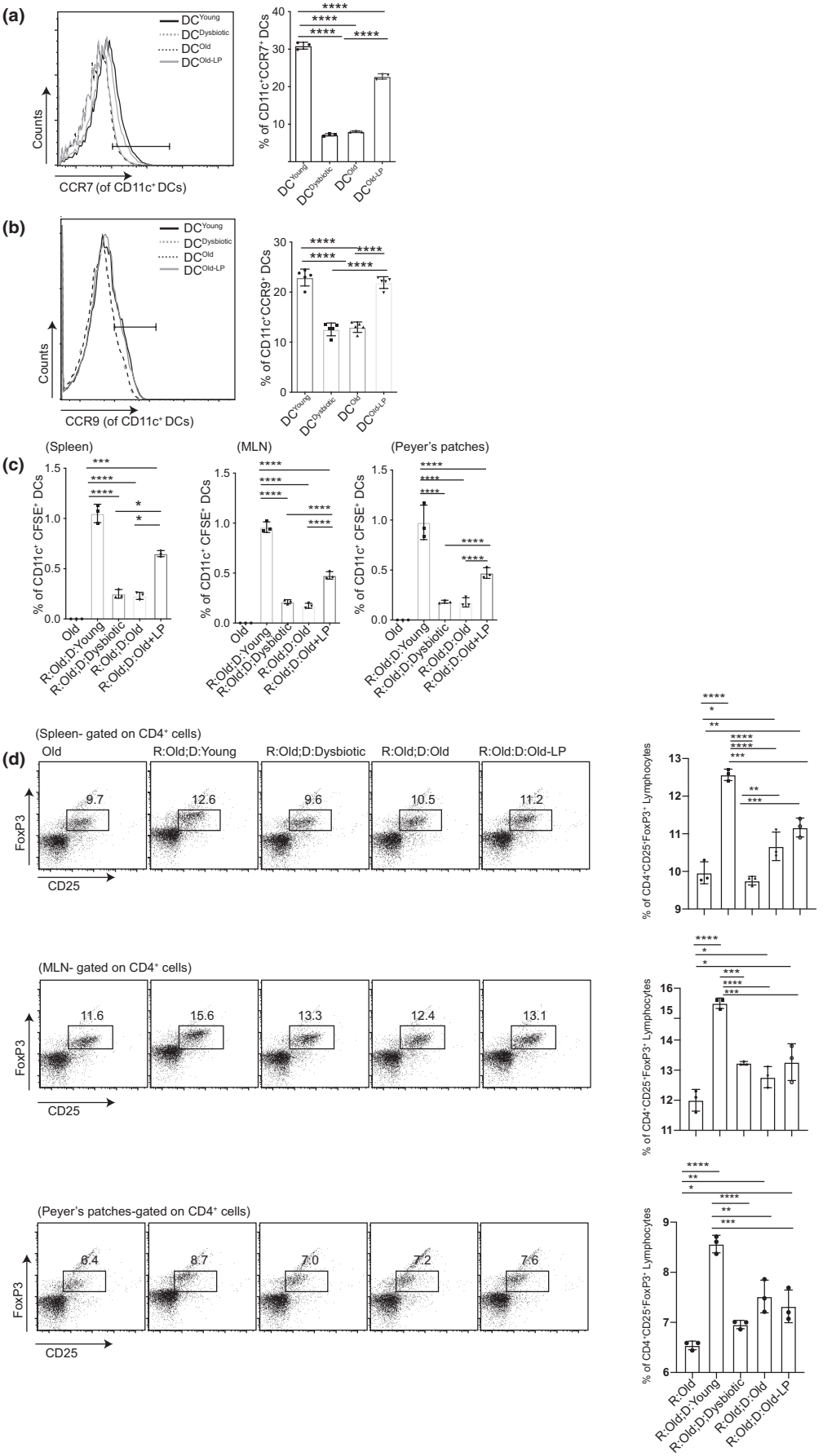

inflammation, neurodegenerative diseases, metabolic disorders, and cancer (Belkaid & Hand, 2014; Zheng, Fang, et al., 2020). However, the mechanism of age-associated immune dysfunction through gut dysbiosis remains largely unexplored. Consequently, in the current study, we have tried to uncover the influence of aging on gut microbiota and its impact on DCs. Additionally, we explored the prospect of a key probiotic strain for restoring age-mediated DC dysfunction.

Dendritic cells play an essential role in regulating immunity and tolerance by connecting innate and adaptive immune systems (Raker et al., 2015). Tolerogenic DCs maintain central and peripheral tolerance by regulation of optimum effector T cell and regulatory T-cell responses (Hasegawa & Matsumoto, 2018). However, with age, the regulatory function of DCs is impaired. The current study explores the gut-age axis by monitoring dysbiosis-associated functional defects of dendritic cells (DCs). We did a comparative analysis of the gut microbiome of young animals with aged and gut-disrupted young mice and simultaneously compared the DCs from all of them for their phenotypic characteristics and functional capacity. As compared to the young group (DC^{Young}), the DCs generated from aged (DC^{Old}) and young gut-disrupted animals ($DC^{Dysbiotic}$) exhibited the following differences: (i) loss of tolerance, as supported by upregulation in the level of pro-inflammatory molecules IL-6, IL-1β, TNF-α, IL-12, IFN-γ, NF-κB, p65, RELA, and decline in the anti-inflammatory moieties IL-2, IL-10, TGF-β, IL-4, IDO, arginase, NO, IRF-4, IRF-8 PDL1, BTLA4, and ALDH2; (ii) impaired functionality, as evinced by the failure to control the hyperactivation of T cells; (iii) inability to generate the optimum frequency of Tregs; (iv) contraction of *Lactobacillus* from the gut of the old and Abx treated young mice; and (v) replenishment of gut of old mice with *Lactobacillus plantarum* restored the tolerogenic phenotype and function of old DCs.

We observed that NF-κB signaling was required for the homeostatic maturation and function of DC^{Young} while overactivation was observed in $DC^{Dysbiotic}$ and DC^{Old}. NF-κB is a master regulator of inflammation, and its dysregulated activation is associated with several autoimmune, inflammatory pathogenesis (Barnabei et al., 2021) and aging (Adler et al., 2007). Over-expression of NF-κB subunit RelA/p65 induces a senescent phenotype in cultured cells, while the low level in the progeroid mouse model has been interrelated with the delay in age-associated pathologies (Flores et al., 2017; Seitz et al., 2000). In agreement, we demonstrate that overt activation of NF-κB in $DC^{Dysbiotic}$ and DC^{Old} is due to increased phosphorylation of p65, interestingly, p65 phosphorylation decline in $DC^{Old\text{-}LP}$ on feeding the old animals with LP. We assume that the decline in phosphorylation of p65 in $DC^{Old\text{-}LP}$ is associated with secreted factors, as an inhibitor of p65 (JSH-23) and supernatant of DC^{Young} culture show a similar effect on DC^{Old} for NF-κB downregulation through p65 phosphorylation. Increased activation of NF-κB was associated with the maturation status of old and dysbiotic DC. In comparison with DC^{Young} both $DC^{Dysbiotic}$ and DC^{Old} exhibited heightened expression of co-stimulatory and MHC molecules and decrease in the level of inhibitory molecules. Further, reduced phagocytosis was noticed, since $DC^{Dysbiotic}$ and DC^{Old} poorly captured antigens and apoptotic bodies. Our findings further suggest that gut dysbiosis affects the tolerogenic properties of DC as enhanced $CD4^+$ T-cell proliferation, increased release of pro-inflammatory cytokines and reduction in the pool of Tregs and the level of anti-inflammatory cytokines were observed. Unregulated T-cell proliferation upon aging has been linked previously to loss of DC tolerance (Agrawal & Gupta, 2011). Since, the secretion of anti-inflammatory cytokines and reduced secretion of pro-inflammatory cytokines by DC contribute to tolerance induction (Wakkach et al., 2003). We conclude that gut dysbiosis leads to the activation of NF-κB signaling in DC and activates pro-inflammatory phenotype conducive for $CD4^+$ T-cell activation. Interestingly, LP reconstitution restored the phenotype and functional properties of old DCs as evident by optimum expression of co-stimulatory and MHCII expression on $DC^{Old\text{-}LP}$, improved phagocytic activity and controlled proliferation of $CD4^+$ T cells.

Our analysis of the gene expression signature through global transcriptomic profiling of all four groups of DCs reveals a striking difference between DC^{Young} and DC^{Old} where the later is similar to $DC^{Dysbiotic}$ for gene expression. Interestingly, LP reconstituted old DC ($DC^{Old\text{-}LP}$) aligned with DC^{Young} in the molecular screening. A convincing repression of NF-κB inhibitor genes was observed in both $DC^{Dysbiotic}$ and DC^{Old} compared to DC^{Young}. Activation of NF-κB genes coincided with the repression of *Tgfb* genes and receptors. TGFβ has been linked with tolerogenic function in DC (Zhong et al., 2019), and transcriptional activation of *Smad7* in response to pro-inflammatory cytokine stimulation through NF-κB activation has been shown to suppress TGFβ/SMAD signaling (Bitzer et al., 2000). In our experimental settings, we have shown downregulation of *Tgfb* expression, and the corresponding decrease in TGFβ in the supernatant of DC^{Old} and $DC^{Dysbiotic}$ $CD4^+$ T-cell co-culture. Our transcriptomic profiling re-confirmed our results; we observed downregulation of *Tgfb*, *Tgfb* receptors and associated receptors (Tgfb1, Tgfr3, and Tgfbrap1) in

FIGURE 6 Inoculation of *Lactobacillus plantarum* into the gut of old mice modulates the transcriptomic gene profile. RNA was isolated from LPS-stimulated $DC^{Old\text{-}LP}$, DC^{Old}, $DC^{Dysbiotic}$, and DC^{Young} for gene array profiling by Agilent GeneChips. Data analysis was done, and differential gene expression between the groups was compared. (a) UpSet plot representing the intersection between the sets of differentially expressed genes from various comparisons in the limma setup with a vertical bar plot reporting the intersection size, the dot plot was reporting the set participation in the intersection, and the horizontal bar plot reporting the set sizes. The heatmap (b) represents the differentially expressed features associated with the immune response (left panel), differentially expressed metabolism-related features (right panel). Rows represent the features, and columns signify the samples. The 'Color Key' denotes the log-transformed expression values. Data are from three independent sets, with each data set representing a pool of three animals ($n = 3$ mice/group).

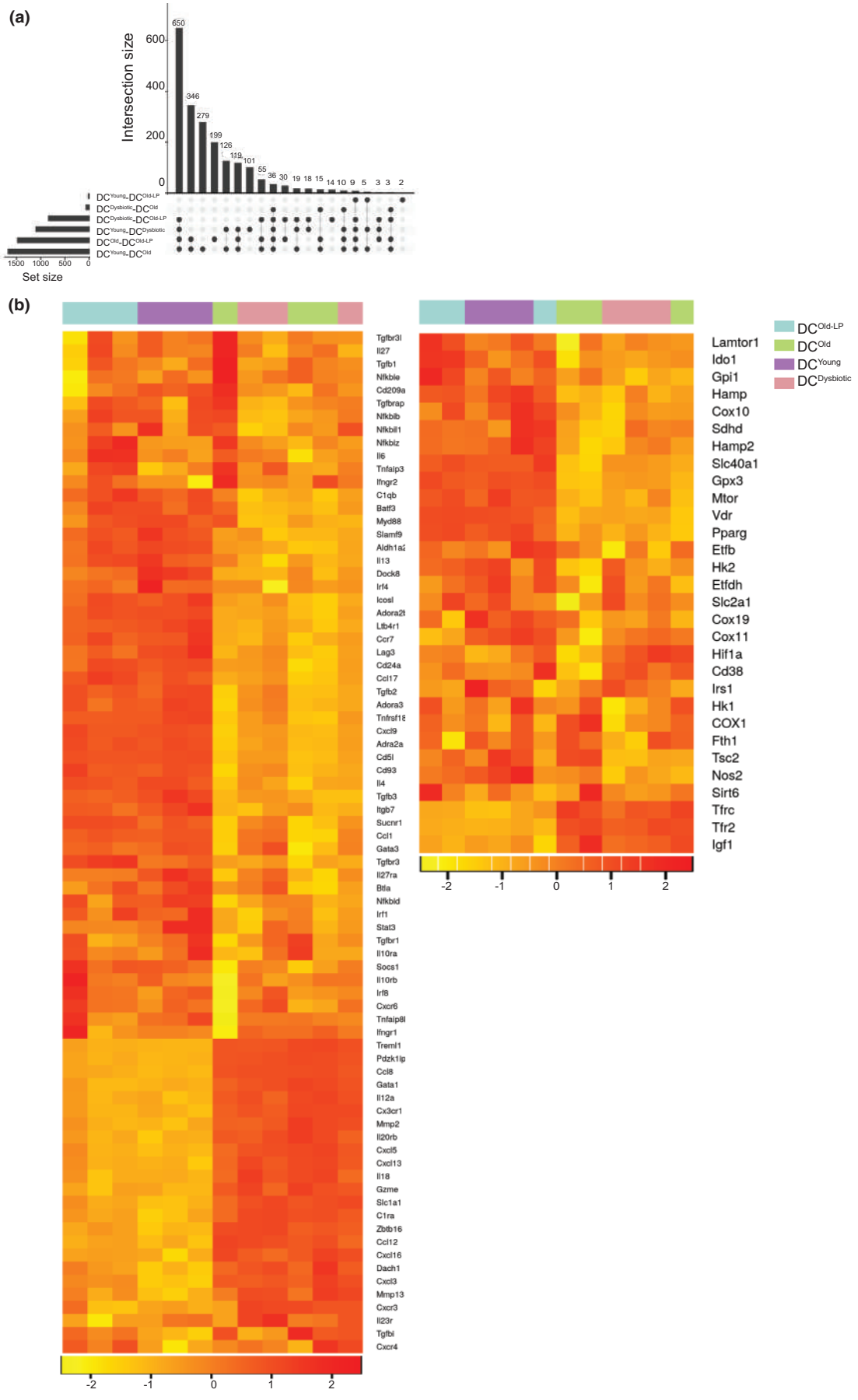

DC^{Old} and $DC^{Dysbiotic}$ compared to DC^{Young}. LP reconstitution restores the TGFβ signaling by downregulating the NF-κB activation.

The tolerogenic phenotype of DCs to induce T-cell hyporesponsiveness is orchestrated by a complex network of immunoregulatory molecules (Domogalla et al., 2017) and metabolic rewiring (Adamik et al., 2022). Transcription factors IRF4, IRF8, and BATF3 have been shown to promote tolerogenic phenotype of DCs by promoting Tregs generation through negative regulation of proinflammatory cytokine transcription and induction of *Raldh*, *Pdl1*, and *Pdl2* expression (Vander Lugt et al., 2017), and prevention of inflammasome activation in splenic DCs (McDaniel et al., 2020). Likewise, we observed a downregulation in the expression of *Irf4*, *Irf8*, *Pdl1*, *Btla*, and *Aldh2* with a potent reduction in Treg inducing capacities of both $DC^{Dysbiotic}$ and DC^{Old} but not DC^{Young}. Intriguingly, LP replenishment restores the tolerogenic properties of DCs by upregulating the expression of immunoregulatory molecules. The Treg induction was boosted, and it coincided with enhanced migratory capacity of DCs. Further, the downregulation in the pattern of NO, iNOS, arginase 1 and IDO in $DC^{Dysbiotic}$ and DC^{Old} that contributed to their immunogenic phenotype was also restored through LP reconstitution. The NO, iNOS, arginase 1, and IDO have been implicated in imparting tolerogenic behavior of DC (Panfili et al., 2019; Verinaud et al., 2015). NO responsible for the tolerogenic behavior of DCs is a product of L-arginine metabolism and its level is controlled in cells by iNOS (Moncada, 1999) while immunoregulatory enzyme IDO elicits peripheral tolerance in DCs. Another important observation in this study included the rewiring of metabolic processes in DC^{Old} by switching from mitochondrial OXPHOS to a glycolytic pathway with greater consumption of glucose compared to DC^{Young} and $DC^{Old\text{-}LP}$. Notably, DCs at a steady-state condition showing tolerogenic behavior normally engage in mitochondrial OXPHOS for energy requirements. However, after TLR-based activation they become immunogenic with the remarkable switch towards glycolysis, similar to Warburg metabolism (Krawczyk et al., 2010).

Overall, the parallel observations in $DC^{Dysbiotic}$ and DC^{Old} suggest that disruption in gut microbiota due to aging or antibiotic treatment of young mice can contribute to the loss of tolerance in DCs. We have uncovered a notable contribution of gut microbiota contributing to the loss of immune tolerance in the dendritic cells on aging. Our data show a significant role of NF-κB signaling in immune tolerance at old age, through the regulation of cytokine signaling. Furthermore, disruption of the gut on aging or antibiotic treatment of young group also results in the disappearance of beneficial commensals like *Lactobacillus plantarum*, resulting in the loss of tolerance in DCs. Interestingly, *LP* replenishment restores tolerogenic phenotype and properties of old DCs through modulation of metabolism and immunity-associated gene network profiling. The study for the first time demonstrates the role of aging on gut dysbiosis, which ultimately resulted in the loss of functionality in DCs in maintaining tolerance. Finally, this study suggests the immunotherapeutic role of LP to treat age-related disruption in the gut for the tolerogenic function of dendritic cells.

4 | METHODS

4.1 | Animals and ethical statement

Animal experiments were performed with C57BL/6 female mice. 2–3 months old mice were considered young and 22–24 months were considered old. All the animals were procured from IMTECH Center for Animal Resources and Experimentation (iCARE), Institute of Microbial Technology (IMTECH), Chandigarh. Institutional Animal Ethics Committee (No. 55/1999/CPCSEA), Ministry of Environment and Forest, Government of India has approved the study and all the experiments and protocols are in accordance with the guidelines of the same.

4.2 | Gut dysbiosis mice model

Young mice were given drinking water with a broad-spectrum antibiotic (Abx) cocktail (Ampicillin, 1 g/L; neomycin sulfate, 1 g/L; metronidazole, 1 g/L and vancomycin, 0.5 g/L) Himedia (Mumbai, India) ad libitum in drinking water for 21 days to disrupt the gut microbiota, with change in Abx containing water after every 3 days. To assess the effect of Abx-mediated dysbiosis on the gut bacterial burden, serially diluted fecal samples from all groups were plated on a BHI medium under aerobic and anaerobic conditions. Facultative anaerobic conditions were maintained by keeping the plates in airtight sealed glass chambers in presence of Anaerogas packs-LE002A-5NO, Himedia (Mumbai, India).

4.3 | Chemicals and reagents

All reagents were acquired from Sigma Aldrich (St. Louis, MO) or else specified. All recombinant cytokines were purchased from BD Biosciences (San Diego, CA). Fluorochrome-tagged Abs viz. CD11c-PEcy7 (#558079), MHCII-PerCP-efluor710 (#46–5320-82), CD86-PE (#12–0862-85), CD80-FITC (#553768), CD40- PerCPcy5.5 (#124623), Tim3-APC (#134007), CCR7-APC (#120107), and CCR9-PE (#565576) were procured from BD Biosciences (San Jose, CA), eBioscience (San Diego, CA), and Biolegend (San Diego, CA). Secondary anti-mouse and anti-rabbit Abs for flow cytometry and confocal microscopy were from Invitrogen-Thermo Fisher Scientific (Waltham, MA). ELISA reagents and Abs against IL-6, IFN-γ, IL-17, IL-12, TGF-β, IL-4, TNF-α, IL-2, and IL-10 were purchased from BD Biosciences (San Diego, CA). Primers for qRT PCR, were synthesized by Sigma Aldrich (St. Louis, MO) and Integrated DNA Technologies, Inc. (Coralville, IA). Anti-mouse phospho p65 (# 3033), p65 (# 8242), iNOS (# 13120), and β-actin (# 3700) Abs were from Cell Signalling Technology (Danvers, MA), anti-mouse IDO (# sc-137,012) from Santa Cruz Biotechnology, (Santa Cruz, CA) and anti-mouse arginase1 (# 610709) from BD Biosciences, (San Diego, CA) were used in Western blot. Other chemicals and reagents like RPMI-1640, fetal bovine serum were from GIBCO (Grand Island, NY), L-glutamine, l-pyruvate, streptomycin and

penicillin- from Serva (Heidelberg, Germany). All tissue culture-grade plasticwares were from BD Biosciences (San Diego, CA), Corning™ (Corning, NY) and Nunc™ (Rochester, New York).

4.4 | Bacterial strains used in the in vivo experiments

Lactobacillus plantarum MTCC 2621 obtained from Microbial Type Culture Collection (MTCC), IMTECH (Chandigarh, India) was cultured in DeMan, Rogosa Sharpe broth (Merck, Darmstadt, Germany) at 37°C, 5% CO_2. The bacterial suspension was pellet down by centrifugation at 3000 *g* for 10 min and washed with 1xPBS twice, and CFU was adjusted to 1×10^8. Thereafter, the same CFU in 200 μL sterile PBS was orally gavaged to mice every alternate day for 21 days, until mice were sacrificed. Fecal samples were obtained on Days 0, 7, and 21 to assess the accumulation of bacteria inside the gut.

4.5 | Dendritic cell cultures

Bone marrow cells from the femurs and tibia of mice were flushed with cold RPMI media. After RBC lysis by ACK lysis buffer, the cells (2×10^6/well) were plated in a 6-well plate. The BMCs were cultured in RPMI-1640 supplemented with 10% FCS, penicillin (100 U/mL), L-glutamine (100 mM), streptomycin (100 mg/mL), rmGM-CSF (2 ng/mL) (#554586) and 4 ng/mL rmIL-4 (#-550067), BD Biosciences (San Diego, CA), for DC cultures. On 3rd day, the culture was supplemented with fresh complete RPMI media with rmGM-CSF (2 ng/mL) and rmIL-4 (4 ng/mL) at half of its initial volume. Loosely adherent cells were harvested by gentle pipetting on the 7th day and used for further experiments. The methodology was followed as per the already mentioned protocol (Lutz et al., 1999). Later, for maturation of BMDCs (2×10^6/well) were stimulated with LPS-1 μg/mL, L2630-Sigma Aldrich (St. Louis, MO) in 6-well plate.

4.6 | Flow cytometry

Single-cell suspension was incubated for 30 min at 4°C with Fc block (anti-mouse CD16/32 Ab) to prevent non-specific binding of Abs. Next, cell-surface staining was done with fluorochrome-tagged monoclonal antibodies for another 30 min at 4°C as per the experiment. For intracellular staining, cell surface stained cells were fixed and permeabilized using True-nuclear™ transcription factor kit-Biolegend (San Diego, CA) and stained for intracellular targets in accordance with the manufacturer's protocol. The data was obtained with BD FACSVerse and analyzed through BD FlowJo software (San Jose, CA).

4.7 | Cytokine estimation

The cytokines were estimated in the culture SNs by sandwich ELISA. Briefly, 96-well ELISA plates were coated with purified rat anti-mouse IL-6, IFN-γ, IL-17, IL-12, TGF-β, IL-4, TNF-α, IL-2 (all at 2 μg/mL), and IL-10 (4 μg/mL) antibodies in phosphate buffer (0.01 M-pH 9.2 or pH 6) overnight (O/N) at 4°C as per the manufacturer's protocol BD Biosciences (San Diego, CA). The next day, blocking was done with BSA (1%) in PBS for 2 h at room temperature (RT). Subsequently, 50 μL samples (culture SNs) along with the respective standards of the recombinant cytokines were added to each well followed by O/N incubation at 4°C. After incubation and subsequent washing, 50 μL biotinylated anti-mouse antibodies (2 μg/mL) for respective cytokines were added to plates and incubated for 2 h at RT. Further, plates were incubated with streptavidin-HRP at 1:10,000 dilution at 37°C for 40 min. After subsequent washing, 1× TMB solution was used for color development and the reaction was stopped by H_2SO_4(7%). Absorbance was read at 450 nm on a spectrophotometer, Synergy H1, BioTek (Santa Clara, CA). The quantification of cytokines (pg/mL) was done using a standard curve of recombinant cytokines log2 serial dilutions.

4.8 | Quantitative real-time PCR (qRT-PCR)

Trizol reagent was used to isolate total RNA from LPS-stimulated DCs according to the manufacturer's protocol-Invitrogen (Carlsbad, CA). RNA samples were incubated with amplification grade DNase1 enzyme to remove DNA contamination. 1 μg purified RNA with a standard ratio of 260/280 1.9–2.0 was used to synthesize cDNA with a reverse transcription kit, according to the manufacturer's protocol-Applied Biosystems (Foster City, CA). Following that, qRT-PCR was carried out using SYBR green PCR mix-Applied Biosystems (San Diego, CA) according to the manufacturer's protocol. The real-time PCR analysis was performed using the comparative Ct method on an Applied Biosystems step one plus PCR (Waltham, MA). The results are presented as a relative expression after normalization with β-actin. The primer sequences used in PCR are listed in Table S1.

4.9 | DC-T cell co-cultures

$CD4^+$ T cells were purified from single-cell suspension of the mouse splenocytes with BD IMag™ mouse CD4 T lymphocyte enrichment set–DM, BD Biosciences (San Diego, CA) by MACS negative selection following the manufacturer's protocol. Later, sorted T cells were co-cultured with LPS-stimulated DCs in a 1:5 ratio (DC: T cell) with a total seeding population of 2×10^5 cells per well of 96-well plates.

4.10 | Proliferation assay

$CD4^+$ T cells were labelled with carboxyfluorescein succinimidyl ester (CFSE, 2 μM)- Sigma Aldrich (St. Louis, MO) in PBS for 8 min at 37°C. Any unbound CFSE was washed with RPMI with 10% FCS. Stained cells were then co-cultured with DCs in 96-well flat bottom plates coated with anti-mouse CD3 (5 μg/mL) and soluble anti-mouse CD28 (2 μg/mL) antibodies at 37°C with 5% CO_2 for 72 h.

The proliferation of labeled T cells was assessed, using flow cytometry. The culture SNs were collected to later estimate the cytokines through ELISA. For syngeneic and allogeneic setup, $CD4^+$ T cells were obtained from C57BL/6 and BALB/c mice, respectively.

4.11 | In vitro Tregs induction assay

The same procedure was followed as described in DC-T cell co-culture procedure and maintained for up to 5 days for induction of T regulatory cells (Tregs). On the 5th day, cells were harvested and stained for Treg-specific markers; anti-mouse CD4-FITC (# 11-0042-82), CD25-PE-Cy7 (# 25-0251-82), and FOXP3-PE (# 12–5773-82) all from eBioscience (San Diego, CA); and CD127-APC (# 158205) Biolegend (San Diego, CA) fluorochrome-tagged monoclonal antibodies.

4.12 | Adoptive transfer of DCs

LPS-stimulated DCs (5×10^6) from different groups of mice viz. young, young dysbiotic, old and old-LP were injected intravenously (i.v.) into old mice in 200 μL of PBS.

4.13 | Nitric oxide (NO) production

After 24 hours, the culture SNs of LPS-stimulated BMDCs were collected and NO was measured according to Griess method (Pahari et al., 2016). In brief, a 1:1 ratio of SNs was added to the Griess reagent (50 μL)- Sigma Aldrich (St. Louis, MO) and incubated for 5 min at room temperature. Later, the absorbance was measured at 550 nm. NO was quantified in comparison with sodium nitrite ($NaNO_2$) as a standard (μM).

4.14 | Phagocytosis assay

LPS-stimulated DCs (1×10^6 per sample) were incubated with dextran-FITC (40,000 Da)- Sigma Aldrich (St. Louis, MO) at 37°C for 30 min, or on ice as a control, for the dextran antigen uptake. After proper washing, uptake was then assessed by flow cytometry. For phagocytic uptake of apoptotic bodies, Jurkat T cells labelled with CFSE were treated with actinomycin D for 14–15 h. to induce apoptosis in the same. Later, apoptotic cells were co-cultured with LPS-stimulated DCs for 3–4 h, and uptake was monitored by flow cytometry.

4.15 | In vivo DC migration

LPS-stimulated DCs from different groups of mice were labelled with CFSE (2 μM), and 5×10^6 cells were adoptively transferred through an intravenous (i.v.) route into Old mice in 200 μL of sterile PBS. After 5 days, animals were sacrificed and cells from the spleen, mesenteric lymph node and Peyer's patches were stained for fluorochrome-tagged anti-mouse CD11c antibody. Later, the $CD11c^+CFSE^+$ population was monitored to assess migrated DC population. Furthermore, cells from the same tissues as mentioned were stained by fluorochrome-tagged anti-mouse CD4, CD127, CD25 and FOXP3 to assess the induction of Tregs using flow cytometry.

4.16 | Inhibition of the NF-κB pathway

The DCs harvested on the seventh day of culture were stimulated with LPS (1 μg/mL) in presence of a selective inhibitor for nuclear translocation of NF-κB p65, JSH-23 (7 μM) #481408, Sigma Aldrich (St. Louis, MO) in 24-well plates (0.5×10^6 cells/well) in 1 mL complete media for 24 h. Later, cells were washed with PBS after harvesting and used for further experiments.

4.17 | Dextran-FITC intestinal permeability assay

Evaluation of intestinal epithelial barrier permeability was done utilizing the dextran-FITC permeability assay (Furuta et al., 2001; Meisel et al., 2018). In brief, mice were fasted for 4 h and then 60 mg dextran-FITC (MW 4000), #46944, Sigma Aldrich (St. Louis, MO) per 100 g body weight was given through oral gavage. After 3 h of gavage, blood samples (400–500 μL) were obtained from the tail vein and plasma was extracted by centrifugation (2000 g for 10 min at 4°C). Thereafter, 50 μL blood plasma was transferred in duplicates into a flat-bottom 96-well plate (Corning, NY), and fluorescence reading was measured in fluorescence spectrophotometer setup in Synergy H1, BioTek (Santa Clara, CA) with emission and excitation wavelengths of 520 nm and 490 nm, respectively. Plasma dextran-FITC concentration was assessed using a standard curve established by serial dilution of the same.

4.18 | Western blotting

The whole cell lysate was prepared by lysing LPS-stimulated DCs in RIPA lysis buffer (Tris HCl25 mM, NaCl150 mM, EDTA5 mM, Triton X-1000.1%, sodium deoxycholate 1%, SDS 0.1%) supplemented with PMSF, phosphatase and protease inhibitor cocktail after 40 min incubation on ice. Lysates were centrifuged at 8000 *g* for 10 min, and the protein concentration of the lysate was measured by the BCA method. 40 μg of protein was added to Laemmli buffer and boiled (10 min, 95°C). Proteins were separated in 10–12% SDS-PAGE gels and transferred to the PVDF membrane. Later, 5% BSA was used to block the membranes followed by incubation with the primary antibody on a shaker overnight at 4°C. All primary antibodies were diluted at a 1:500–1000 ratio for immunoblotting. HRP-conjugated secondary anti-mouse and anti-rabbit antibodies

were used (1:10000) for the detection of primary antibody binding. Each step included regular washings and incubations. Finally, blots were developed using Novex™ ECL Chemiluminescent Substrate Reagent Kit, Invitrogen-Thermo Fisher Scientific, (Waltham, MA) and visualization was done on iBright™ FL1500 Imaging System, Invitrogen-Thermo Fisher Scientific (Waltham, MA). Blot analysis and quantification were done using ImageJ analysis software. Abs to phospho p65, p65, anti- IDO, iNOS, arginase1, and β-actin (loading control) were used for Western blotting.

4.19 | Glucose uptake assay

ACK lysed bone marrow cells (BMCs) and LPS-stimulated DCs were incubated with 10 μM of 2-NBDG (2-(N-(7-Nitrobenz-2-oxa-1,3-diazol-4-yl) Amino)-2-Deoxyglucose) in glucose-free RPMI-1640 + 10% FCS at 37°C/5% CO_2 for 30 min. Thereafter, cells were washed and 2-NBDG uptake was monitored through flow cytometry, BD FACSVerse™ (San Jose, CA) and data were analysed through BD FlowJo software (San Jose, CA).

4.20 | Fecal DNA extraction

Aseptically obtained mice fecal samples were immediately placed on ice and kept at −80°C for later use. Zymo Research Fecal DNA Isolation Kit (Irvine, CA) was used to isolate fecal DNA from 100 mg of fecal pellets, according to the manufacturer's procedure. Quantification was done on a NanoDrop spectrophotometer, SYNERGY H1-BioTek (Santa Clara, CA). The quantified DNA was then directly used for real-time PCR analysis. 50 ng of extracted genomic DNA from fecal samples was used as a template for a real-time PCR reaction with genus/species-specific primers (0.2 μM), and SYBR green PCR Master-mix, Applied Biosystems (San Diego, CA). Each cycle of PCR reaction was 10 min at 95°C, then 40 cycles of 30 s at 95°C, 1 min at 60°C and performed in step one plus PCR, Applied Biosystems (Waltham, MA). Data were represented as relative abundance for each genus/species after normalization with bacterial universal primer/DNA as an internal control.

4.21 | 16S rRNA sequencing for gut microbiota analysis

DNA was isolated as per the already discussed protocol from mice fecal samples. Later, DNA was further processed for amplicon-based sequencing of the V3-V4 hyper-variable region of the 16S rRNA gene. Fusion primer 16S amplicon PCR primers Fw 5′ TCGTCGGCAGCGTCAGATGTGTATAAGAGACAGCCTACGGGNGGCWGCAG 3′ and Rv 5′ GTCTCGTGGGCTCGGAGATGTGTATAAGAGACAGGACTACHVGGGTATCTAATCC 3′ (Klindworth et al., 2013) was used to amplify V3-V4 region of 16S rRNA using 12.5 ng of DNA. Sequencing libraries were prepared from amplified V3-V4 region of 16S rRNA by Index PCR using Nextera XT index kit as per manufacturer instructions (Illumina, #15044223 Rev. B). The quality of the final libraries was checked using high-sensitivity D1000 screen tape in Tape-Station 2200 Agilent Technologies (Santa Clara, CA), and final library quantification was performed in Qubit Fluorometer. Paired-end (2 × 250 bp) sequencing of these libraries was performed in NovaSeq 6000 (Illumina, San Diego, CA). Sample preparation and sequencing were done at the National Institute of Biomedical Genomics (Kalyani, India). The raw data were first checked for quality, and then, DADA2 was used to remove chimeric information. The demultiplexed sequences were then trimmed to lengths of 250 and 230 for forward and reverse, respectively. After that, the frequency table and data were obtained. Model classifier, which was created using the reference Green gene database, was used to classify taxa. The taxonomic plots were then created using the model classifier parameters such as forward primer CCTACGGGNGGCWGCAG and reverse primer GACTACHVGGGTATCTAATCC. The OTU table has been created from taxonomic classification. MAFFT was used to align the sequences, which were then masked to obtain masked aligned sequences. Subsequently, for diversity analysis, phylogenetic trees were created. With the parameter sampling depth 582,778, PCoA and diversity analysis plots were obtained using rooted and unrooted trees.

4.22 | Microarray-based gene expression analysis

RNA was isolated from DCs after LPS stimulation (1 μg/mL) using TRIzol reagent according to the manufacturer's protocol, Sigma Aldrich (St. Louis, MO). Later, the DNase1 enzyme was added for the digestion and removal of genomic DNA. Thereafter, RNA was quantified with the NanoDrop ND-100 Spectrophotometer, NanoDrop Technologies (Wilmington, DE), and quality for the same was examined with the Tapestation 4200™, Agilent Technologies (Santa Clara, CA). Samples with RIN (RNA integrity number) score of more than 6 and a 28S:18S rRNA ratio of around 2:1 were included for the further process. Thereafter, labelling and hybridization were done using Agilent one-color (Cy3 fluorochrome), a microarray-related gene expression platform in accordance with the manufacturer's instructions for evaluating mRNA expression. Briefly, 500 ng of RNA was labelled with a one-color Low-Input Quick Amp labelling kit, 5190–2305 (Agilent Technologies, Palo Alto, CA, USA). Cy3-labelled mRNA samples were hybridized onto a mouse 8 × 60 K Gene Expression V2 Array kit, G4858A, Agilent Technologies, (Palo Alto, CA) for 16 h at 55°C in a rotator oven with subsequent washing. DNA microarray scanner, Agilent Technologies, (Palo Alto, CA) was used to scan the array slides, and Agilent Feature Extraction software 10.5 (Palo Alto, CA) to extract hybridization signals. Thereafter, with the help of limma R package, the quantile normalization method was implemented to normalize the quantitative microarray data. Using the same package, differential feature estimation was performed by lmFit () function to fit a linear model to expression data of each feature and eBayes (empirical

Bayes) function used to obtain adj.*p*.value and logFC. Threshold adj.*p*.value ≤ 0.05 and abs (logFC) ≥ 0.5 were used to obtain significant differential features. R package gprofiler2 was used for the enrichment of functional annotations. Summarization of gene ontology and treemap plot were done with R package rrvgo.

4.23 | Statistical analysis

One-way ANOVA followed by Tukey's multiple comparison test and two-way ANOVA followed by Sidak's multiple comparisons test were done using GraphPad Prism 6 software (San Diego, CA). A p value <0.05 was considered significant.

AUTHOR CONTRIBUTIONS

HB performed the experiments and contributed to experimental design, data analysis, discussion and writing. RPS helped in flow cytometry data acquisition with HB and analyzed the 16S rRNA sequencing data. SS conducted experiments with HB. JNA conceptualized, designed and supervised the study, and contributed to the discussion and writing of the manuscript. RK conceptualized, designed and supervised the study, analyzed the data and wrote the manuscript. All authors revised and commented on the manuscript. All authors approved the final manuscript.

ACKNOWLEDGMENTS

HB and RPS are thankful to the Council of Scientific and Industrial Research (CSIR) fellowship and SS to the Indian Council of Medical Research (ICMR) for providing Junior and Senior Research fellowships.

FUNDING INFORMATION

This study is supported by the grants from CSIR, India grants OLP134, HUM (No. BSC0119) and CSIR-FIRST (No. MLP062).

CONFLICT OF INTEREST STATEMENT

The authors declare that they have no conflict of interest.

DATA AVAILABILITY STATEMENT

The 16s rRNA sequencing data from this study have been deposited at the GenBank Sequence Read Archive with the accession number PRJNA879291. The microarray raw data are submitted to the GEO repository with GEO accession number GSE 213155.

ORCID

Hilal Bashir https://orcid.org/0000-0003-3605-1726
Javed N. Agrewala https://orcid.org/0000-0003-0227-1042
Rashmi Kumar https://orcid.org/0000-0003-3444-1018

REFERENCES

Adamik, J., Munson, P. V., Hartmann, F. J., Combes, A. J., Pierre, P., Krummel, M. F., Bendall, S. C., Argüello, R. J., & Butterfield, L. H. (2022). Distinct metabolic states guide maturation of inflammatory and tolerogenic dendritic cells. *Nature Communications*, *13*(1), 5184. https://doi.org/10.1038/s41467-022-32849-1

Ade, N., Antonios, D., Kerdine-Romer, S., Boisleve, F., Rousset, F., & Pallardy, M. (2007). NF-kappaB plays a major role in the maturation of human dendritic cells induced by NiSO(4) but not by DNCB. *Toxicological Sciences*, *99*(2), 488–501. https://doi.org/10.1093/toxsci/kfm178

Adler, A. S., Sinha, S., Kawahara, T. L., Zhang, J. Y., Segal, E., & Chang, H. Y. (2007). Motif module map reveals enforcement of aging by continual NF-kappaB activity. *Genes & Development*, *21*(24), 3244–3257. https://doi.org/10.1101/gad.1588507

Agrawal, A., Agrawal, S., Cao, J. N., Su, H., Osann, K., & Gupta, S. (2007). Altered innate immune functioning of dendritic cells in elderly humans: A role of phosphoinositide 3-kinase-signaling pathway. *Journal of Immunology*, *178*(11), 6912–6922. https://doi.org/10.4049/jimmunol.178.11.6912

Agrawal, A., Agrawal, S., & Gupta, S. (2017). Role of dendritic cells in inflammation and loss of tolerance in the elderly. *Frontiers in Immunology*, *8*, 896. https://doi.org/10.3389/fimmu.2017.00896

Agrawal, A., & Gupta, S. (2011). Impact of aging on dendritic cell functions in humans. *Ageing Research Reviews*, *10*(3), 336–345. https://doi.org/10.1016/j.arr.2010.06.004

Anderson, A. C., Joller, N., & Kuchroo, V. K. (2016). Lag-3, Tim-3, and TIGIT: Co-inhibitory receptors with specialized functions in immune regulation. *Immunity*, *44*(5), 989–1004. https://doi.org/10.1016/j.immuni.2016.05.001

Banchereau, J., & Steinman, R. M. (1998). Dendritic cells and the control of immunity. *Nature*, *392*(6673), 245–252. https://doi.org/10.1038/32588

Barnabei, L., Laplantine, E., Mbongo, W., Rieux-Laucat, F., & Weil, R. (2021). NF-kappaB: At the Borders of autoimmunity and inflammation. *Frontiers in Immunology*, *12*, 716469. https://doi.org/10.3389/fimmu.2021.716469

Belkaid, Y., & Hand, T. W. (2014). Role of the microbiota in immunity and inflammation. *Cell*, *157*(1), 121–141. https://doi.org/10.1016/j.cell.2014.03.011

Bermudez-Brito, M., Borghuis, T., Daniel, C., Pot, B., de Haan, B. J., Faas, M. M., & de Vos, P. (2018). *L. plantarum* WCFS1 enhances Treg frequencies by activating DCs even in absence of sampling of bacteria in the Peyer patches. *Scientific Reports*, *8*(1), 1785. https://doi.org/10.1038/s41598-018-20243-1

Bitzer, M., von Gersdorff, G., Liang, D., Dominguez-Rosales, A., Beg, A. A., Rojkind, M., & Bottinger, E. P. (2000). A mechanism of suppression of TGF-beta/SMAD signaling by NF-kappa B/RelA. *Genes & Development*, *14*(2), 187–197.

Bosco, N., & Noti, M. (2021). The aging gut microbiome and its impact on host immunity. *Genes and Immunity*, *22*(5–6), 289–303. https://doi.org/10.1038/s41435-021-00126-8

Carreno, L. J., Riedel, C. A., & Kalergis, A. M. (2011). Induction of tolerogenic dendritic cells by NF-kappaB blockade and Fcgamma receptor modulation. *Methods in Molecular Biology*, *677*, 339–353. https://doi.org/10.1007/978-1-60761-869-0_22

Cho, S. J., Moon, J. S., Lee, C. M., Choi, A. M., & Stout-Delgado, H. W. (2017). Glucose transporter 1-dependent glycolysis is increased during aging-related lung fibrosis, and phloretin inhibits lung fibrosis. *American Journal of Respiratory Cell and Molecular Biology*, *56*(4), 521–531. https://doi.org/10.1165/rcmb.2016-0225OC

Coquerelle, C., & Moser, M. (2010). DC subsets in positive and negative regulation of immunity. *Immunological Reviews*, *234*(1), 317–334. https://doi.org/10.1111/j.0105-2896.2009.00887.x

de Heusch, M., Oldenhove, G., Urbain, J., Thielemans, K., Maliszewski, C., Leo, O., & Moser, M. (2004). Depending on their maturation state, splenic dendritic cells induce the differentiation of CD4(+) T lymphocytes into memory and/or effector cells in vivo. *European Journal of Immunology*, *34*(7), 1861–1869. https://doi.org/10.1002/eji.200424878

Domogalla, M. P., Rostan, P. V., Raker, V. K., & Steinbrink, K. (2017). Tolerance through education: How tolerogenic dendritic cells shape immunity. *Frontiers in Immunology*, *8*, 1764. https://doi.org/10.3389/fimmu.2017.01764

Esmaeili, S. A., Mahmoudi, M., Rezaieyazdi, Z., Sahebari, M., Tabasi, N., Sahebkar, A., & Rastin, M. (2018). Generation of tolerogenic dendritic cells using *Lactobacillus rhamnosus* and *Lactobacillus delbrueckii* as tolerogenic probiotics. *Journal of Cellular Biochemistry*, *119*(9), 7865–7872. https://doi.org/10.1002/jcb.27203

Fallarino, F., Grohmann, U., You, S., McGrath, B. C., Cavener, D. R., Vacca, C., Orabona, C., Bianchi, R., Belladonna, M. L., Volpi, C., Santamaria, P., Fioretti, M. C., & Puccetti, P. (2006). The combined effects of tryptophan starvation and tryptophan catabolites down-regulate T cell receptor zeta-chain and induce a regulatory phenotype in naive T cells. *Journal of Immunology*, *176*(11), 6752–6761. https://doi.org/10.4049/jimmunol.176.11.6752

Ferreira Dos Santos, T., Alves Melo, T., Almeida, M. E., Passos Rezende, R., & Romano, C. C. (2016). Immunomodulatory effects of *Lactobacillus plantarum* Lp62 on intestinal epithelial and mononuclear cells. *BioMed Research International*, *2016*, 8404156. https://doi.org/10.1155/2016/8404156

Flores, R. R., Clauson, C. L., Cho, J., Lee, B. C., McGowan, S. J., Baker, D. J., Niedernhofer, L. J., & Robbins, P. D. (2017). Expansion of myeloid-derived suppressor cells with aging in the bone marrow of mice through a NF-kappaB-dependent mechanism. *Aging Cell*, *16*(3), 480–487. https://doi.org/10.1111/acel.12571

Funeshima, N., Fujino, M., Kitazawa, Y., Hara, Y., Hara, Y., Hayakawa, K., Okuyama, T., Kimura, H., & Li, X. K. (2005). Inhibition of allogeneic T-cell responses by dendritic cells expressing transduced indoleamine 2,3-dioxygenase. *The Journal of Gene Medicine*, *7*(5), 565–575. https://doi.org/10.1002/jgm.698

Furuta, G. T., Turner, J. R., Taylor, C. T., Hershberg, R. M., Comerford, K., Narravula, S., Podolsky, D. K., & Colgan, S. P. (2001). Hypoxia-inducible factor 1-dependent induction of intestinal trefoil factor protects barrier function during hypoxia. *The Journal of Experimental Medicine*, *193*(9), 1027–1034. https://doi.org/10.1084/jem.193.9.1027

Geiger, H., de Haan, G., & Florian, M. C. (2013). The ageing haematopoietic stem cell compartment. *Nature Reviews. Immunology*, *13*(5), 376–389. https://doi.org/10.1038/nri3433

Grohmann, U., Fallarino, F., & Puccetti, P. (2003). Tolerance, DCs and tryptophan: Much ado about IDO. *Trends in Immunology*, *24*(5), 242–248. https://doi.org/10.1016/s1471-4906(03)00072-3

Hackstein, H., & Thomson, A. W. (2004). Dendritic cells: Emerging pharmacological targets of immunosuppressive drugs. *Nature Reviews. Immunology*, *4*(1), 24–34. https://doi.org/10.1038/nri1256

Hadeiba, H., Sato, T., Habtezion, A., Oderup, C., Pan, J., & Butcher, E. C. (2008). CCR9 expression defines tolerogenic plasmacytoid dendritic cells able to suppress acute graft-versus-host disease. *Nature Immunology*, *9*(11), 1253–1260. https://doi.org/10.1038/ni.1658

Hasegawa, H., & Matsumoto, T. (2018). Mechanisms of tolerance induction by dendritic cells In vivo. *Frontiers in Immunology*, *9*, 350. https://doi.org/10.3389/fimmu.2018.00350

Hawiger, D., Inaba, K., Dorsett, Y., Guo, M., Mahnke, K., Rivera, M., Ravetch, J. V., Steinman, R. M., & Nussenzweig, M. C. (2001). Dendritic cells induce peripheral T cell unresponsiveness under steady state conditions in vivo. *The Journal of Experimental Medicine*, *194*(6), 769–779. https://doi.org/10.1084/jem.194.6.769

Honda, K., & Littman, D. R. (2016). The microbiota in adaptive immune homeostasis and disease. *Nature*, *535*(7610), 75–84. https://doi.org/10.1038/nature18848

Horton, C., Shanmugarajah, K., & Fairchild, P. J. (2017). Harnessing the properties of dendritic cells in the pursuit of immunological tolerance. *Biomed Journal*, *40*(2), 80–93. https://doi.org/10.1016/j.bj.2017.01.002

Hughes, J. B., Hellmann, J. J., Ricketts, T. H., & Bohannan, B. J. (2001). Counting the uncountable: Statistical approaches to estimating microbial diversity. *Applied and Environmental Microbiology*, *67*(10), 4399–4406. https://doi.org/10.1128/AEM.67.10.4399-4406.2001

Iberg, C. A., & Hawiger, D. (2020). Natural and induced tolerogenic dendritic cells. *Journal of Immunology*, *204*(4), 733–744. https://doi.org/10.4049/jimmunol.1901121

Josefsdottir, K. S., Baldridge, M. T., Kadmon, C. S., & King, K. Y. (2017). Antibiotics impair murine hematopoiesis by depleting the intestinal microbiota. *Blood*, *129*(6), 729–739. https://doi.org/10.1182/blood-2016-03-708594

Kemgang, T. S., Kapila, S., Shanmugam, V. P., & Kapila, R. (2014). Cross-talk between probiotic lactobacilli and host immune system. *Journal of Applied Microbiology*, *117*(2), 303–319. https://doi.org/10.1111/jam.12521

Kim, C., Fang, F., Weyand, C. M., & Goronzy, J. J. (2017). The life cycle of a T cell after vaccination – where does immune ageing strike? *Clinical and Experimental Immunology*, *187*(1), 71–81. https://doi.org/10.1111/cei.12829

Klindworth, A., Pruesse, E., Schweer, T., Peplies, J., Quast, C., Horn, M., & Glockner, F. O. (2013). Evaluation of general 16S ribosomal RNA gene PCR primers for classical and next-generation sequencing-based diversity studies. *Nucleic Acids Research*, *41*(1), e1. https://doi.org/10.1093/nar/gks808

Krawczyk, C. M., Holowka, T., Sun, J., Blagih, J., Amiel, E., DeBerardinis, R. J., Cross, J. R., Jung, E., Thompson, C. B., Jones, R. G., & Pearce, E. J. (2010). Toll-like receptor-induced changes in glycolytic metabolism regulate dendritic cell activation. *Blood*, *115*(23), 4742–4749. https://doi.org/10.1182/blood-2009-10-249540

Lamubol, J., Ohto, N., Kuwahara, H., & Mizuno, M. (2021). *Lactiplantibacillus plantarum* 22A-3-induced TGF-beta1 secretion from intestinal epithelial cells stimulated CD103(+) DC and Foxp3(+) Treg differentiation and amelioration of colitis in mice. *Food & Function*, *12*(17), 8044–8055. https://doi.org/10.1039/d1fo00990g

Lee, K. A., Flores, R. R., Jang, I. H., Saathoff, A., & Robbins, P. D. (2022). Immune senescence, immunosenescence and aging. *Frontiers in Aging*, *3*, 900028. https://doi.org/10.3389/fragi.2022.900028

Li, K., Yang, M., Tian, M., Jia, L., du, J., Wu, Y., Li, L., Yuan, L., & Ma, Y. (2022). *Lactobacillus plantarum* 17-5 attenuates Escherichia coli-induced inflammatory responses via inhibiting the activation of the NF-kappaB and MAPK signalling pathways in bovine mammary epithelial cells. *BMC Veterinary Research*, *18*(1), 250–259. https://doi.org/10.1186/s12917-022-03355-9

Li, S., Zhang, M., Xiang, F., Zhao, J., Jiang, C., & Zhu, J. (2011). Dendritic cells expressing BTLA induces CD8+ T cell tolerance and attenuates the severity of diabetes. *Vaccine*, *29*(44), 7747–7751. https://doi.org/10.1016/j.vaccine.2011.07.125

Lutz, M. B., Kukutsch, N., Ogilvie, A. L., Rossner, S., Koch, F., Romani, N., & Schuler, G. (1999). An advanced culture method for generating large quantities of highly pure dendritic cells from mouse bone marrow. *Journal of Immunological Methods*, *223*(1), 77–92. https://doi.org/10.1016/s0022-1759(98)00204-x

Macho Fernandez, E., Valenti, V., Rockel, C., Hermann, C., Pot, B., Boneca, I. G., & Grangette, C. (2011). Anti-inflammatory capacity of selected lactobacilli in experimental colitis is driven by NOD2-mediated recognition of a specific peptidoglycan-derived muropeptide. *Gut*, *60*(8), 1050–1059. https://doi.org/10.1136/gut.2010.232918

Marwah, V. S., Scala, G., Kinaret, P. A. S., Serra, A., Alenius, H., Fortino, V., & Greco, D. (2019). eUTOPIA: solUTion for omics data PreprocessIng and analysis. *Source Code for Biology and Medicine*, *14*, 1. https://doi.org/10.1186/s13029-019-0071-7

McDaniel, M. M., Kottyan, L. C., Singh, H., & Pasare, C. (2020). Suppression of inflammasome activation by IRF8 and IRF4 in cDCs is critical for T cell priming. *Cell Reports*, *31*(5), 107604. https://doi.org/10.1016/j.celrep.2020.107604

Meisel, M., Hinterleitner, R., Pacis, A., Chen, L., Earley, Z. M., Mayassi, T., Pierre, J. F., Ernest, J. D., Galipeau, H. J., Thuille, N., Bouziat, R.,

Buscarlet, M., Ringus, D. L., Wang, Y., Li, Y., Dinh, V., Kim, S. M., McDonald, B., Zurenski, M. A., … Jabri, B. (2018). Microbial signals drive pre-leukaemic myeloproliferation in a Tet2-deficient host. *Nature*, *557*(7706), 580–584. https://doi.org/10.1038/s41586-018-0125-z

Moncada, S. (1999). Nitric oxide: Discovery and impact on clinical medicine. *Journal of the Royal Society of Medicine*, *92*(4), 164–169. https://doi.org/10.1177/014107689909200402

Mondanelli, G., Bianchi, R., Pallotta, M. T., Orabona, C., Albini, E., Iacono, A., Belladonna, M. L., Vacca, C., Fallarino, F., Macchiarulo, A., Ugel, S., Bronte, V., Gevi, F., Zolla, L., Verhaar, A., Peppelenbosch, M., Mazza, E. M. C., Bicciato, S., Laouar, Y., … Grohmann, U. (2017). A relay pathway between arginine and tryptophan metabolism confers immunosuppressive properties on dendritic cells. *Immunity*, *46*(2), 233–244. https://doi.org/10.1016/j.immuni.2017.01.005

Oh, S. A., Wu, D. C., Cheung, J., Navarro, A., Xiong, H., Cubas, R., Totpal, K., Chiu, H., Wu, Y., Comps-Agrar, L., Leader, A. M., Merad, M., Roose-Germa, M., Warming, S., Yan, M., Kim, J. M., Rutz, S., & Mellman, I. (2020). PD-L1 expression by dendritic cells is a key regulator of T-cell immunity in cancer. *Nature Cancer*, *1*(7), 681–691. https://doi.org/10.1038/s43018-020-0075-x

Ohl, L., Mohaupt, M., Czeloth, N., Hintzen, G., Kiafard, Z., Zwirner, J., Blankenstein, T., Henning, G., & Förster, R. (2004). CCR7 governs skin dendritic cell migration under inflammatory and steady-state conditions. *Immunity*, *21*(2), 279–288. https://doi.org/10.1016/j.immuni.2004.06.014

Pahari, S., Khan, N., Aqdas, M., Negi, S., Kaur, J., & Agrewala, J. N. (2016). Infergen stimulated macrophages restrict mycobacterium tuberculosis growth by autophagy and release of nitric oxide. *Scientific Reports*, *6*, 39492. https://doi.org/10.1038/srep39492

Panfili, E., Mondanelli, G., Orabona, C., Bianchi, R., Gargaro, M., Fallarino, F., Puccetti, P., Grohmann, U., Volpi, C., & Belladonna, M. L. (2019). IL-35Ig-expressing dendritic cells induce tolerance via arginase 1. *Journal of Cellular and Molecular Medicine*, *23*(5), 3757–3761. https://doi.org/10.1111/jcmm.14215

Pathak, M., Padghan, P., Halder, N., Shilpi, K. N., Sonar, S. A., & Lal, G. (2020). CCR9 signaling in dendritic cells drives the differentiation of Foxp3(+) Tregs and suppresses the allergic IgE response in the gut. *European Journal of Immunology*, *50*(3), 404–417. https://doi.org/10.1002/eji.201948327

Peche, H., Trinite, B., Martinet, B., & Cuturi, M. C. (2005). Prolongation of heart allograft survival by immature dendritic cells generated from recipient type bone marrow progenitors. *American Journal of Transplantation*, *5*(2), 255–267. https://doi.org/10.1111/j.1600-6143.2004.00683.x

Ragonnaud, E., & Biragyn, A. (2021). Gut microbiota as the key controllers of "healthy" aging of elderly people. *Immunity & Ageing*, *18*(1), 2. https://doi.org/10.1186/s12979-020-00213-w

Raker, V. K., Domogalla, M. P., & Steinbrink, K. (2015). Tolerogenic dendritic cells for regulatory T cell induction in man. *Frontiers in Immunology*, *6*, 569. https://doi.org/10.3389/fimmu.2015.00569

Savill, J., Dransfield, I., Gregory, C., & Haslett, C. (2002). A blast from the past: Clearance of apoptotic cells regulates immune responses. *Nature Reviews. Immunology*, *2*(12), 965–975. https://doi.org/10.1038/nri957

Seitz, C. S., Deng, H., Hinata, K., Lin, Q., & Khavari, P. A. (2000). Nuclear factor kappaB subunits induce epithelial cell growth arrest. *Cancer Research*, *60*(15), 4085–4092.

Si, C., Zhang, R., Wu, T., Lu, G., Hu, Y., Zhang, H., Xu, F., Wei, P., Chen, K., Tang, H., Yeretssian, G., & Xiong, H. (2016). Dendritic cell-derived nitric oxide inhibits the differentiation of effector dendritic cells. *Oncotarget*, *7*(46), 74834–74845. https://doi.org/10.18632/oncotarget.11361

Sim, W. J., Ahl, P. J., & Connolly, J. E. (2016). Metabolism is central to tolerogenic dendritic cell function. *Mediators of Inflammation*, *2016*, 2636701–2636710. https://doi.org/10.1155/2016/2636701

Steinman, R. M., Hawiger, D., & Nussenzweig, M. C. (2003). Tolerogenic dendritic cells. *Annual Review of Immunology*, *21*, 685–711. https://doi.org/10.1146/annurev.immunol.21.120601.141040

Thevaranjan, N., Puchta, A., Schulz, C., Naidoo, A., Szamosi, J. C., Verschoor, C. P., Loukov, D., Schenck, L. P., Jury, J., Foley, K. P., Schertzer, J. D., Larché, M. J., Davidson, D. J., Verdú, E. F., Surette, M. G., & Bowdish, D. M. E. (2017). Age-associated microbial dysbiosis promotes intestinal permeability, systemic inflammation, and macrophage dysfunction. *Cell Host & Microbe*, *21*(4), 455–466 e454. https://doi.org/10.1016/j.chom.2017.03.002

Trombetta, E. S., & Mellman, I. (2005). Cell biology of antigen processing in vitro and in vivo. *Annual Review of Immunology*, *23*, 975–1028. https://doi.org/10.1146/annurev.immunol.22.012703.104538

Uribe-Herranz, M., Rafail, S., Beghi, S., Gil-de-Gómez, L., Verginadis, I., Bittinger, K., Pustylnikov, S., Pierini, S., Perales-Linares, R., Blair, I. A., Mesaros, C. A., Snyder, N. W., Bushman, F., Koumenis, C., & Facciabene, A. (2020). Gut microbiota modulate dendritic cell antigen presentation and radiotherapy-induced antitumor immune response. *The Journal of Clinical Investigation*, *130*(1), 466–479. https://doi.org/10.1172/JCI124332

van Baarlen, P., Troost, F. J., van Hemert, S., van der Meer, C., de Vos, W. M., de Groot, P. J., Hooiveld, G. J., Brummer, R. J., & Kleerebezem, M. (2009). Differential NF-kappaB pathways induction by *Lactobacillus plantarum* in the duodenum of healthy humans correlating with immune tolerance. *Proceedings of the National Academy of Sciences of the United States of America*, *106*(7), 2371–2376. https://doi.org/10.1073/pnas.0809919106

Vander Lugt, B., Riddell, J., Khan, A. A., Hackney, J. A., Lesch, J., DeVoss, J., Weirauch, M. T., Singh, H., & Mellman, I. (2017). Transcriptional determinants of tolerogenic and immunogenic states during dendritic cell maturation. *The Journal of Cell Biology*, *216*(3), 779–792. https://doi.org/10.1083/jcb.201512012

Verinaud, L., Issayama, L. K., Zanucoli, F., de Carvalho, A. C., da Costa, T. A., di Gangi, R., Bonfanti, A. P., Ferreira, I. T., de Oliveira, A. L., Machado, D. R., & Thomé, R. (2015). Nitric oxide plays a key role in the suppressive activity of tolerogenic dendritic cells. *Cellular & Molecular Immunology*, *12*(3), 384–386. https://doi.org/10.1038/cmi.2014.94

Vogel, A., Martin, K., Soukup, K., Halfmann, A., Kerndl, M., Brunner, J. S., Hofmann, M., Oberbichler, L., Korosec, A., Kuttke, M., Datler, H., Kieler, M., Musiejovsky, L., Dohnal, A., Sharif, O., & Schabbauer, G. (2022). JAK1 signaling in dendritic cells promotes peripheral tolerance in autoimmunity through PD-L1-mediated regulatory T cell induction. *Cell Reports*, *38*(8), 110420. https://doi.org/10.1016/j.celrep.2022.110420

Wakkach, A., Fournier, N., Brun, V., Breittmayer, J. P., Cottrez, F., & Groux, H. (2003). Characterization of dendritic cells that induce tolerance and T regulatory 1 cell differentiation in vivo. *Immunity*, *18*(5), 605–617. https://doi.org/10.1016/s1074-7613(03)00113-4

Wu, X., & Li, L. (2012). Rosiglitazone suppresses lipopolysaccharide-induced matrix metalloproteinase-2 activity in rat aortic endothelial cells via Ras-MEK1/2 signaling. *International Journal of Cardiology*, *158*(1), 54–58. https://doi.org/10.1016/j.ijcard.2010.12.105

Yu, P., Ke, C., Guo, J., Zhang, X., & Li, B. (2020). *Lactobacillus plantarum* L15 alleviates colitis by inhibiting LPS-mediated NF-kappaB activation and ameliorates DSS-induced gut microbiota dysbiosis. *Frontiers in Immunology*, *11*, 575173. https://doi.org/10.3389/fimmu.2020.575173

Zheng, D., Liwinski, T., & Elinav, E. (2020). Interaction between microbiota and immunity in health and disease. *Cell Research*, *30*(6), 492–506. https://doi.org/10.1038/s41422-020-0332-7

Zheng, Y., Fang, Z., Xue, Y., Zhang, J., Zhu, J., Gao, R., Yao, S., Ye, Y., Wang, S., Lin, C., Chen, S., Huang, H., Hu, L., Jiang, G. N., Qin, H., Zhang, P., Chen, J., & Ji, H. (2020). Specific gut microbiome signature predicts the early-stage lung cancer. *Gut Microbes*, *11*(4), 1030–1042. https://doi.org/10.1080/19490976.2020.1737487

Zhong, M., Zhong, C., Cui, W., Wang, G., Zheng, G., Li, L., Zhang, J., Ren, R., Gao, H., Wang, T., Li, X., Che, J., & Gohda, E. (2019). Induction of tolerogenic dendritic cells by activated TGF-beta/Akt/Smad2 signaling in RIG-I-deficient stemness-high human liver cancer cells. *BMC Cancer*, *19*(1), 439. https://doi.org/10.1186/s12885-019-5670-9

Zhu, B., Buttrick, T., Bassil, R., Zhu, C., Olah, M., Wu, C., Xiao, S., Orent, W., Elyaman, W., & Khoury, S. J. (2013). IL-4 and retinoic acid synergistically induce regulatory dendritic cells expressing Aldh1a2. *Journal of Immunology*, *191*(6), 3139–3151. https://doi.org/10.4049/jimmunol.1300329

SUPPORTING INFORMATION

Additional supporting information can be found online in the Supporting Information section at the end of this article.

How to cite this article: Bashir, H., Singh, S., Singh, R. P., Agrewala, J. N., & Kumar, R. (2023). Age-mediated gut microbiota dysbiosis promotes the loss of dendritic cells tolerance. *Aging Cell*, *22*, e013838. https://doi.org/10.1111/acel.13838

Cellular and Molecular Life Sciences (2022) 79:567
https://doi.org/10.1007/s00018-022-04596-5

ORIGINAL ARTICLE

Mycobacterium tuberculosis exploits MPT64 to generate myeloid-derived suppressor cells to evade the immune system

Sanpreet Singh[1] · Sudeep K. Maurya[1] · Mohammad Aqdas[1] · Hilal Bashir[1] · Ashish Arora[3] · Vijayender Bhalla[1,4] · Javed N. Agrewala[1,2]

Received: 30 June 2022 / Revised: 19 September 2022 / Accepted: 9 October 2022

Abstract

Mycobacterium tuberculosis (Mtb) is a smart and successful pathogen since it can persist in the intimidating environment of the host by taming and tuning the immune system. *Mtb* releases MPT64 (Rv1980c) protein in high amounts in patients with active tuberculosis (TB). Consequently, we were curious to decipher the role of MPT64 on the differentiating dendritic cells (DCs) and its relation to evading the immune system. We observed that pre-exposure of differentiating DCs to MPT64 (DC^{MPT64}) transformed them into a phenotype of myeloid-derived suppressor cells (MDSCs). DC^{MPT64} expressed a high level of immunosuppressive molecules PD-L1, TIM-3, nitric oxide (NO), arginase 1, IDO-1, IL-10 and TGF-β, but inhibited the production of pro-inflammatory cytokines TNF-α, IL-6 and IL-12. DC^{MPT64} chemotaxis function was diminished due to the reduced expression of CCR7. DC^{MPT64} promoted the generation of regulatory T cells (Tregs) but inhibited the differentiation of Th1 cells and Th17 cells. Further, high lipid and methylglyoxal content, and reduced glucose consumption by DC^{MPT64}, rendered them metabolically quiescent and consequently, reduced DC^{MPT64} ability to phagocytose *Mtb* and provided a safer shelter for the intracellular survival of the mycobacterium. The mechanism identified in impairing the function of DC^{MPT64} was through the increased production and accumulation of methylglyoxal. Hence, for the first time, we demonstrate the novel role of MPT64 in promoting the generation of MDSCs to favor *Mtb* survival and escape its destruction by the immune system.

Keywords *Mtb* · Dendritic cells · MDSCs · Tregs

Introduction

Mycobacterium tuberculosis (*Mtb)* persists skillfully by deceiving the host immune system. It adopts multiple contrivances, viz., disrupts the fusion of phagosome-lysosome [1], neutralizes the function of reactive nitrogen and oxygen-free radicals [2], induces necrosis of macrophages [3, 4], impairs the antigen processing and presentation [5, 6], hampers apoptosis of infected cells [7], inhibits autophagy and lysosomal functions [8] and impedes the production of interferons [9]. Suggesting that the pathogen is not only utilized by the host to generate protective immunity, but the bacterium too successfully subjugates the host immune system [10, 11].

The *Mtb* uses its proteins, like Acr1, to successfully inhibit the maturation of DCs [12, 13]; DCs exposed to ManLAM failed to fully mature and showed a decline in the level of MHCI and MHCII, CD83, CD86 and CCR7 [14], and LprA, LprG and LpgH too downregulates the MHCII expression [15–17]. Further, an encounter of DCs with *Mtb* secretory Ag (MTSA) during differentiation promotes the survival of the intracellular bacterium by inhibiting the production of ROS [18]. Moreover, ESAT-6 has been reported to inhibit the phagolysosome fusion [19]. Similarly, PtpA and SapM proteins inhibit phagosome maturation. PtpA suppresses the acidification of phagosomes [20] and Ndk interacts with the Rac1 protein of host cells and prevents the

✉ Javed N. Agrewala
jagrewala@gmail.com

1 Immunology Laboratory, CSIR-Institute of Microbial Technology, Chandigarh 160036, India

2 Immunology Laboratory, Department of Biomedical Engineering, Indian Institute of Technology Ropar, Rupnagar 140001, India

3 Department of Biochemistry and Structural Biology, CSIR-Central Drug Research Institute, Lucknow 226031, India

4 Biosensor Laboratory, CSIR-Institute of Microbial Technology, Chandigarh, India

Published online: 25 October 2022

assembly of the NOX2 [21]. Many proteins, such as PknE (protein kinaseE), Ndk, nuoG, SecA2 and PtpA, have been reported to induce necrosis and apoptosis of infected host cells [7, 22, 23]. Furthermore, *Mtb* elicits the generation of MDSCs that fail to activate T cells [24]. Along with Tregs, MDSCs presence is reported in TB granulomas to suppress effector T cell function and therefore promote the progression of the disease [24]. MDSCs utilize nitric oxide (NO), arginase 1 and methylglyoxal (MGO) with other constituents that cause nitrosylation of T cell receptors, apoptosis of T cells and induction of Tregs [25–27]. The vast detrimental effect of MDSCs is mediated by the strong suppression of Th1 and Th17 immunity along with a decline in the secretion of innate cytokines [28]. Consequently, it becomes crucial to decode the function of unexplored proteins exploited by *Mtb* to support the generation of MDSCs to escape the immune system.

MPT64 is a secretory protein (m.wt. ~ 24 kDa) and is less studied for its immunomodulatory role [29]. It belongs to a new family of beta grasp proteins [30]. The level of MPT64 is high in the serum and sputum of active TB patients [31]. Moreover, MPT64 enhances the secretion of IL-1β, IL-6, TNF-α and IL-10 by the macrophages, and therefore may be responsible for suppressing the immune system [32]. Recently, it has been shown that MPT64 inhibits the apoptosis of macrophages through upregulation of bcl-2 and increases the survival of *Mtb* [33]. Further, the MPT64 mutant strain (Mtb*Δmpt64*) generates less bacterial burden in mice, as compared to wildtype *Mtb* [34].

Keeping in view the aforesaid facts, we have tried to delineate here the immunomodulatory role of MPT64 on the activation and differentiation of DCs. Interestingly, we observed that the early encounter of DCs with MPT64 (DC^{MPT64}) during their differentiation skewed them towards a myeloid suppressor cell phenotype. The DC^{MPT64} showed the accumulation of methylglyoxal, an advanced glycation end product, which along with other soluble mediators is implicated in suppressing the host immune system. DC^{MPT64} preferably generated Tregs and suppressed the activation of Th1 cells and Th17 cells. The DC^{MPT64} demonstrated decreased tendency to phagocytose and kill *Mtb*. Consequently, it may be concluded from the study that *Mtb* utilizes MPT64 to make DC^{MPT64} a safe shelter for its persistence, and this may be one of the mechanisms adopted by the mycobacterium to escape the host immune system.

Materials and methods

Dendritic cell culture

Bone marrow cells (BMCs) were isolated from the femur and tibiae of C57BL/6 mice and were differentiated into DCs, as mentioned elsewhere [35]. Briefly, the BMCs were treated with ACK lysis buffer (0.15 M NH_4Cl, 10 mM $KHCO_3$, and 88 mM Na_2EDTA) to lyse RBCs. BMCs (2×10^6) were cultured in 24-well plates in complete medium [RPMI-1640 + FCS-10% supplemented with penicillin (100 U/ml), L-glutamine (100 mM), streptomycin (100 mg/ml)] and GM-CSF (2 ng/ml) and IL-4 (4 ng/ml). The cultures were kept for 7d in a humidified CO_2 (5%) incubator at 37 °C. The medium was replenished after 3 d. Abbreviations used in this text: DCs: BMCs cultured with GM-CSF + IL-4; DC^{MPT64}, DC^{CFP-10} and DC^{ESAT-6}: BMCs cultured with GM-CSF + IL-4 along with MPT64, CFP-10 and ESAT-6, respectively.

Arginase activity assay

Arginase was estimated through arginase activity assay. DCs and DC^{MPT64} (5×10^5) were cultured in 48-well plates for 6 d in RPMI-1640 + FCS-10%. The cells were isolated on the 7th day and washed with 1X PBS, and water (100 µl) containing Triton X-100 (0.1%) and protease inhibitor was added and incubated at 37 °C for 30 min. Later, Tris–HCL (100 µl, 25 mM), $MnCl_2$ (333 µM) and pH 7.5 were added followed by heating the reaction mixture at 56 °C for 10 min to activate the enzyme. Later, L-arginine (200 µl, 0.5, mol/L, pH 9.7) was added as an arginase substrate and heated the mixture for 30 min at 37 °C. The reaction was stopped with an acid solution (400 µl, H_2SO_4:H_3PO_4:H_2O; 1:3:7). Finally, α-isonitrosopropiophenone (50 µl, 9% ethanol) was added to the reaction mixture for colorimetric detection of urea, followed by heating the mixture for 45 min at 56 °C. Finally, the reaction mixture was kept in dark at RT for 10 min. The urea formed was calorimetrically determined by taking absorbance at 540 nm [36, 37].

Expression of surface markers by flow cytometer

DCs, DC^{MPT64} and DC^{CFP-10} (5×10^5) were cultured in a complete medium for 6 d. Cells were harvested on the 7th day and surface stained with fluorochrome-labelled Abs to CD11c, CD11b, F4/80, Ly6c, Ly6G, CCR7, Fox-P3, CD25, CD4, CD8, TCRβ and TCRγ/δ. Cells were acquired through flow cytometry and expression was monitored through BD DIVA software.

In vivo cell migration assay

DCs, DC^{MPT64} and DC^{CFP-10} (2×10^6) were cultured in 6-well plates complete medium for 6 d. Next, the cells were re-suspended in CFSE (1 ml, 2 µM) and incubated for 8 min at 37 °C. Later, FBS (2 ml) was added and cultures were centrifuged at 2000 rpm at RT for 3 min. The cell pellet was washed 2× with PBS-1X + FBS-20%. The CFSE-labelled

cells were intravenously injected into C57BL/6 mice. After 24 h and 48 h, the animals were sacrificed and splenocytes were monitored for the presence of CFSE-labelled DCs by flow cytometer. Results were analyzed through BD DIVA software and represented in terms of fold-change migration. Later, the expression of CCR7 was monitored on these cells through flow cytometry.

Soluble antigen uptake assay

DCs and DC^{MPT64} (2×10^5) were cultured in 24-well plates for 6 d in complete media at 37 °C/5% CO_2. Later, cells were pulsed with FITC-dextran (100 µg/ml) and monitored for 30 min/37 °C. The cells were washed 4 × with PBS-1X-BSA-1%. Finally, cells were acquired through a flow cytometer and analyzed for dextran-FITC uptake through BD DIVA software.

Mycobacterial uptake and intracellular survival

DCs and DC^{MPT64} (5×10^5) were cultured in 24-well plate for 6 d in complete media. On the 7th day cells were washed with PBS-1X and infected with *Mtb* strains H37Ra (GFP-*Mtb*) or H37Rv for 4 h (3 h for *M. smegmatis*) at MOI of 1:5 in antibiotic-free RPMI-1640 media. Extensive washings with PBS-1X were given to the cells. Later, to kill the extracellular bacilli, amikacin (2 µg/ml) (for H37Rv) and gentamycin (50 µg/ml) (for H37Ra and *M. smegmatis*) were added to antibiotic-free RPMI-1640 media into cell cultures for 1 h at 37 °C. Then, cells were extensively washed with PBS-1X. To monitor the uptake after 4 h of *Mtb* (GFP-H37Ra, H37Rv, *M. smegmatis*) infection, cells were lysed with saponin (0.1%) and lysates (100 µl) were plated on 7H11 plates. Further, to monitor the survival of *Mtb* (H37Rv) within DCs and DC^{MPT64}, infected cells were rested for 72 h at 37 °C in 5% CO_2. The cells were lysed with saponin (0.1%) and lysates (100 µl) were plated in 7H11 plates. Bacterial growth was enumerated after 21 d by colony-forming units (CFUs).

Isolation of CD4 T cells and CD8 T cells

CD4 T cells and CD8 T cells were isolated from mouse spleen and lymph nodes by magnetic-activated cell sorting (MACS) through negative selection, as per the manufacturer's instruction (BD Biosciences, San Diego, CA). Briefly, splenocytes were isolated from C57BL/6 and BALB/c mice and were processed into a single-cell suspension. Next, CD4 T cells and CD8 T cells enrichment cocktail was added to these splenocytes. Generally, a mouse CD4 T cell enrichment cocktail (5 µl/1×10^6 cells) was added and incubated for 15 min on ice. Then, cells were centrifuged at 300 g for 7 min, and to this pellet streptavidin-magnetic beads (5 µl) were added and incubated for 30 min at 6–12 °C. Afterwards, CD4 T cells were isolated using BD IMagnet™. Similarly, CD8 T cells were isolated using CD8 T cells enrichment kit.

Syngeneic T cell proliferation

CD4 T cells and CD8 T cells were purified from the C57BL/6 mice splenocytes by MACS as per the manufacturer's instruction (BD Biosciences, San Diego, CA). CD4 T cells and CD8 T cells were re-suspended in 1 ml PBS (1X) supplemented with CFSE (2 µM) and incubated for 8 min/37 °C. Later, excess of CFSE was quenched using FCS (2 ml) and cells were washed twice with PBS-1X. T cells were co-cultured with DC^{MPT64} (ratio 10:1) in a 96-well flat bottom plate pre-coated with anti-CD3 (1 µg/ml) and anti-CD28 (0.5 µg/ml) Abs for 72 h. T cell proliferation was assessed through CFSE dye dilution assay by flow cytometry. Data were analyzed through BD DIVA software.

Allogeneic T cell proliferation

CD4 T cells and CD8 T cells were purified from the BALB/c mice splenocytes by MACS as per the manufacturer's instruction (BD Biosciences, San Diego, CA). CD4 T cells and CD8 T cells were re-suspended in 1 ml PBS (1X) supplemented with CFSE (2 µM) and incubated for 8 min/37 °C. Later, excess CFSE was quenched using FCS (2 ml) and cells were washed twice with PBS-1X. T cells (BALB/c) were co-cultured with DC^{MPT64} (C57BL/6) (ratio 10:1) (1.1×10^5 cells/well) in a 96-well flat bottom plate pre-coated with anti-CD3 (1 µg/ml) and anti-CD28 (0.5 µg/ml) Abs for 72 h. T cell proliferation was assessed through CFSE dye dilution assay by flow cytometry. Data were analyzed through BD DIVA software.

The expression of TCRβ and TCRγ/δ chains and apoptosis of T cells

Anti-CD3 and anti-CD28 stimulated naïve CD4 T cells and CD8 T cells were co-cultured with DC^{MPT64} and control DCs and DC^{CFP-10} (DC:T cell, 1:10) for 72 h/37 °C/5% CO_2. Later, the cells were stained with fluorochrome-labelled anti-TCRβ chain and TCRγ/δ chain Abs and analyzed through flow cytometry. Further, the apoptosis in T cells upon culturing with DCs, DC^{MPT64} and DC^{CFP-10} was enumerated through staining with FITC-labelled Annexin V (5 µl/tube) for 15 min in dark. After incubation, the binding buffer (400 µl) was added to these cells and analyzed immediately

by flow cytometry. Data were analyzed through BD DIVA software.

DC^{MPT64}-mediated suppression of CD4 T cells and CD8 T cells through NO secretion

The suppressive activity of DC^{MPT64} was measured through trans-well plate experiments. CFSE-labelled naïve CD4 T cells and CD8 T cells were stimulated with anti-CD3 and CD28 Abs and poured into the lower chamber of the trans-well plate. DC^{MPT64} and control DC^{CFP-10} and DCs were added into the upper chamber of the trans-well plate. Further, the same cultures were set in a normal tissue culture plate. The cells were incubated for 72 h at 37 °C/5% CO_2. Furthermore, the role of NO-mediated suppression of CD4 T cells and CD8 T cells by DC^{MPT64} was validated by treating the cultures with iNOS inhibitor (NM: N-monomethyl-L-arginine) (20 µM) for 72 h. The proliferation of T cells was measured by CFSE dye dilution assay through flow cytometry and analyzed by BD DIVA software.

Statistical analysis

Data analysis was done using '*t* test' (one- and two-tailed) and one-way analysis of variance (ANOVA) (Dunnett and Bonferroni tests) using GraphPad Prism 6 software (GraphPad Software, La Jolla, CA). The '*p* value' of less than 0.05 was considered significant.

Results

MPT64 impairs the maturation of DC^{MPT64}

Mtb uses an array of approaches to elude its destruction by modulating the host immune system. DCs are the only APCs that can activate naïve T cells. Interestingly, it has been observed that DCs upon *Mtb* infection lose their function [38]. Hence, it is crucial to comprehend how *Mtb* implicates its components to detriment the function of DCs. Therefore, we thought to decipher the influence of the exposure of MPT64 on the differentiating DCs. BMCs were cultured in the presence of GM-CSF and IL-4 with (DC^{MPT64}) or without (DCs) MPT64. The control cultures were set using CFP-10 (DC^{CFP-10}) and ESAT-6 (DC^{ESAT-6}) proteins of *Mtb*. We noted a decline in the $CD11c^+$ cells, but augmentation in the pool of $F4/80^+$ cells, in a dose-dependent manner (Fig. 1A). However, the greatest expansion of $F4/80^+$ cells and lowest percentage of $CD11c^+$ cells were observed with 12 µg/ml of MPT64. Hence, this concentration was used in all the subsequent experiments.

To validate that the decline in the frequency of $CD11c^+$ cells was not due to overgrowth and death of the cells, we checked their viability. No change in the viability of neither $CD11c^+$ cells nor $F4/80^+$ cells was noted (Supplementary Fig. 3A). We also checked the specificity of MPT64. To prove this, we used CFP-10 and ESAT-6 proteins of *Mtb*. We noticed that the increase of the $F4/80^+$ cells and decline in the $CD11c^+$ cells were solely associated with a function of MPT64 and not CFP-10 and ESAT-6 proteins (Supplementary Fig. 3B). Thus, it establishes the specificity of MPT64 in transforming the BMCs under DCs differentiating conditions (IL-4 + GM-CSF) into MDSCs.

An optimum expression of co-stimulatory and MHC molecules by the APC is decisive for the presentation of antigen and activation of T cells. Decline or absence in the expression of co-stimulatory molecules leads to T cell anergy, a state of unresponsiveness. Hence, we next evaluated the expression of these molecules on DC^{MPT64}. DC^{MPT64} increased CD40, CD80 and CD11b levels but declined MHC II expression (Fig. 1B). Further, it has been reported that DCs not only activate but also suppress the immunity [39]. Therefore, we were curious to monitor the expression of co-inhibitory molecules on DCs. We noticed that DC^{MPT64} displayed higher levels of PD-L1, TIM-3, and Ly6C, as compared to control DCs (Fig. 1C–D). Both PD-L1 and TIM-3 are known for the induction of tolerance, as well as recognized as co-inhibitory markers [40]. The cells with $Ly6C^{hi}$, $F4/80^{hi}$, $CD11b^{hi}$, $CD40^{hi}$, $CD80^{hi}$, $PD\text{-}L1^{hi}$ and $TIM\text{-}3^{hi}$ phenotypes represent monocytic MDSCs (myeloid-derived suppressor cells). It can be inferred from these findings that pre-exposure of early DCs to MPT64 during differentiation converts them to MDSCs. Recently, MDSCs have been reported to be localized within the TB granulomas along with DCs and macrophages. MDSCs are heterogeneous cell populations having different morphology and functionality.

We have used purified and endotoxin-free MPT64, CFP-10 and ESAT-6 in all the experiments (Supplementary Fig. 1A, B). The MPT64 was characterized through MASCOT, it is the same as wild-type MPT64 protein [29] (Supplementary Fig. 2). We also verified the specificity of the experiments using CFP-10 and ESAT-6 proteins of *Mtb* that were produced under the same conditions [36].

MPT64 inhibits the release of pro-inflammatory cytokines by DC^{MPT64}

DC performs a diametric role, it can activate and suppress the immune response. The cytokines secreted by DCs are very critical for *Mtb* survival [42]. Pro-inflammatory cytokines, like IL-6, IL-12, and TNF-α, inhibit the growth of *Mtb*, whereas anti-inflammatory cytokines, such as IL-10

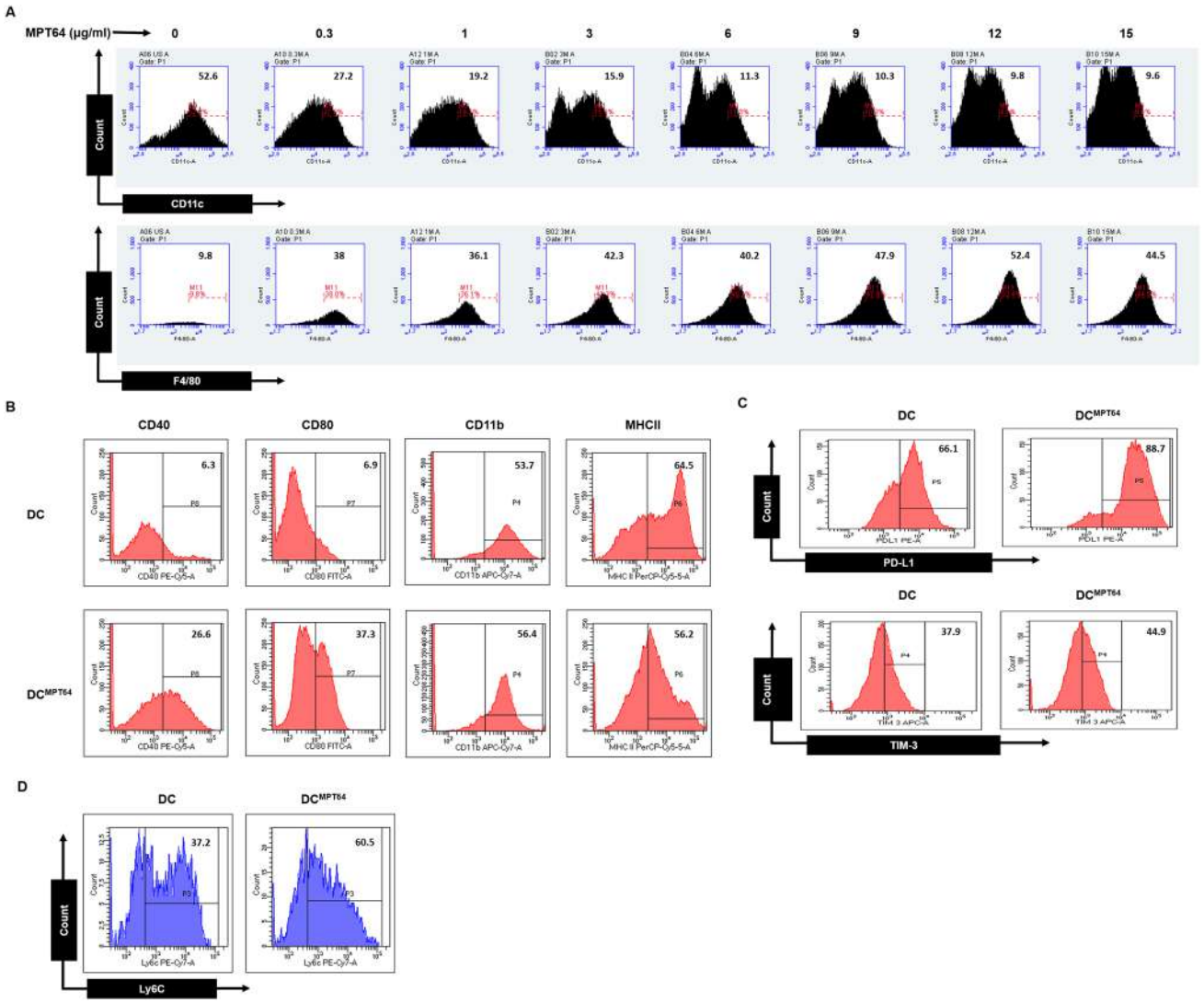

Fig. 1 MPT64 impairs the maturation of DC. Bone marrow cells (BMCs) cultured with GM-CSF + IL-4 (DCs) along with MPT64 (DC^{MPT64}) were monitored for the expression of **A** CD11c and F4/80 through flow cytometry upon exposure to various concentrations of MPT64 (0–15 µg/ml). The insets of the histogram display percentage positive cells. **B** The expression of CD40, CD80, CD11b, MHCII and **C** PD-L1 and TIM-3 was assessed through flow cytometry on DC^{MPT64} and control DCs. The values in the inset of the histogram show percentage of positive cells. **D** The expression of Ly6C on DC^{MPT64} and control DCs was monitored through flow cytometry and shown as histograms. The data are representative of 2–3 independent experiments.*$p < 0.05$, **$p < 0.01$, ***$p < 0.001$, ****$p < 0.0001$

and TGF-β, encourage the persistence of *Mtb* [43, 44]. Moreover, cytokines are the third important signal requisite for the activation of T cells. Therefore, it was imperative to examine the cytokines produced by DC^{MPT64}. DC^{MPT64} showed a significant reduction in the yield of IL-6 ($p < 0.01$), IL-12 ($p < 0.0001$) and TNF-α ($p < 0.0001$), as compared to control DCs and DC^{CFP-10} (Fig. 2A–C). In contrast, a higher level of IL-10 ($p < 0.0001$) was noted in DC^{MPT64} (Fig. 2D). These results illustrate that MPT64 restricts DCs to produce cytokines that impede *Mtb* function but promote cytokines that may help mycobacterium sustenance.

MPT64 induces morphological changes in DC^{MPT64} and obstructs their migratory function

DCs play a decisive role in activating the immune system against *Mtb* infection [45, 46]. DCs have many long arborizing projections on their surface known as dendrites, which help in capturing of antigens and interaction with T cells [47]. Activated DCs appear morphologically vivid with elongated dendrites. They robustly capture antigens for processing and presentation to T cells [48]. Hence, we wanted to monitor the change in the morphology of

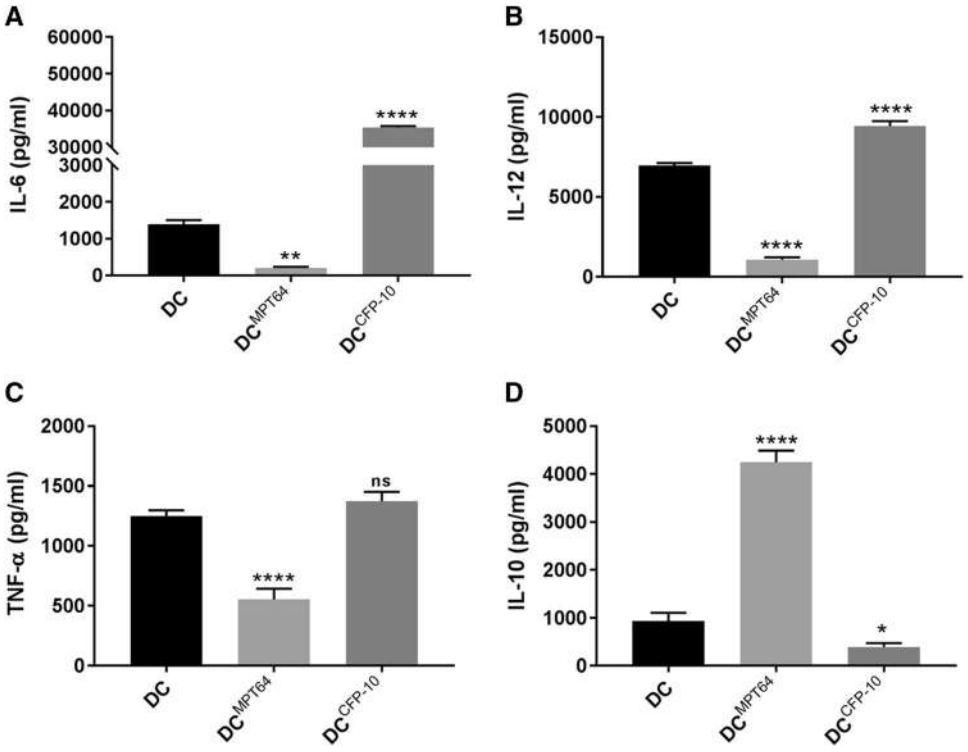

Fig. 2 Exposure of MPT64 to DC^{MPT64} during maturation impedes the secretion of pro-inflammatory cytokines IL-6, IL-12 and TNF-α but augments the release of IL-10. DC^{MPT64} and control DC^{CFP-10} and DCs were cultured for 6 days in complete medium. Later, SNs were collected for the estimation of **A** IL-6, **B** IL-12, **C** TNF-α and **D** IL-10 by ELISA. Data represented as mean ± SD are from triplicate wells ($n=3$) and 2 independent experiments. *$p<0.05$, **$p<0.01$, ***$p<0.001$, ****$p<0.0001$

MPT64-treated DCs. Surprisingly, DC^{MPT64} exhibited an absence of dendrites, as compared to control DCs (Fig. 3A). These changes were further documented by confocal microscopy (Supplementary Fig. 4A). This corroborates with our previous observations that MPT64 prompts the generation of MDSCs, as these cells have diminished morphology with less efficacy of activating adaptive immune response (Fig. 1).

Mtb conventionally infects macrophages and DCs. Lipid depots within the host cells act as an energy reservoir for the survival of *Mtb* [49]. MDSCs have high lipid content and act as a nutrient-rich niche to benefit the *Mtb* survival [50]. Further, the lipid within DCs hampers their functionality [51]. Hence, we planned to check whether lipid accumulation within DC^{MPT64} curbs their functionality. Intriguingly, we observed that DC^{MPT64} showed augmented lipid deposition, as compared to control DCs and DC^{CFP-10} by both flow cytometry and confocal microscopy (Fig. 3B and Supplementary Fig. 4B). It can be inferred from these results that *Mtb* employs its MPT64 protein to promote lipid accumulation in DC^{MPT64}, which might be responsible for their suppressive function.

Migration of antigen-captured APCs to lymphoid organs is crucial for the induction of adaptive immune response. DCs capture antigens from the site of infection and migrate to the secondary lymphoid organs to activate T cells. Such DCs express an optimum level of CCR7, a chemokine that is responsible for their chemotaxis [48]. Migration of DCs to the site of infection or lymphoid organs with captured antigen relies highly on CCR7 expression [52]. Till now, we observed that DC^{MPT64} exhibit high expression of co-inhibitory markers with less expression of MHC II markers and therefore imparts suppressive phenotype. Hence, we were eager to know, whether DC^{MPT64} have retained their migratory potential or not. Surprisingly, DC^{MPT64} exhibited a significant ($p<0.05$) reduction in the expression of CCR7 (Fig. 3C, D and Supplementary Fig. 5A). Further, to confirm this finding in vivo, we adoptively transferred CFSE-labelled DC^{MPT64} into mice. A significant drop was apparent in the migration of DC^{MPT64} but not control DCs to the spleen after 24 h ($p<0.0001$) and 48 h ($p<0.001$) of inoculation (Fig. 3E, F). Such DC^{MPT64} displayed a significantly ($p<0.01$) lower level of CCR7 (Fig. 3G, H). Our results correlate well with the findings that the deposition of high lipid content in the cells hampers their migration and functionality [51].

MPT64 abates the efficacy of DC^{MPT64} to activate and differentiate T cells

For the complete elimination of pathogens, both innate and adaptive immunity play a very important role. APCs upon recognizing pathogens activate the primary immune response through the secretion of antibodies, cytokines and other soluble mediators. Pathogen-captured DCs migrate to secondary lymphoid organs to activate pathogen-reactive T cells [53]. Inhibition of the activation of T cells has been referred to as a 'gold' standard for

considering any cell as MDSCs [54]. Since DC^{MPT64} exhibited an MDSCs-like phenotype, we were next interested to see whether DC^{MPT64} inhibit the proliferation of CD4 T cells and CD8 T cells. We co-cultured DC^{MPT64} with syngeneic CD4 T cells ($p < 0.0001$) and CD8 T cells ($p < 0.001$) and observed a significant decrease in their proliferation (Fig. 4A, B). Likewise, these results were further supported by observing a substantial decline in the proliferation of allogeneic CD4 T cells ($p < 0.05$) and CD8 T cells ($p < 0.001$) (Fig. 4C, D). These findings suggest the suppressive nature of DC^{MPT64}, as has been reported in the case of MDSCs. Therefore, DC^{MPT64} exhibit their tendency to inhibit the induction of T cell response.

The adaptive immune system plays a compelling contribution in controlling the spread of *Mtb*. Lymphocytes have a significant role in the pathogenesis and development of immunity [55]. Activation of T cells by DCs leads to the secretion of array of cytokines, such as IL-17, IFN-γ, TGF-β and IL-10. These cytokines have a robust role in the induction and differentiation of Th1 cells, Th17 cells and Treg cells. Th1 cells and Th17 cells play a central role in protecting against *Mtb* [56]. In contrast, Th2 cells and Tregs support the progression of the disease [57, 58]. We detected a reduction in IFN-γ ($p < 0.0001$) and IL-17 ($p < 0.0001$), but an increase in IL-10 ($p < 0.0001$) and TGF-β ($p < 0.0001$) when syngeneic CD4 T cells were cultured with DC^{MPT64} (Fig. 4E–H). These results were confirmed using allogeneic CD4 T cells. A reduction in IFN-γ ($p < 0.0001$) and IL-17 ($p < 0.0001$), but an increase in the IL-10 ($p < 0.0001$) and TGF-β ($p < 0.0001$), was noticed (Fig. 4I–L). Therefore, these results testify that DC^{MPT64} obstruct the differentiation of Th1 cells and Th17 cells but supports the generation of Tregs.

DC^{MPT64} induce the generation of Tregs

Tolerance of immune response has been identified in the case of diseases, like TB and cancer. Conventionally, immune system of host always maintain a balance between the generation of immune response and tolerance. DCs not only stimulate innate and adaptive immunity but also impart tolerance [39, 59]. Till now, we have noticed that DC^{MPT64} exhibit high expression of PD-L1, TIM-3 and IL-10. Both PD-L1 and TIM-3 are well known for the generation of tolerance in DCs [40, 60]. Moreover, we have shown that DC^{MPT64} have the efficacy to abate the activation and differentiation of CD4 T cells and CD8 T cells. T cells stimulated by DC^{MPT64} produced significantly higher levels of TGF-β and IL-10 (Fig. 4G, H, K, L). Therefore, we examined if DC^{MPT64} can in vivo evoke the generation of $FoxP3^+$ Tregs. Hence, OVA pulsed-DC^{MPT64} were adoptively transferred into mice twice at an interval of 7d (Fig. 5A). A significant augmentation was demonstrated in the percentage of $CD4^+$ and $CD8^+$ Tregs ($p < 0.05$) (Fig. 5B–E and Supplementary Fig. 5B, C). Our data substantiate the previous findings that MDSCs promote Tregs during TB infection [61]. These results also suggest that *Mtb* may be exploiting its MPT64 to elude the immune response by engendering Tregs.

MPT64 impairs the ability of DC^{MPT64} to phagocytose mycobacterium

DCs and macrophages are the most potent immune cells with strong phagocytic activity. DCs upon uptake of pathogen translocate MHC I or II complex on its surface with enhanced expression of co-stimulatory molecules and cytokines [48]. Surprisingly, we observed that MPT64-exposed DC^{MPT64} show less expression of MHC II. Interestingly, it has been well reported that MDSCs have less phagocytosis potential and favor the survival of the pathogen [62]. *Mtb*-infected macrophages and DCs show deterioration in engulfing antigens. To check this, we infected DC^{MPT64} with *Mtb* GFP-H37Ra, *Mtb* H37Rv and *M. smegmatis* and examined their uptake by flow cytometer (GFP-H37Ra) and CFUs (H37Rv and *M. smegmatis*). DC^{MPT64} indicated significant downregulation in phagocytosis of both the virulent (H37Rv) ($p < 0.001$) and avirulent (H37Ra) ($p < 0.001$) mycobacteria (Fig. 6A, B). These results were further confirmed, when we noted a substantial ($p < 0.0001$) decline by DC^{MPT64} to engulf *M. smegmatis*, another strain of mycobacteria by CFUs (Fig. 6C). Further, impairment in phagocytosis of *Mtb* GFP-H37Ra by DC^{MPT64} was validated by confocal imaging (Fig. 6D). Furthermore, DC^{MPT64} also exhibited remarkable inhibition ($p < 0.0001$) in the uptake of dextran-FITC, a soluble form of an antigen (Fig. 6E, F).

Enhancement of the intracellular survival of *Mtb* in the DC^{MPT64}

Like alveolar macrophages, *Mtb* can also persist in MDSCs [26, 63]. We observed that DC^{MPT64} exhibit a suppressive phenotype and augments the generation of Tregs through inhibition of Th1 cells and Th17 cells. MDSCs have a very contentious role in tuberculosis and literature have shown that through modulation of immune response MDSCs promote *Mtb* survival [64]. Next, we thought of checking the intracellular survival of *Mtb* in DC^{MPT64}. *Mtb* showed remarkably ($p < 0.0001$) higher growth in the DC^{MPT64}, as compared to control DCs (Fig. 7). The results indicate that *Mtb* exploits its MPT64 protein to establish its survival in the DCs by skewing its differentiation to MDSCs.

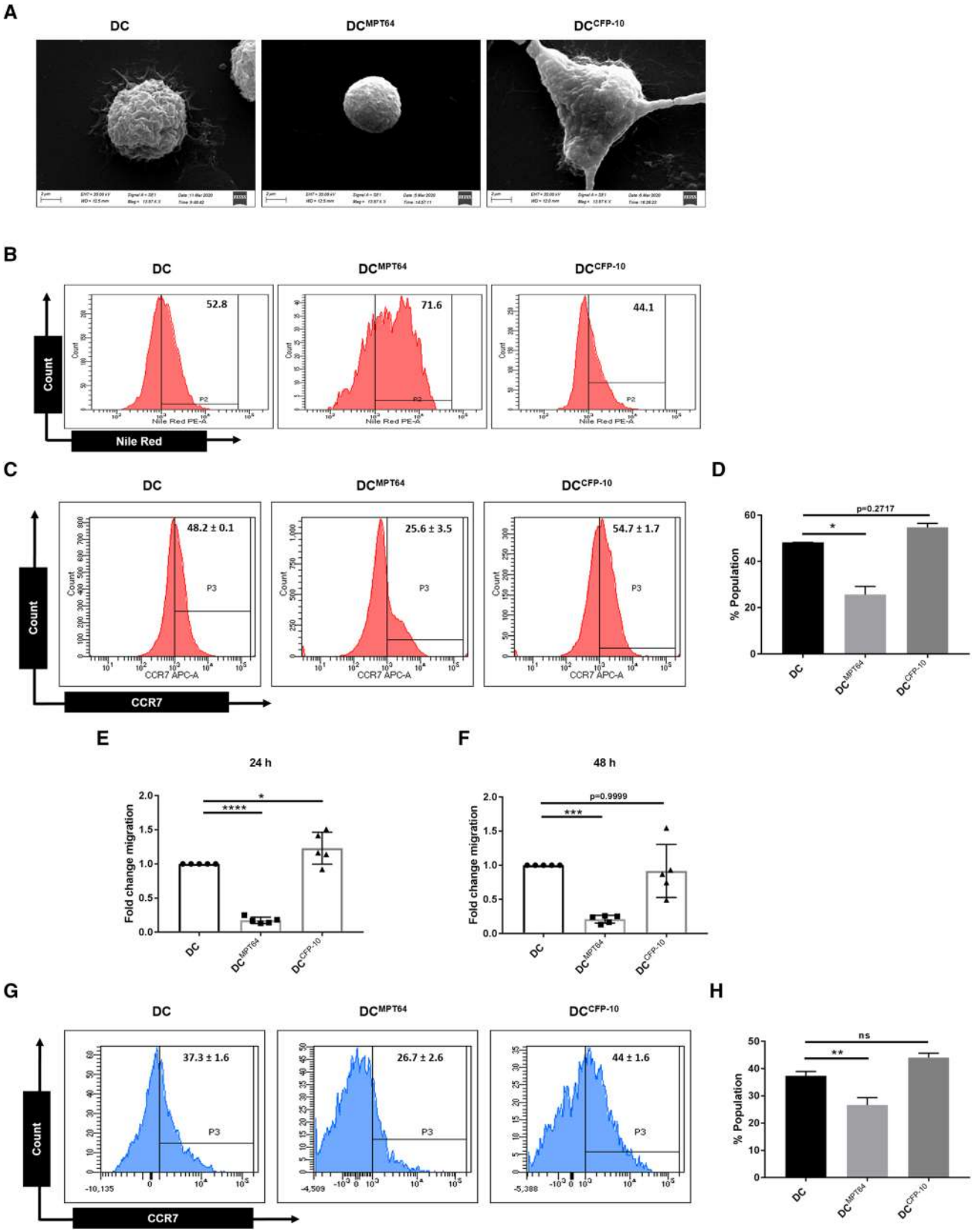
A
DC
DC^MPT64
DC^CFP-10
B
DC
DC^MPT64
DC^CFP-10
52.8
71.6
44.1
Count
Nile Red
Nile Red PE-A
P2
C
DC
DC^MPT64
DC^CFP-10
48.2 ± 0.1
25.6 ± 3.5
54.7 ± 1.7
P3
Count
CCR7
CCR7 APC-A
D
% Population
p=0.2717
*
DC
DC^MPT64
DC^CFP-10
E
24 h
Fold change migration
*
****
F
48 h
p=0.9999
***
G
DC
DC^MPT64
DC^CFP-10
37.3 ± 1.6
26.7 ± 2.6
44 ± 1.6
P3
Count
CCR7
H
% Population
ns
**

◂**Fig. 3** Induction of morphological changes and impairment in the migratory function of DC^{MPT64}. **A** DC^{MPT64} and control DC^{CFP-10} and DCs were cultured on poly-L-Lysine pre-coated glass coverslips in 12-well plates for 6 d. Later, cells were fixed with modified Karnovsky fixative and imaged under scanning electron microscopy (SEM). Pictures were clicked at 13.97 K (scale bar: 2 µm). The data are representative of two independent experiments. **B** DC^{MPT64}, DC^{CFP-10} and DCs were stained with Nile red dye for monitoring the lipid accumulation within cells through flow cytometry. Values in the inset of the histogram depict the percent positive cells ($n=1$). **C–D** DC^{MPT64}, DC^{CFP-10} and DCs were monitored for the surface expression of CCR7 ($n=2$). Data are represented as percentage positive cells (mean ± SEM) through flow cytometer histograms and bar diagrams. **E–F** DC^{MPT64}, DC^{CFP-10} and DCs were CFSE-labelled and injected i.v. in the mice. After 24 and 48 h, the presence of $CFSE^+$ cells was monitored in the spleen. The data are expressed as a fold-change migration of DC^{MPT64} through scatter plots. Each dot denotes an individual animal ($n=5$). **G–H** The surface expression of CCR7 was observed ex vivo on DC^{MPT64} migrated to the spleen ($n=4$). The percentage positive (mean ± SEM) DC^{MPT64} is illustrated through a flow cytometry and bar diagram. Data are representative of 2 independent experiments. $*p<0.05$, $**p<0.01$, $***p<0.001$, $****p<0.0001$, *ns* non-significant

The mechanism involved in suppressing the function of DC^{MPT64} by MPT64 is through the involvement of arginase, STAT-3, NO and IDO

Innate immune cells restrict *Mtb* infection through various mechanisms, such as phagocytosis, opsonization, inflammasome activation and producing various inflammatory mediators [2]. We next elucidated the mechanism involved in imparting suppression by DC^{MPT64}. DC^{MPT64} showed modulation in the expression of $CD11c^{lo}$, $CD11b^{hi}$, $F4/80^{hi}$, $CD40^{hi}$, $CD80^{hi}$, $MHCII^{lo}$, $Ly6C^{hi}$, $Ly6G^{lo}$, $PD\text{-}L1^{hi}$, $TIM\text{-}3^{hi}$, $IL\text{-}10^{hi}$, $TGF\text{-}\beta^{hi}$, $IL\text{-}6^{lo}$, $IL\text{-}12^{lo}$, $TNF\text{-}\alpha^{lo}$ and $CCR7^{lo}$, the molecules that are responsible for immunosuppression (Figs. 1, 2, 3). Based upon the presence of specific set of markers these cells have been characterized as M-MDSC. After extensive analysis, we observed the mechanism involved in suppression was through an elevated level ($p<0.05$) of the arginase in DC^{MPT64}, as tested by biochemical assay and confirmed by Western blotting (Fig. 8A, B). The higher quantity of arginase was well correlated with increased STAT-3 expression (Fig. 8C). STAT-3 controls arginase 1 in MDSCs [65]. MDSCs produce a higher amount of arginase, which contributes to the inhibition of the immunity [66]. We next examined indoleamine 2,3-dioxygenase (IDO) and ROS in DC^{MPT64}. IDO and ROS are important immunosuppressive molecules produced by MDSCs [67–69]. DC^{MPT64} showed augmentation in IDO and a decline in the expression of NF-κB and secretion of ROS (Fig. 8D, F). Similarly, a significant release in the NO ($p<0.0001$) and iNOS was noticed, along with a noticeable upregulation of STAT-1 (Fig. 10I–K). STAT-1 is required for the iNOS activation [70], which establishes the specificity of our results.

During microbial infections, NF-κB contributes to managing the immune response. It enhances the release of pro-inflammatory cytokines and chemokines and fosters the migration of the cells to the site of infection. We observed a remarkable reduction of NF-κB, as compared to control DCs (Fig. 8E). In essence, the results illustrate that *Mtb* skillfully exploits MPT64 to modulate the expression of an array of molecules on DC^{MPT64} to fine-tune the immune system for its survival.

Acquisition of dormant metabolic phenotype by DC^{MPT64}

Various mechanisms have been delineated for the immune surveillance and elicitation of the optimum immune response against infections [55, 71]. MDSCs work as a double edge sword against host in TB infection, as they not only provide a safer resort for *Mtb* survival but also slash the adaptive immune response. *Mtb* utilizes lipids as a potent nutritional source for its survival and progression within host cells [49]. During TB infection, MDSCs shift their glycolysis machinery to the fatty acid oxidation [72]. Therefore, we analyzed the metabolic components of DC^{MPT64}. Initially, we monitored the glucose uptake potential of DC^{MPT64} and noted a significant decline ($p<0.001$) in the glucose (2-NBDG) level, as compared to control DCs (Fig. 9A, B). These results were further confirmed by confocal microscopy; a significant fall in the glucose uptake was seen in DC^{MPT64} (Fig. 9C). Negative control (DC^{neg}) signifies DCs cultured in media supplemented with glucose (Fig. 9A, B).

Glycolysis plays a significant role in the activation of immune cells [73, 74]. Impairment in glycolysis leads to the induction of a steady state in the cells and makes them metabolically inert. We observed that DC^{MPT64} utilize less glucose from surroundings. Further, accumulation of methylglyoxal (MGO) in MDSCs is an indication of their suppressive nature [27]. Hence, we next wanted to monitor the metabolic status of DC^{MPT64}. Likewise, we observed significantly high ($p<0.001$) MGO in DC^{MPT64} by flow cytometry (Fig. 9D, E). These results were further corroborated by confocal imaging (Fig. 9F). DCs stressed with H_2O_2 served as a positive control (DC^{pos}). Furthermore, we observed a significant reduction in Glut1 ($p<0.05$) in DC^{MPT64} (Fig. 9G). Glut1 is the main glucose transport channel in immune and non-immune cells. Additionally,

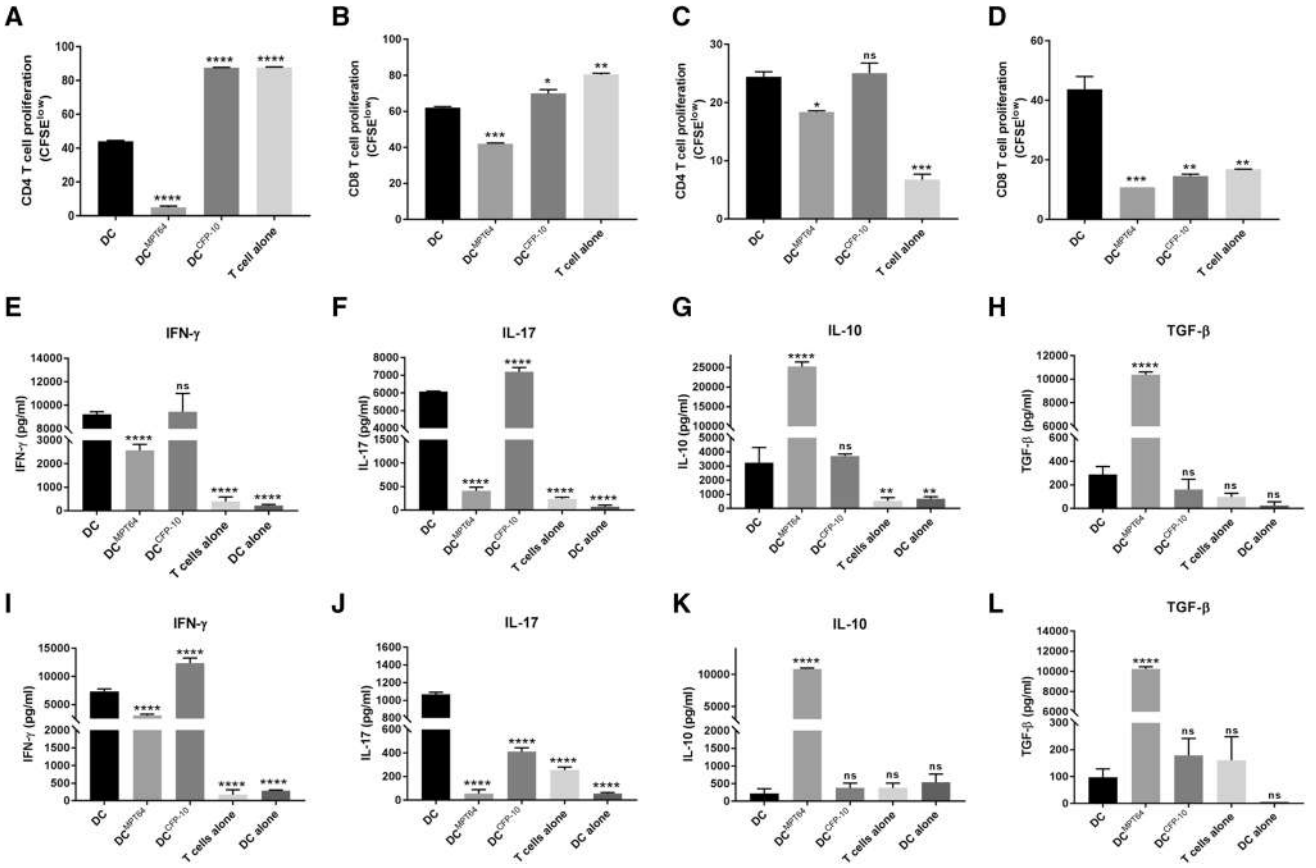

Fig. 4 MPT64 impairs the function of DC^{MPT64} to activate and differentiate CD4 T cells and CD8 T cells. The proliferation of syngeneic CD4 T cells and CD8 T cells by DC^{MPT64}. CFSE-labelled syngeneic naïve **A** CD4 T cells; **B** CD8 T cells were stimulated with plate-bound anti-CD3 and anti-CD28 Abs and co-cultured with syngeneic DC^{MPT64} and control DC^{CFP-10} and DCs (T cell: DCs; 10:1 ratio). The allogeneic proliferation of CD4 T cells and CD8 T cells by DC^{MPT64}. Allogeneic naïve **C** CD4 T cells; **D** CD8 T cells isolated from BALB/c mice were co-cultured with allogeneic (C57BL/6) DCs (T cell: DCs; 10:1 ratio). **A**–**D** After 72 h, T cell proliferation was enumerated by CFSE dye dilution assay. The bar diagram represents the percentage of positive cells (mean ± SEM) ($n = 2$), and data are representative of 2–3 independent experiments. **E**–**L** Estimation of the production of cytokines. After 72 h of culture, the SNs were collected from syngeneic (**E**–**H**) and allogeneic (**I**–**L**) and monitored by ELISA for the production of IFN-γ, IL-17, IL-10 and TGF-β. Data represented as mean ± SD are of triplicate wells and ($n = 3$) from 2 independent experiments.*$p < 0.05$, **$p < 0.01$, ***$p < 0.001$, ****$p < 0.0001$, *ns* non-significant

a striking reduction in the expression of the hexokinase 2 ($p < 0.05$) enzyme was detected in DC^{MPT64} (Fig. 9H). Noteworthy, augmentation in the messenger RNA of semicarbazide-sensitive amine oxidase (SSAO) ($p < 0.01$) was seen in DC^{MPT64} (Fig. 9I). It has been reported that intracellular MGO was regulated by glyoxalase and glutathione [75]. A marked reduction in the expression of glyoxalase 1 ($p < 0.01$) in DC^{MPT64} was noticed (Fig. 9J). This finding depicts that there was dysregulation between generation and neutralization of MGO. MGO generation occurs through the by-products (glyceraldehyde3-phosphate and dihydroxyacetone phosphate) of glycolysis, and acetone and aminoacetone by SSAO [76–78]. Together, these results imply that DCs encountering MPT64 during their differentiation renders them metabolically dormant with suppressive function.

The mechanism of inhibition of the proliferation of T cells is through methylglyoxal

During TB infection, innate immune cells engulf the pathogen and initiate a cascade of events. Due to the non-specificity of the innate immune system, the adaptive immune system operates finally to curtail the infection. T cells play a crucial role in the pathogenesis and protection of TB disease [55]. Till now, the results suggest that DC^{MPT64} secrete soluble mediators, as well as displays certain molecules on its surface that are responsible for their suppressive activity. It has been well evidenced that the expression of co-inhibitory molecules, such as PD-L1 and TIM-3, over the surface of myeloid cells imparts suppressive functionality that leads to the induction of tolerance [40, 60]. Moreover, the presence of methylglyoxal in MDSCs dampens T cell function

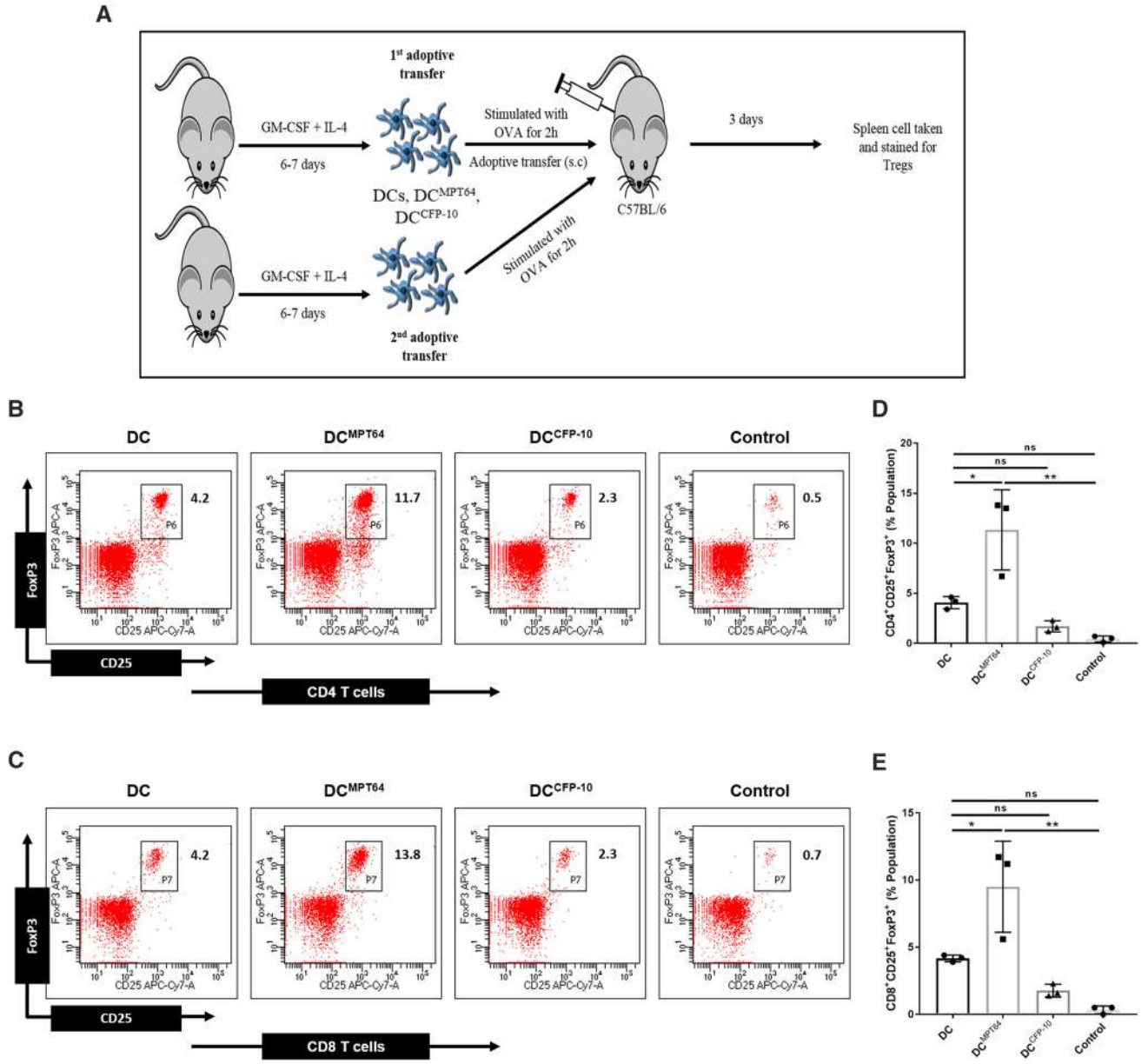

Fig. 5 MPT64-stimulated DC^{MPT64} supports the in vivo generation of Tregs. **A** Diagrammatic representation of the experimental design. Antigen-pulsed DC^{MPT64} and control DC^{CFP-10} and DCs were injected (s.c) twice at an interval of 7 d into the mice. After 3 d, animals were sacrificed and the pool of **B** CD4 T cells; **C** CD8 T cells expressing $CD25^+$ and $FoxP3^+$ were enumerated by flow cytometry and depicted as (**B**, **C**) dot plots; (**D**, **E**) bar diagrams. DCs adoptively transferred without antigen (OVA) were taken as a control. Each dot in the scatter plot signifies data from one mouse ($n=3$). The values (mean ± SEM), in the inset are percentage positive cells and representative of 3 independent experiments. $*p<0.05$, $**p<0.01$, $***p<0.001$, $****p<0.0001$, *ns* non-significant

[27]. Hence, we were curious to know whether inhibition in T cell proliferation by DC^{MPT64} was through secretory molecules or cognate interaction. Consequently, DC^{MPT64} were cultured with CD4 T cells either in a normal tissue culture plate (contact dependent) or in a trans-well culture plate (contact independent). We observed a significant reduction in CD4 T cells ($p<0.001$) proliferation when cultured with DC^{MPT64} either in a contact-dependent or -independent fashion (Fig. 10A, B). These results were further validated with CD8 T cells ($p<0.01$) (Fig. 10C, D). Thus, the DC^{MPT64} inhibit the proliferation of T cells through the secretory, as well as surface molecules.

Nitric oxide is reported to inhibit T cell proliferation [79]. Nitric oxide and iNOS, and their transcription regulator STAT-1 are expressed in higher amounts by DC^{MPT64} (Fig. 10I–K). Consequently, we wanted to examine if NO may be a soluble factor responsible for deterring T cell proliferation. Therefore, the iNOS inhibitor

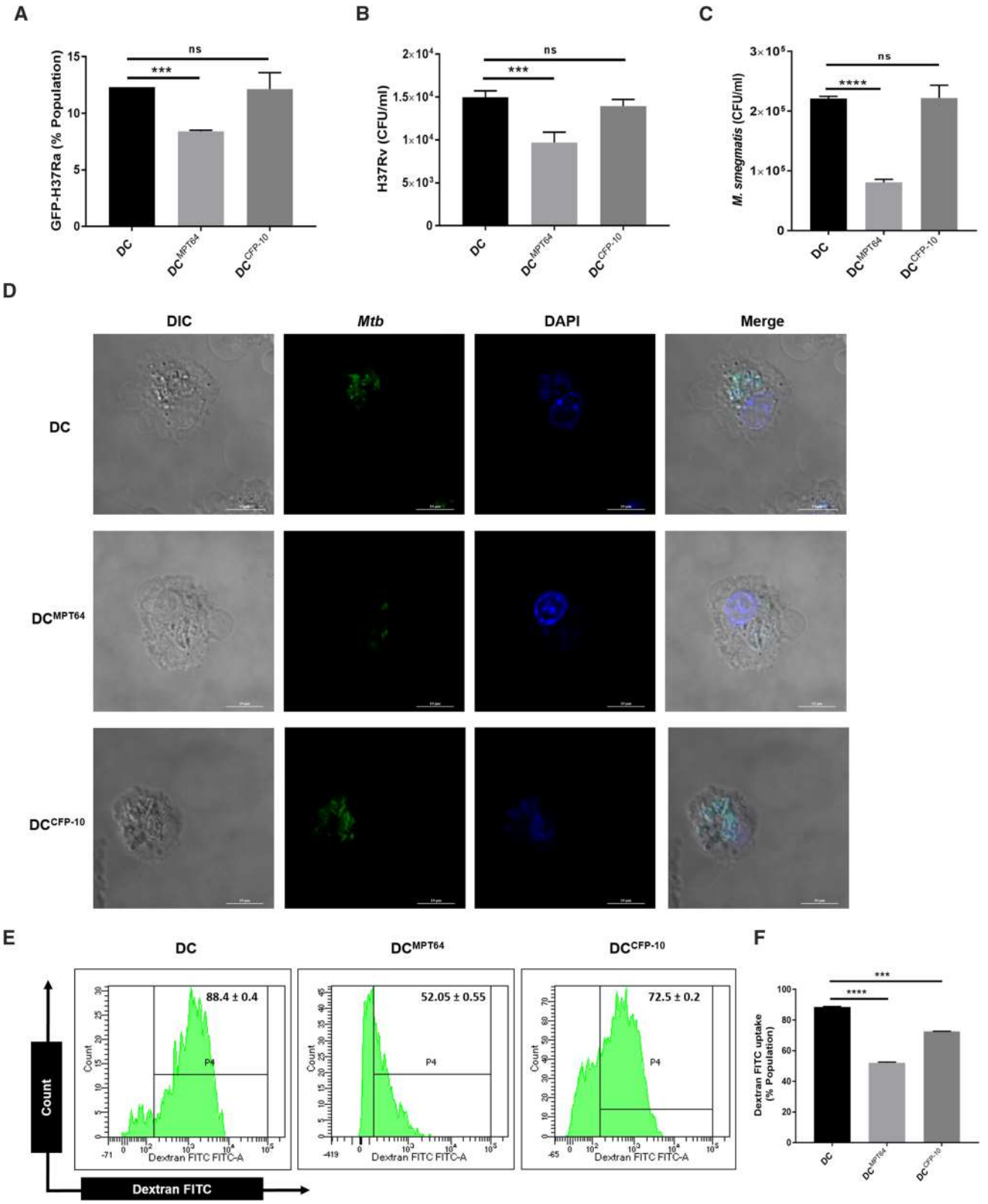

N-monomethyl-L-arginine (NM) was added to the cultures of DC^{MPT64} and CD4 T cells. We observed slight regaining (non-significant) in the proliferation of CD4 T cells (Fig. 10E, F) and CD8 T cells (Fig. 10G, H).

◂**Fig. 6** MPT64 restricted *Mtb* uptake by DC^{MPT64}. The DC^{MPT64} and control DCs were monitored for phagocytosis (3–4 h) (MOI—1:5, DC: bacterium) of **A** GFP-H37Ra; **B** H37Rv; **C** *M. smegmatis*. The extracellular bacilli were killed by incubating cultures with gentamycin/amikacin for 1 h. The engulfment of the bacteria was enumerated by **A** flow cytometer ($n=2$); **B**, **C** CFUs ($n=3$); **D** confocal microscopy (scale bar: 10 µM; magnification: 60×). **E**, **F** DC^{MPT64} were also monitored for antigen (dextran-FITC) uptake by flow cytometry and depicted as **E** histogram and **F** bar diagram ($n=2$). Data are illustrative of 2–3 independent experiments. *$p<0.05$, **$p<0.01$, ***$p<0.001$, ****$p<0.0001$

Myeloid cells depict different metabolic statuses depending upon their state. These metabolic variations can be from a glycolytic metabolism to lipid metabolism, leading to induction or inhibition of various functional and differentiation processes [80]. The adaptive immune system plays a decisive role in controlling TB. Hence, we examined whether DC^{MPT64} induce a metabolically quiescent stage in T cells. A sizeable decline in glucose uptake by CD4 T cells and CD8 T cells was noticed when cultured with DC^{MPT64} (Fig. 11A, B). Further, a remarkable decrease in the MGO level of CD4 T cells was noticed when cultured with DC^{MPT64} but not with control $DC^{CFP\text{-}10}$ and DCs (Fig. 11C). These results were further confirmed with CD8 T cells (Fig. 11D). Thus, it may be concluded that MGO produced by DC^{MPT64} might be restricting the proliferation of T cells. Ultimately, it can be inferred from these results that DC^{MPT64} inhibit the proliferation of T cells through molecules expressed on its surface and soluble mediators.

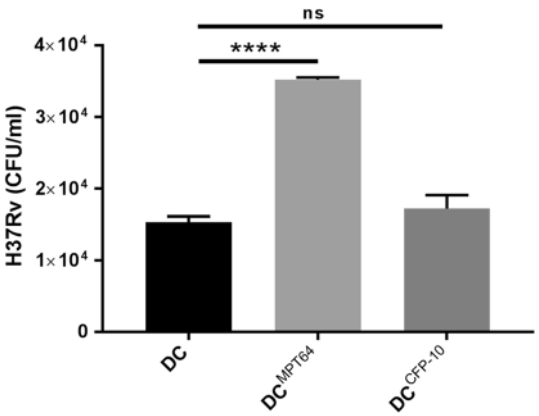

Fig. 7 MPT64 augmens *Mtb* survival in DC^{MPT64}. The DC^{MPT64} were infected with H37Rv (MOI – 1:5) for 4 h. The extracellular bacilli were killed by incubating the cultures with amikacin for 1 h. DC^{MPT64} were further cultured for 72 h. Later, the infected DC^{MPT64} were lysed and the survival of *Mtb* was estimated by CFUs. The data (mean ± SD) shown as bar diagrams are indicative of CFU/ml of *Mtb* and representative of triplicate samples ($n=3$) and two independent experiments. *$p<0.05$, **$p<0.01$, ***$p<0.001$, ****$p<0.0001$

MPT64-stimulated DC^{MPT64} downregulate the expression of T cell receptors and augment T cell apoptosis

T cell recognizes peptide-MHC complex presented on the surface of DCs through its T cell receptor (TCR). The TCR is composed of α and β or γ and δ glycoproteins. The TCRs chains get downregulated in the presence of a high level of NO and ROS [79]. We noticed remarkable downregulation in the expression of the TCRβ chain ($p<0.01$) and TCRγ/δ ($p<0.05$) of CD4 T cells when T cells were cultured with DC^{MPT64} but not control $DC^{CFP\text{-}10}$ and DCs (Fig. 12A–D). These results were further validated with CD8 T cells since a significant decline in the TCRβ chain ($p<0.05$) and TCRγ/δ ($p<0.05$) was noted (Fig. 12E–H).

Literature suggests that myeloid suppressor cell induces apoptosis of T cells. Furthermore, it has been shown that nitrogen and oxygen intermediates impede T cell function through nitration of TCR and apoptosis [81, 82]. We have shown that DC^{MPT64} exhibit high NO secretion along with expression of various other co-inhibitory markers. Therefore, we were interested to examine the effect of DC^{MPT64} in the induction of apoptosis in T cells. Likewise, we noticed considerable apoptosis ($p<0.01$) in CD4 T cells, when co-cultured with DC^{MPT64} but not control DCs or $DC^{CFP\text{-}10}$ (Fig. 12I, J). These results were further authenticated with CD8 T cells ($p<0.001$) (Fig. 12K, L).

Overall the results suggest that MPT64 impairs the function DCs if encountered during their differentiation.

Discussion

Mycobacterium tuberculosis has latently infected nearly 2 billion people globally and therefore is a great threat to society [83]. *Mtb* is a smart pathogen, which has developed various immune evasion strategies against the host [10, 84–86]. *Mtb* secretes an array of molecules, which are involved in subverting the immune response for its persistence. Hence, it is imperative to identify such components. It has been hypothesized that secretory proteins of *Mtb* are the first moieties to encounter the host immune system [87]. Among secretory proteins, Ag85 family, ESAT-6 family, MPT63, MPT64, Acr1 and lipoproteins constitute a major part of the secretome [88]. MPT64 (Rv1980c) is one of the actively secretory proteins of replicating *Mtb* with m.wt. of 24 kDa [29, 89]. It has been observed that the expression level of MPT64 in serum, sputum and granulomas of active TB patients is fairly high [90]. It is recognized by Th1 cells and is a potential diagnostic or vaccine candidate. The modulatory role of MPT64 has been explored to some extent on macrophages, epithelioid cells and multinucleated

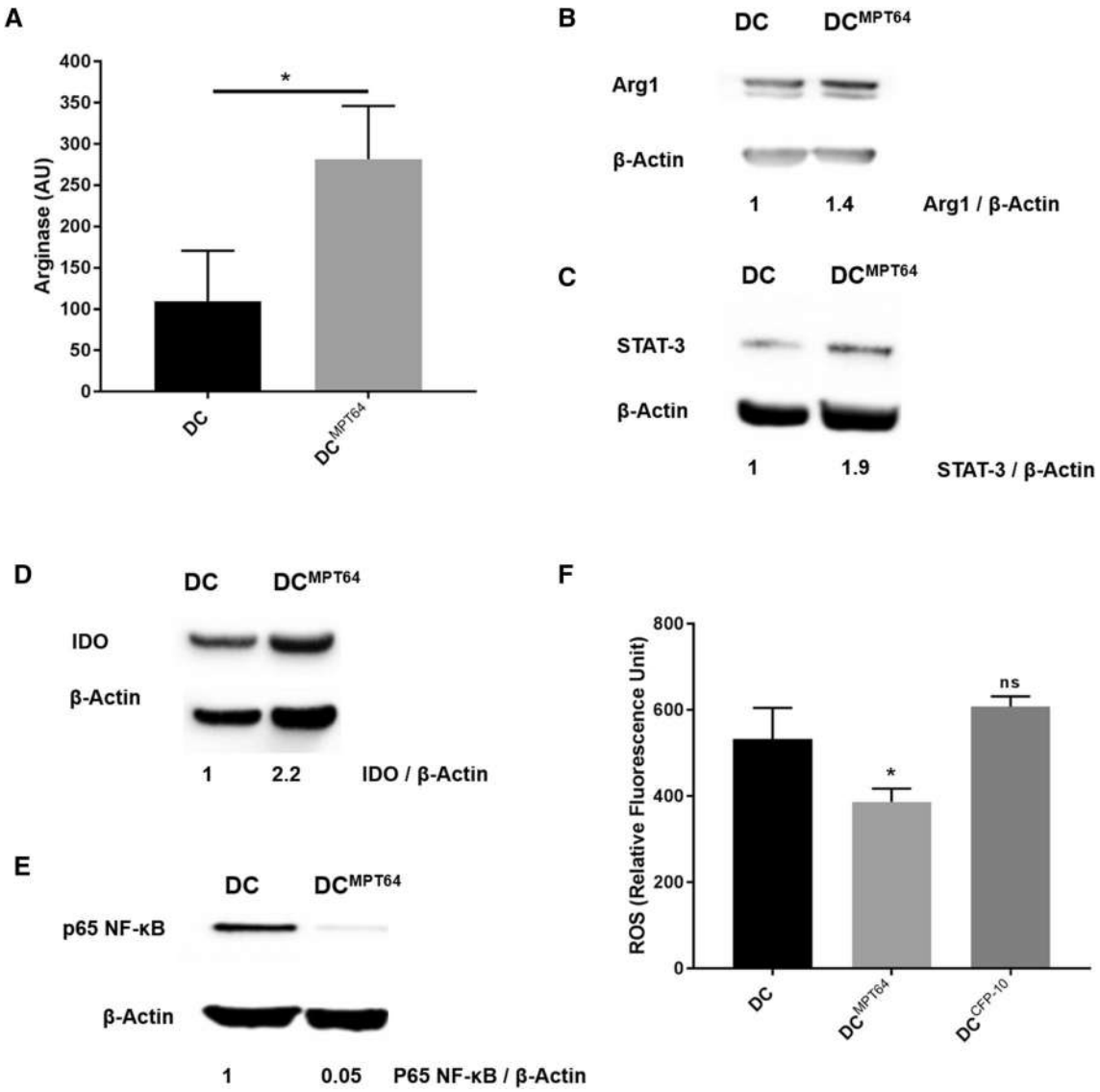

Fig. 8 MPT64 upregulates Arg1 and IDO but inhibits ROS and NF-κB expression in DC^{MPT64}. DC^{MPT64} and control DC^{CFP-10} and DCs were cultured for 6 d in a complete medium. Later, **A** arginase was estimated by arginase activity assay ($n=3$). The cell lysate was used for Western blotting for the expression of **B** arginase 1; **C** STAT-3; **D** IDO; **E** NF-κB p65. **F** ROS were analysed by labelling with oxidation-sensitive dye H2DCFDA ($n=3$). The data are representative of 2–3 independent experiments. *$p<0.05$, **$p<0.01$, ***$p<0.001$, ****$p<0.0001$, *ns* non-significant

giant cells but its influence on differentiating DCs remains elusive [91, 92].

For the first time, we have delineated the role of MPT64 in evading the immune system by impairing the differentiation of the DCs and the following major findings were observed: MPT64 (i) skewed the maturation of BMDCs to MDSCs but not DCs, under DC differentiating milieu (IL-4 + GM-CSF); (ii) suppressed the function of DCs by upregulating the expression of the co-inhibitory molecules PD-L1, TIM-3 and Ly6C; (iii) downregulating the display of MHC II molecules the display of MHC II molecules and inhibiting the secretion of pro-inflammatory cytokines; (iv) impaired the migratory function of DCs by reducing CCR7 expression; (v) promoted the generation of Tregs and restricted the expansion of Th1 cells and Th17 cells; (vi) inhibited the function of DCs to phagocytose *Mtb* but augmented its intracellular survival; and (vii) the mechanism of immunosuppression deciphered was due to the surface exhibition of co-inhibitory molecules and induction of metabolically quiescent morphology.

It was amazing to note that on exposure to MPT64 during their differentiation, DCs failed to activate both CD4 T cells and CD8 T cells and developed a suppressive phenotype like of MDSCs, viz., $CD11c^{lo}$, $MHCII^{lo}$, $Ly6C^{hi}$, $TIM\text{-}3^{hi}$,

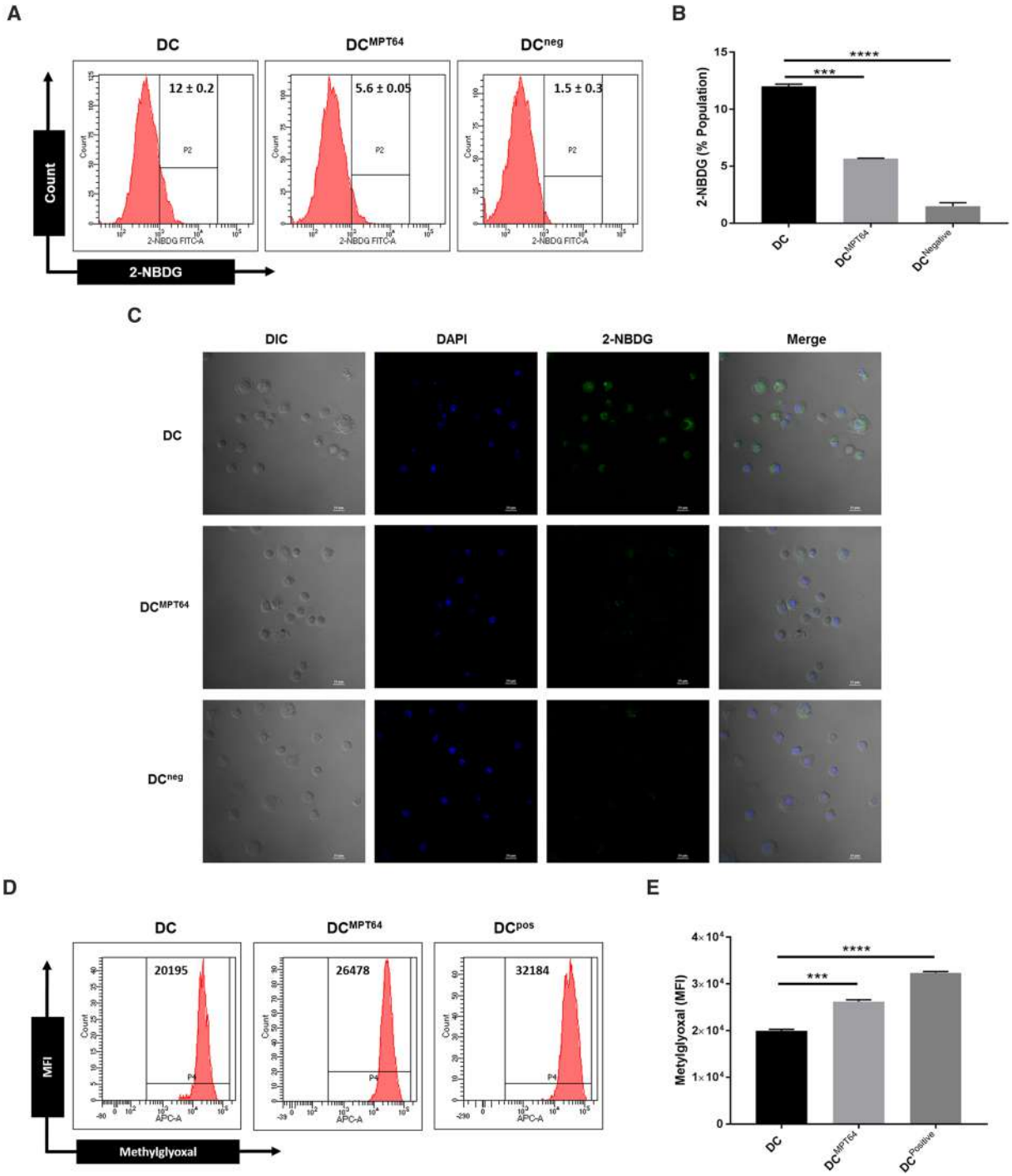

Fig. 9 Acquisition of dormant metabolic phenotype by DC^{MPT64} upon MPT64 exposure. DC^{MPT64} were metabolically characterized and studied for the **A**–**B** impairment of the uptake of glucose analogue 2-NBDG by flow cytometry. The histogram and bar diagrams show the percentage of positive cells (mean ± SEM). DCs cultured with glucose were taken as a negative control (DC^{neg}) ($n = 2$). **C** The decreased level of glucose uptake was monitored by confocal microscopy (scale bar: 10 µM, magnification: 60×). **D** The expression of methylglyoxal was examined by flow cytometry. H_2O_2-treated DCs (DC^{pos}) were taken as a positive control. Data are represented as histograms showing MFI and **E** bar diagrams ($n = 2$). **F** DC^{MPT64} were stained with anti-methylglyoxal Abs (red), along with DAPI (blue) to visualize the nucleus and phalloidin (green) for actin. The images were obtained through a confocal microscope (scale bar: 10 µm, magnification: 60×). The histogram (right side) depicts the intensity of methylglyoxal, actin and DAPI, as indicated by white arrows. **G**–**J** The expression of Glut1, Hk2, SSAO and GLO1 was monitored by RT-qPCR ($n = 3$). The data are representative of 2–3 independent experiments. $^{*}p < 0.05$, $^{**}p < 0.01$, $^{***}p < 0.001$, $^{****}p < 0.0001$

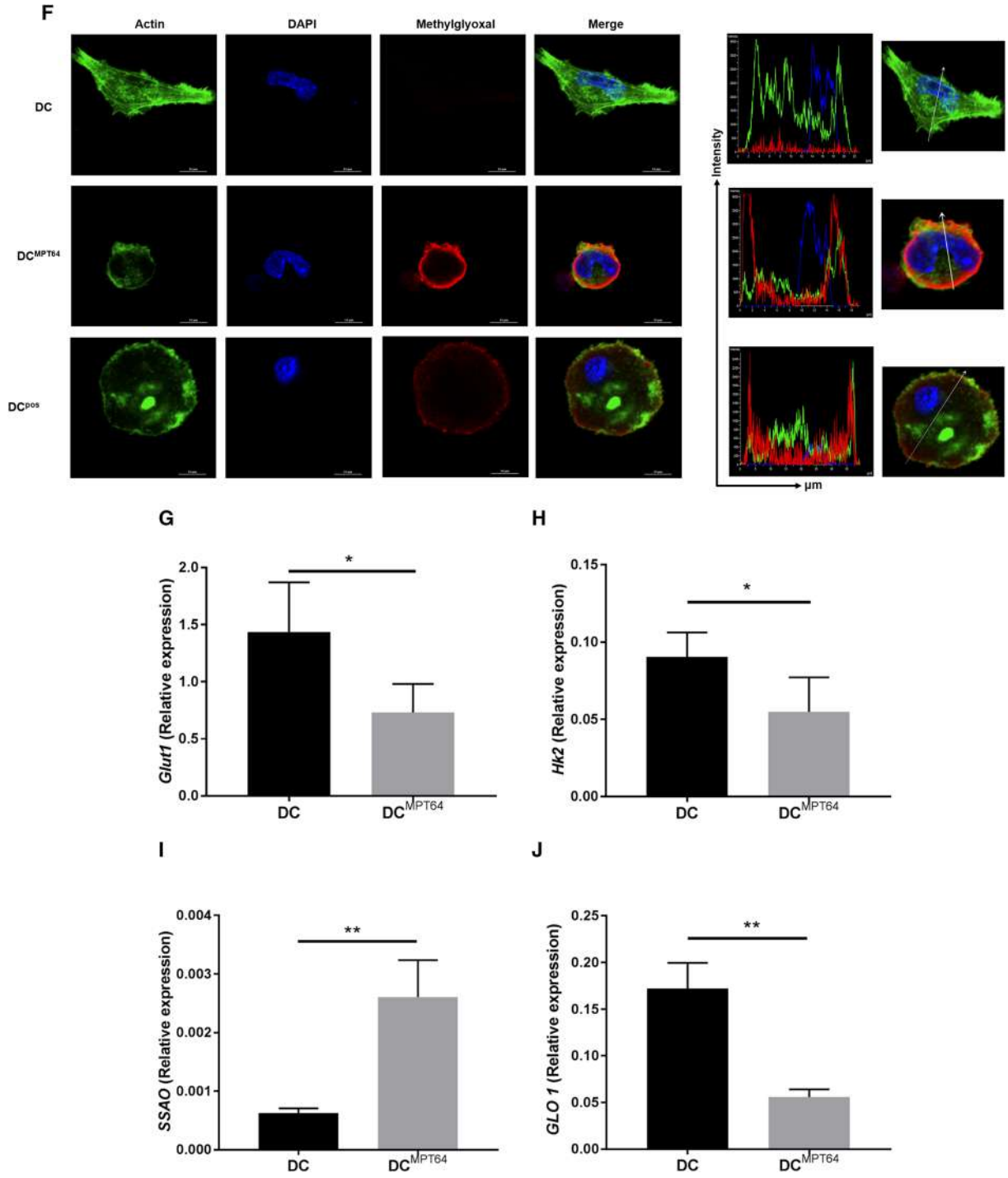

Fig. 9 (continued)

PD-L1^{hi}, CCR7^{lo}, IL-10^{hi}, TGF-β^{hi}, arginase^{hi} and IDO^{hi}. Furthermore, the inhibitory nature of DC^{MPT64} was further validated by the accumulation of lipids and MGO, reduced glucose (2-NBDG) uptake, weakened Glut1 and hexokinase 2 expressions and reduced ability to kill *Mtb*. DC^{MPT64} showed reduced expression of MHCII; hence, their antigen

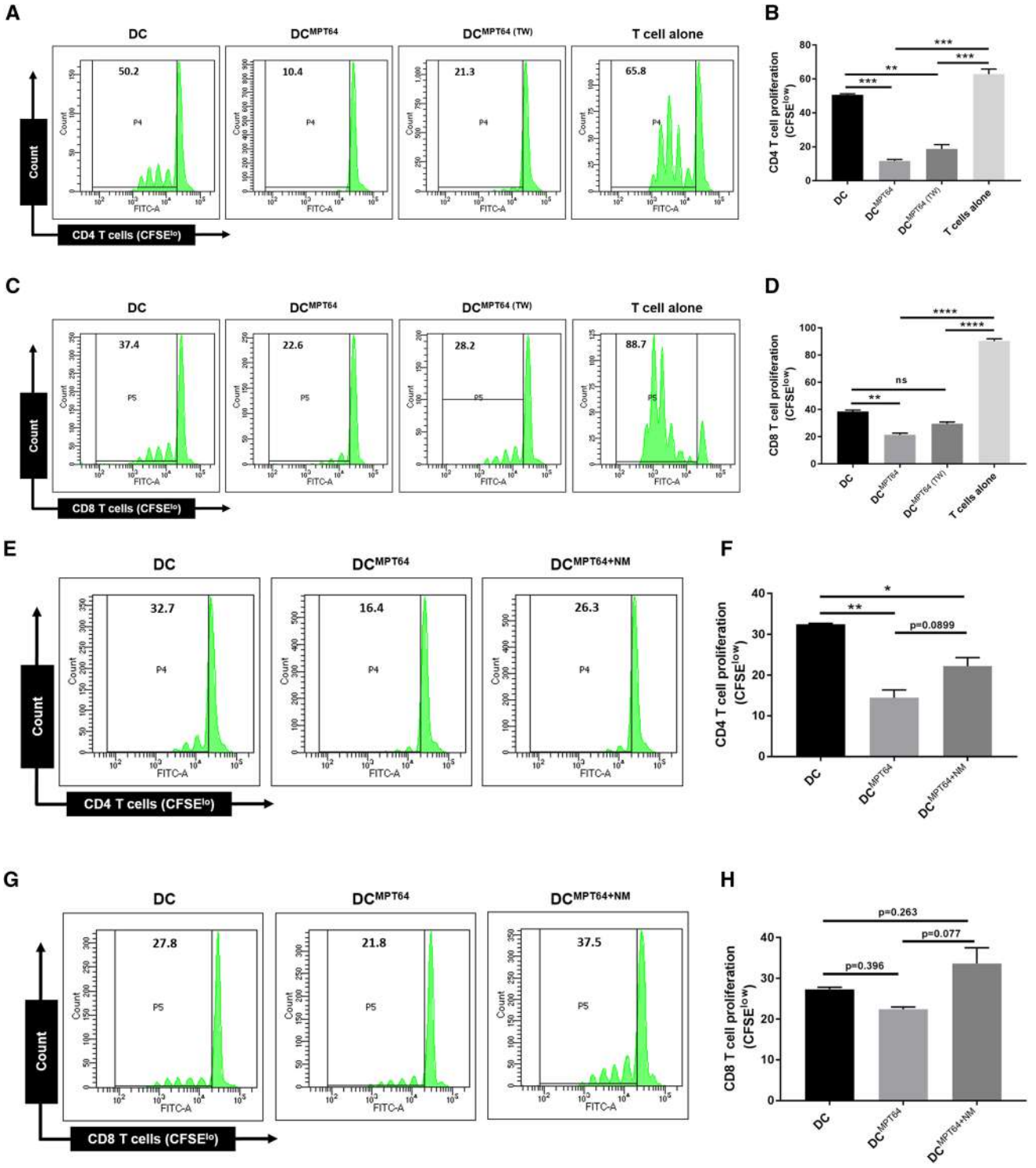

Fig. 10 MPT64-exposed DC^{MPT64} released NO and inhibited the proliferation of CD4 T cells and CD8 T cells. DC^{MPT64} and control DCs were co-cultured in 'regular' and 'trans-well' (TW) plates with CFSE-labelled and anti-CD3 and CD28 Abs stimulated naïve **A**, **B** CD4 T cells; **C**, **D** CD8 T cells. Similarly, DC^{MPT64} and control DCs were co-cultured with CFSE-labelled and anti-CD3 and CD28 Abs stimulated **E**, **F** CD4 T cells; **G**, **H** CD8 T cells in the presence or absence of iNOS inhibitor (NM). The cultures were set for 72 h and proliferation was demonstrated by flow cytometry ($n=2$). **F**, **H** The results (mean ± SEM) are also illustrated as a bar diagram of the percentage of CFSE^{lo} CD4 T cells and CD8 T cells. The SNs of the cultures were used to estimate **I** NO ($n=3$). The lysate of the cells was used to check the expression of **J** iNOS; **K** STAT-1 by Western blotting. The data are representative of 2–3 independent experiments. *$p<0.05$, **$p<0.01$, ***$p<0.001$, ****$p<0.0001$

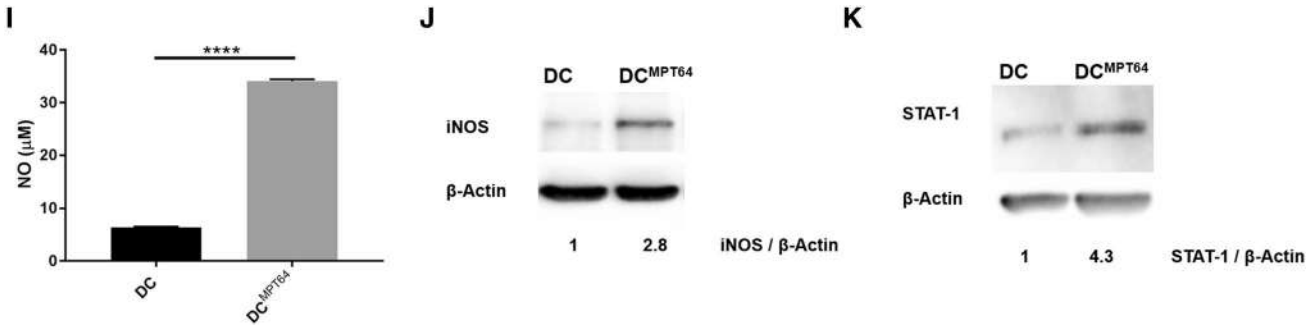

Fig. 10 (continued)

presentation capacity to T cells was compromised. *Mtb* has evolved a mechanism to modulate the MHC expression [55]. Inhibitory markers on DC^{MPT64} point towards their MDSCs-like function. The predominance of MDSCs is noticed in the TB granulomas, which promotes the survival of *Mtb* [93, 94]. Although, MDSCs role is well established in cancer but not yet in TB.

DC^{MPT64} showed upregulation of PD-$L1^{hi}$/TIM-3^{hi} and promoted Tregs development. The interaction of APCs with T cells through PD-L1-PD1 supports Tregs formation [95]. In TB patients, suppression of T cell proliferation is reported due to PD-$L1^{hi}$ on APCs [63]. MDSCs secrete anti-inflammatory cytokines, but pro-inflammatory cytokines to a lesser extent [96]. Likewise, DC^{MPT64} exhibited a high yield of IL-10 and TGF-β. DC^{MPT64} expressed a lower level of CCR7 chemokine that compromised their ability to migrate to lymphoid organs and prime T cells. The migration of DCs to the site of infection to capture antigens or lymph nodes to prime T cells depends on the level of expression of chemokines [97].

Lipids depot in the immune cells impairs their function but serves as an energy reservoir for *Mtb* survival [49]. MDSCs have high lipids content and inhibit the Th1 cell and Th17 cell activation [98]. Similarly, DC^{MPT64} showed high lipid content and inhibited Th1 cell and Th17 cell but stimulated Tregs. MDSCs prefer Tregs induction [99]. Tregs play a cardinal role in suppressing immunity. Further, lipid-rich DC^{MPT64} showed reduced capacity to phagocytose and kill intracellular mycobacteria and served as a protective niche for *Mtb* survival.

It may be important to delineate the metabolic activity of the cells during an infection. *Mtb* utilizes lipids as an energy source from the foamy macrophages [100]. Additionally, on shortage of carbon sources, it initiates glyoxylate shunt for its existence and metabolism of lipids [101]. In the case of MDSCs, the metabolic shift from glycolysis to fatty acid

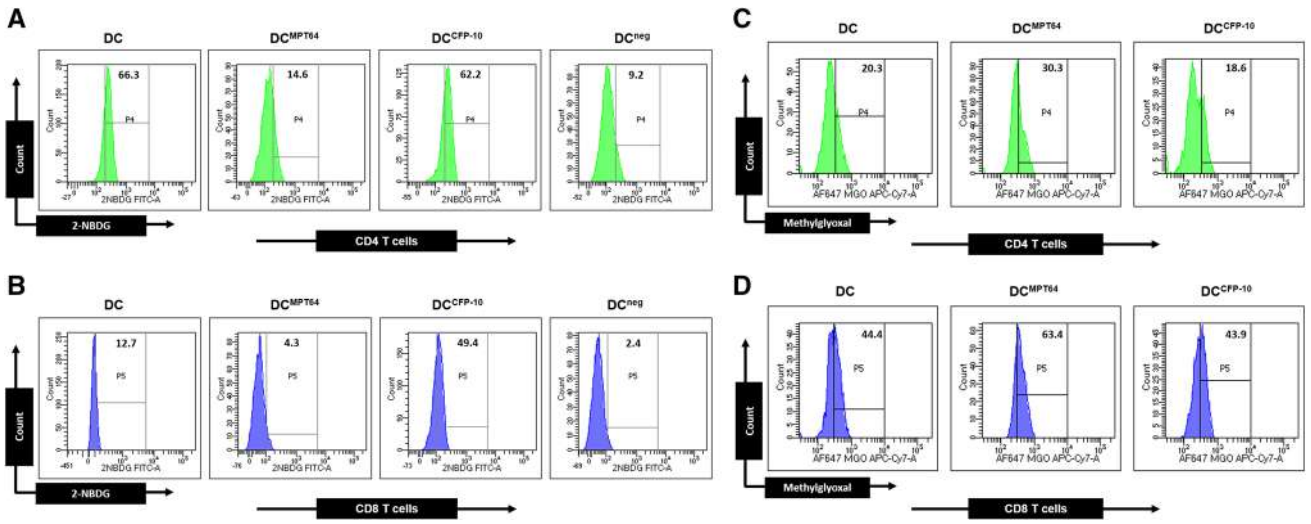

Fig. 11 DC^{MPT64} acquires a metabolically dormant phenotype. DC^{MPT64} and control DCs were co-cultured with the naïve **A**, **C** CD4 T cells; **B**, **D** CD8 T cells and assessed for the uptake of **A**–**B** glucose analogue (2-NBDG); **C**, **D** methylglyoxal through flow cytometry. Values in the inset of histograms refer to the percentage of positive cells for 2-NBDG and methylglyoxal uptake. DCs cultured in glucose conditioned media were used as a negative control (DC^{neg}) for glucose uptake assay. Data are representative of 2–3 independent experiments

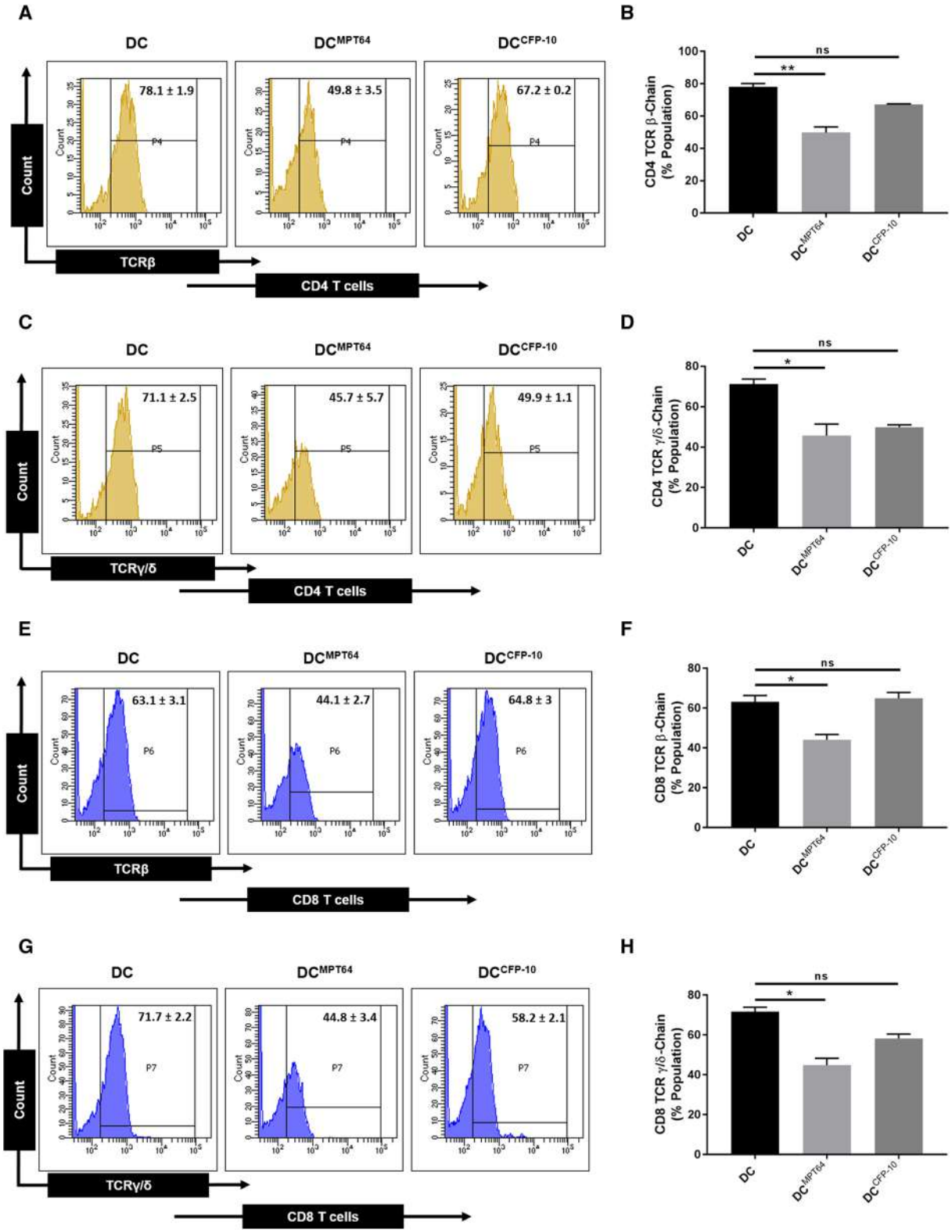

Fig. 12 MPT64-stimulated DC^{MPT64} downregulates the expression of T cells receptor and augments apoptosis of T cells. DC^{MPT64} and control DCs were cultured with the anti-CD3 and CD28 Abs-stimulated naïve **A**–**D** CD4 T cells; **E**–**H** CD8 T cells for 72 h. Later, the cells were analysed for the expression of **A**, **B** TCRβ; **C**, **D** TCRγ/δ chains on CD4 T cells; **E**, **F** TCRβ; **G**, **H** TCRγ/δ chain on CD8 T cells by flow cytometry. The data are expressed as histograms and bar diagrams. Likewise, **I**, **J** CD4 T cells; **K**, **L** CD8 T cells were monitored for apoptosis by staining with Annexin V through flow cytometry. Data (mean ± SEM) ($n = 2$) denoted as histograms and bar diagrams are the percentage of positive cells and representative of 2–3 independent experiments. *$p < 0.05$, **$p < 0.01$, ***$p < 0.001$, ****$p < 0.0001$, *ns* non-significant

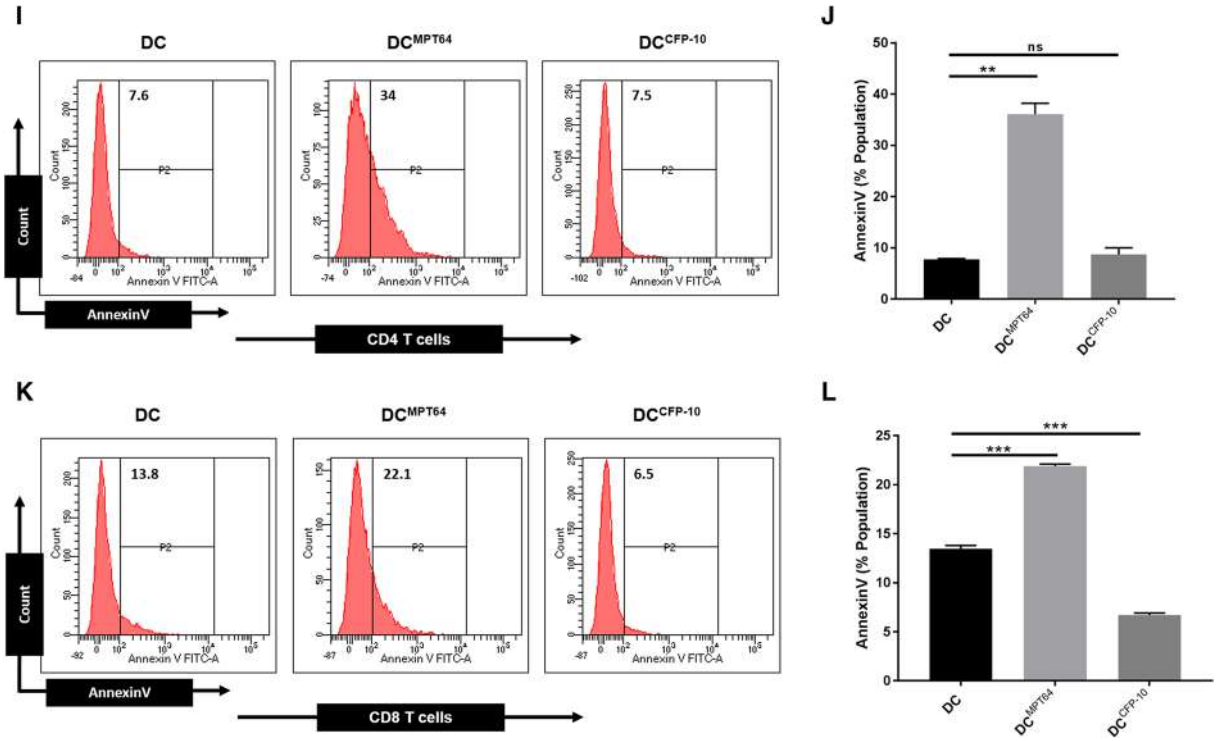

Fig. 12 (continued)

oxidation is known in the case of cancer [72]. Accumulation of methylglyoxal (MGO) imparts suppressive characteristics in MDSCs [27]. Generation of MGO occurs through glyceraldehyde3-phosphate and dihydroxyacetone phosphate during glycolysis and from acetone and aminoacetone by SSAO [76–78]. DC^{MPT64} showed reduced 2-NBDG uptake with impaired Glut1 and hexokinase 2 expression. A deposit of MGO in DC^{MPT64} was noted, which was unutilized due to a decline in glyoxalase 1 level. It showed a decrease in the glycolysis cycle and the generation of advanced glycation end products (MGO), from by-products of glycolysis and aminoacetone. The accumulation of MGO in DC^{MPT64} was further confirmed by flow cytometry and confocal microscopy. It may be inferred that *Mtb* may employ MPT64 to induce MGO for instilling suppressive characteristics in MDSCs.

Finally, we were curious to delineate the mechanism involved by DC^{MPT64} in executing the inhibitory activity. IDO is linked with tolerogenic DCs and Tregs induction by MDSCs [61]. Further, a higher level of NO/iNOS and arginase inhibits the T cell activation [102]. DC^{MPT64} which inhibited T cell proliferation showed augmented expression of NO/iNOS, IDO and arginase 1 and a decline in ROS and NF-κB. Enhanced expression of STAT-1 upregulates iNOS followed by NO secretion, and increased exhibition of STAT-3 stimulates the arginase 1 level, which utilizes L-arginine and generates urea and ornithine, confirming the specificity of our results. Further, induction of iNOS and arginase 1 leads to the generation of ONOO- and RNS that induces malfunctioning of TCR and inhibits T cell proliferation followed by apoptosis. Augmentation of IDO leads to consumption of tryptophan from the cell and surroundings, and therefore deprivation of amino acids in the cell and its microenvironment. Reduction in glucose uptake along with a decline in the expression of Glut1 and Hk2 leads to the formation of MGO, as supported by high levels of SSAO and low expression of GLO1. Augmentation in the secretion of IL-10 and TGF-β leads to Tregs differentiation and inhibition of Th1 cells and Th17 cells. Downregulation in pro-inflammatory response is marked by reduced expression of p65 NF-κB. Higher lipid accumulation works as a source of nutrition for *Mtb* survival in the M-MDSC, as demonstrated by higher the survival rate of *Mtb* [27, 103, 104] (Fig. 13).

DCs have an imperative role in the induction of immune response, but along with that their role in the generation of immune tolerance to self-antigens is also well established. Hence, DCs imparting immune tolerance has been characterized as tolerogenic DCs. Tolerogenic DCs can be well defined on the basis of high expression of co-inhibitory markers, like PD-L1/2, Mer tyrosine kinase, IL-10 and TGF-β [105, 106]. Low expression of co-stimulatory molecules (CD80, CD86, MHC II) and pro-inflammatory

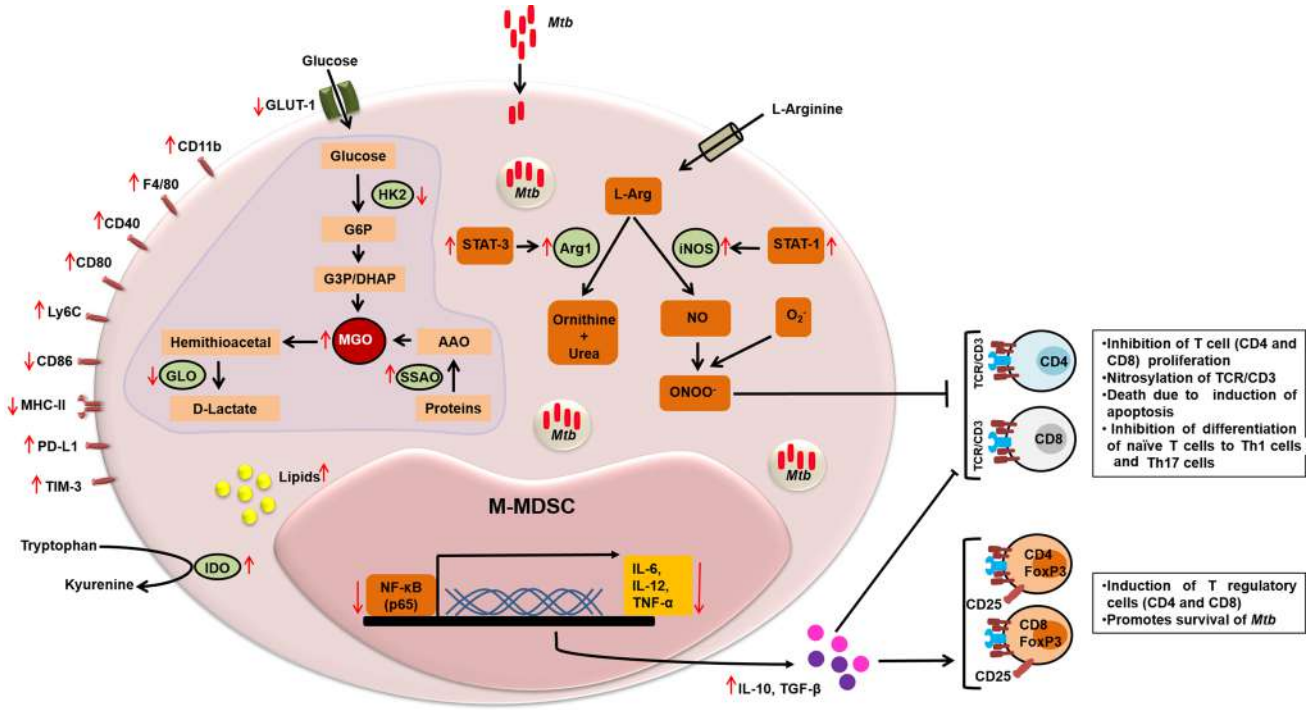

Fig. 13 Proposed mechanism of skewing BMCs towards M-MDSCs by MPT64 protein of *Mtb* under DCs differentiation conditions. Pre-exposure of BMCs to MPT64 under DC differentiating conditions (GM-CSF + IL-4) promotes the generation of M-MDSCs, as evidenced by the enhanced expression of CD11b, Ly6C, F4/80, CD40, CD80, PD-L1, TIM-3 and reduction in the expression of CD86 and MHC II. Enhanced expression of STAT-1 elicits the upregulation of iNOS followed by NO secretion; increased STAT-3 leads to arginase 1 that utilizes L-arginine and generates urea and ornithine. Induction of iNOS and arginase 1 leads to the generation of $ONOO^-$ and RNS that induces malfunctioning of TCR and inhibits T cell proliferation followed by apoptosis. Augmentation of IDO leads to the consumption of tryptophan from the cell and surroundings, and therefore deprivation of amino acids in the cell and its microenvironment. Reduction in glucose uptake along with a decline in the expression of Glut1 and Hk2 leads to the formation of MGO, as supported by high levels of SSAO and low expression of GLO1. Increased secretion of IL-10 and TGF-β leads to Tregs differentiation and inhibition of Th1 cells, Th2 cells and Th17 cells. Downregulation in pro-inflammatory response is marked by reduced expression of p65 NF-κB. Higher lipid accumulation works as a source of nutrition for *Mtb* survival in the M-MDSC, as demonstrated by the higher survival rate of *Mtb*

cytokines (TNF-α, IL-12 and IL-6) are exhibited by these cells [107]. Interestingly, MPT64 stimulation of differentiating DCs leads to the generation of M-MDSCs. These are also well-known immunosuppressive cells resembling tolerogenic DCs in terms of high expression of PD-L1, TIM-3, IL-10 and TGF-β. In contrast to tolerogenic DCs, MDSCs express Ly6C marker along with CD40 and CD80 molecules. These are not exhibited by tolerogenic DCs. Surprisingly, MDSCs do exhibit a high expression of arginase 1 and iNOS, due to which it depletes essential amino acids from the surrounding T cells and limits their proliferation [108, 109]. Hence, contrary to tolerogenic DCs, MDSCs have diverse immune suppressive machinery, which differentiates them from other suppressive immune cells.

In essence, this study for the first time decodes a novel mechanism of immune evasion adopted by *Mtb* through its MPT64 protein. This study suggests that MPT64 may be an excellent drug target to inhibit the persistence of *Mtb* in human cells.

Supplementary Information The online version contains supplementary material available at https://doi.org/10.1007/s00018-022-04596-5.

Acknowledgements SS received a fellowship from the Indian Council of Medical Research (ICMR); MA was the recipient of fellowships from the Department of Science and Technology (DST); SKM and HB were the recipients of fellowships from CSIR.

Author contributions JNA conceptualized the study. JNA, SS and SKM designed the experiments and analyzed data. SS, SKM, MA and HB performed experiments. SS, JNA and VB wrote the manuscript. AA cloned, expressed and purified the proteins. All the authors finally reviewed and approved the submitted manuscript.

Funding The work was supported through funding from the Council of Scientific and Industrial Research (CSIR), India.

Data availability All data generated or analyzed during this study are included in this article and its supplementary information file.

Additionally, data are available from the corresponding author upon reasonable request.

Declarations

Conflict of interest The authors have no relevant financial or non-financial interests to disclose.

Ethical approval The use of *Mtb* for this study was approved by the Biosafety committee of Institute of Microbial Technology (CSIR-IMTECH/IBSC/2018/31). All animal studies were approved by the Institutional Animal Ethics Committee (55/GO/Re/Rc/Bi/Bt/S/99/CPCSEA) and experiments were performed as per the approved protocols and guidelines issued by CPCSEA (Committee for the Purpose of Supervision of Experiments on Animals), Govt. of India.

References

1. Mehra A, Zahra A, Thompson V, Sirisaengtaksin N, Wells A, Porto M et al (2013) Mycobacterium tuberculosis type VII secreted effector EsxH targets host ESCRT to impair trafficking. PLoS Pathog 9(10):e1003734. https://doi.org/10.1371/journal.ppat.1003734
2. Lerner TR, Borel S, Gutierrez MG (2015) The innate immune response in human tuberculosis. Cell Microbiol 17(9):1277–1285. https://doi.org/10.1111/cmi.12480
3. Queval CJ, Brosch R, Simeone R (2017) The macrophage: a disputed fortress in the battle against *Mycobacterium tuberculosis*. Front Microbiol 8:2284. https://doi.org/10.3389/fmicb.2017.02284
4. Wang Z, Jiang H, Chen S, Du F, Wang X (2012) The mitochondrial phosphatase PGAM5 functions at the convergence point of multiple necrotic death pathways. Cell 148(1–2):228–243. https://doi.org/10.1016/j.cell.2011.11.030
5. Cambier CJ, Falkow S, Ramakrishnan L (2014) Host evasion and exploitation schemes of *Mycobacterium tuberculosis*. Cell 159(7):1497–1509. https://doi.org/10.1016/j.cell.2014.11.024
6. Harding CV, Boom WH (2010) Regulation of antigen presentation by *Mycobacterium tuberculosis*: a role for toll-like receptors. Nat Rev Microbiol 8(4):296–307. https://doi.org/10.1038/nrmicro2321
7. Velmurugan K, Chen B, Miller JL, Azogue S, Gurses S, Hsu T et al (2007) Mycobacterium tuberculosis nuoG is a virulence gene that inhibits apoptosis of infected host cells. PLoS Pathog 3(7):e110. https://doi.org/10.1371/journal.ppat.0030110
8. Ouimet M, Koster S, Sakowski E, Ramkhelawon B, van Solingen C, Oldebeken S et al (2016) Mycobacterium tuberculosis induces the miR-33 locus to reprogram autophagy and host lipid metabolism. Nat Immunol 17(6):677–686. https://doi.org/10.1038/ni.3434
9. Mayer-Barber KD, Andrade BB, Barber DL, Hieny S, Feng CG, Caspar P et al (2011) Innate and adaptive interferons suppress IL-1alpha and IL-1beta production by distinct pulmonary myeloid subsets during *Mycobacterium tuberculosis* infection. Immunity 35(6):1023–1034. https://doi.org/10.1016/j.immuni.2011.12.002
10. Zhai W, Wu F, Zhang Y, Fu Y, Liu Z (2019) The immune escape mechanisms of *Mycobacterium tuberculosis*. Int J Mol Sci 20(2):340. https://doi.org/10.3390/ijms20020340
11. Ernst JD (2018) Mechanisms of *M. tuberculosis* immune evasion as challenges to TB vaccine design. Cell Host Microbe 24(1):34–42. https://doi.org/10.1016/j.chom.2018.06.004
12. Siddiqui KF, Amir M, Gurram RK, Khan N, Arora A, Rajagopal K et al (2014) Latency-associated protein Acr1 impairs dendritic cell maturation and functionality: a possible mechanism of immune evasion by *Mycobacterium tuberculosis*. J Infect Dis 209(9):1436–1445. https://doi.org/10.1093/infdis/jit595
13. Amir M, Aqdas M, Nadeem S, Siddiqui KF, Khan N, Sheikh JA et al (2017) Diametric role of the latency-associated protein acr1 of *Mycobacterium tuberculosis* in modulating the functionality of pre- and post-maturational stages of dendritic cells. Front Immunol 8:624. https://doi.org/10.3389/fimmu.2017.00624
14. Dulphy N, Herrmann JL, Nigou J, Rea D, Boissel N, Puzo G et al (2007) Intermediate maturation of *Mycobacterium tuberculosis* LAM-activated human dendritic cells. Cell Microbiol 9(6):1412–1425. https://doi.org/10.1111/j.1462-5822.2006.00881.x
15. Gehring AJ, Dobos KM, Belisle JT, Harding CV, Boom WH (2004) *Mycobacterium tuberculosis* LprG (Rv1411c): a novel TLR-2 ligand that inhibits human macrophage class II MHC antigen processing. J Immunol 173(4):2660–2668. https://doi.org/10.4049/jimmunol.173.4.2660
16. Noss EH, Pai RK, Sellati TJ, Radolf JD, Belisle J, Golenbock DT et al (2001) Toll-like receptor 2-dependent inhibition of macrophage class II MHC expression and antigen processing by 19-kDa lipoprotein of *Mycobacterium tuberculosis*. J Immunol 167(2):910–918. https://doi.org/10.4049/jimmunol.167.2.910
17. Pecora ND, Gehring AJ, Canaday DH, Boom WH, Harding CV (2006) *Mycobacterium tuberculosis* LprA is a lipoprotein agonist of TLR2 that regulates innate immunity and APC function. J Immunol 177(1):422–429. https://doi.org/10.4049/jimmunol.177.1.422
18. Sinha A, Singh A, Satchidanandam V, Natarajan K (2006) Impaired generation of reactive oxygen species during differentiation of dendritic cells (DCs) by *Mycobacterium tuberculosis* secretory antigen (MTSA) and subsequent activation of MTSA-DCs by mycobacteria results in increased intracellular survival. J Immunol 177(1):468–478. https://doi.org/10.4049/jimmunol.177.1.468
19. Simeone R, Bobard A, Lippmann J, Bitter W, Majlessi L, Brosch R et al (2012) Phagosomal rupture by *Mycobacterium tuberculosis* results in toxicity and host cell death. PLoS Pathog 8(2):e1002507. https://doi.org/10.1371/journal.ppat.1002507
20. Wong D, Bach H, Sun J, Hmama Z, Av-Gay Y (2011) *Mycobacterium tuberculosis* protein tyrosine phosphatase (PtpA) excludes host vacuolar-H+-ATPase to inhibit phagosome acidification. Proc Natl Acad Sci USA 108(48):19371–19376. https://doi.org/10.1073/pnas.1109201108
21. Miller JL, Velmurugan K, Cowan MJ, Briken V (2010) The type I NADH dehydrogenase of *Mycobacterium tuberculosis* counters phagosomal NOX2 activity to inhibit TNF-alpha-mediated host cell apoptosis. PLoS Pathog 6(4):e1000864. https://doi.org/10.1371/journal.ppat.1000864
22. Sun J, Singh V, Lau A, Stokes RW, Obregon-Henao A, Orme IM et al (2013) *Mycobacterium tuberculosis* nucleoside diphosphate kinase inactivates small GTPases leading to evasion of innate immunity. PLoS Pathog 9(7):e1003499. https://doi.org/10.1371/journal.ppat.1003499
23. Jayakumar D, Jacobs WR Jr, Narayanan S (2008) Protein kinase E of *Mycobacterium tuberculosis* has a role in the nitric oxide stress response and apoptosis in a human macrophage model of infection. Cell Microbiol 10(2):365–374. https://doi.org/10.1111/j.1462-5822.2007.01049.x
24. Ribechini E, Eckert I, Beilhack A, Du Plessis N, Walzl G, Schleicher U et al (2019) Heat-killed *Mycobacterium tuberculosis* prime-boost vaccination induces myeloid-derived suppressor cells with spleen dendritic cell-killing capability. JCI Insight. https://doi.org/10.1172/jci.insight.128664
25. El Daker S, Sacchi A, Tempestilli M, Carducci C, Goletti D, Vanini V et al (2015) Granulocytic myeloid derived suppressor cells expansion during active pulmonary tuberculosis is

associated with high nitric oxide plasma level. PLoS ONE 10(4):e0123772. https://doi.org/10.1371/journal.pone.0123772
26. Knaul JK, Jorg S, Oberbeck-Mueller D, Heinemann E, Scheuermann L, Brinkmann V et al (2014) Lung-residing myeloid-derived suppressors display dual functionality in murine pulmonary tuberculosis. Am J Respir Crit Care Med 190(9):1053–1066. https://doi.org/10.1164/rccm.201405-0828OC
27. Baumann T, Dunkel A, Schmid C, Schmitt S, Hiltensperger M, Lohr K et al (2020) Regulatory myeloid cells paralyze T cells through cell-cell transfer of the metabolite methylglyoxal. Nat Immunol 21(5):555–566. https://doi.org/10.1038/s41590-020-0666-9
28. Yang B, Wang X, Jiang J, Zhai F, Cheng X (2014) Identification of CD244-expressing myeloid-derived suppressor cells in patients with active tuberculosis. Immunol Lett 158(1–2):66–72. https://doi.org/10.1016/j.imlet.2013.12.003
29. Wang Z, Potter BM, Gray AM, Sacksteder KA, Geisbrecht BV, Laity JH (2007) The solution structure of antigen MPT64 from *Mycobacterium tuberculosis* defines a new family of beta-grasp proteins. J Mol Biol 366(2):375–381. https://doi.org/10.1016/j.jmb.2006.11.039
30. Sehnal D, Bittrich S, Deshpande M, Svobodova R, Berka K, Bazgier V et al (2021) Mol* viewer: modern web app for 3D visualization and analysis of large biomolecular structures. Nucleic Acids Res 49(W1):W431–W437. https://doi.org/10.1093/nar/gkab314
31. Mehaffy C, Dobos KM, Nahid P, Kruh-Garcia NA (2017) Second generation multiple reaction monitoring assays for enhanced detection of ultra-low abundance *Mycobacterium tuberculosis* peptides in human serum. Clin Proteom 14:21. https://doi.org/10.1186/s12014-017-9156-y
32. Fan Q, Lu M, Xia ZY, Bao L (2013) *Mycobacterium tuberculosis* MPT64 stimulates the activation of murine macrophage modulated by IFN-gamma. Eur Rev Med Pharmacol Sci 17(24):3296–3305
33. Wang Q, Liu S, Tang Y, Liu Q, Yao Y (2014) MPT64 protein from *Mycobacterium tuberculosis* inhibits apoptosis of macrophages through NF-kB-miRNA21-Bcl-2 pathway. PLoS ONE 9(7):e100949. https://doi.org/10.1371/journal.pone.0100949
34. Stamm CE, Pasko BL, Chaisavaneeyakorn S, Franco LH, Nair VR, Weigele BA et al (2019) Screening *Mycobacterium tuberculosis* secreted proteins identifies mpt64 as a eukaryotic membrane-binding bacterial effector. mSphere. https://doi.org/10.1128/mSphere.00354-19
35. Lutz MB, Kukutsch N, Ogilvie AL, Rossner S, Koch F, Romani N et al (1999) An advanced culture method for generating large quantities of highly pure dendritic cells from mouse bone marrow. J Immunol Methods 223(1):77–92. https://doi.org/10.1016/s0022-1759(98)00204-x
36. Corraliza IM, Campo ML, Soler G, Modolell M (1994) Determination of arginase activity in macrophages: a micromethod. J Immunol Methods 174(1–2):231–235. https://doi.org/10.1016/0022-1759(94)90027-2
37. Cowburn AS, Crosby A, Macias D, Branco C, Colaco RD, Southwood M et al (2016) HIF2alpha-arginase axis is essential for the development of pulmonary hypertension. Proc Natl Acad Sci USA 113(31):8801–8806. https://doi.org/10.1073/pnas.1602978113
38. Wolf AJ, Linas B, Trevejo-Nunez GJ, Kincaid E, Tamura T, Takatsu K et al (2007) *Mycobacterium tuberculosis* infects dendritic cells with high frequency and impairs their function in vivo. J Immunol 179(4):2509–2519. https://doi.org/10.4049/jimmunol.179.4.2509
39. Popov A, Schultze JL (2008) IDO-expressing regulatory dendritic cells in cancer and chronic infection. J Mol Med (Berl) 86(2):145–160. https://doi.org/10.1007/s00109-007-0262-6
40. Sumpter TL, Thomson AW (2011) The STATus of PD-L1 (B7–H1) on tolerogenic APCs. Eur J Immunol 41(2):286–290. https://doi.org/10.1002/eji.201041353
41. Meher AK, Bal NC, Chary KV, Arora A (2006) *Mycobacterium tuberculosis* H37Rv ESAT-6-CFP-10 complex formation confers thermodynamic and biochemical stability. FEBS J 273(7):1445–1462. https://doi.org/10.1111/j.1742-4658.2006.05166.x
42. Zhu J, Yamane H, Paul WE (2010) Differentiation of effector CD4 T cell populations (*). Annu Rev Immunol 28:445–489. https://doi.org/10.1146/annurev-immunol-030409-101212
43. Redford PS, Murray PJ, O'Garra A (2011) The role of IL-10 in immune regulation during *M. tuberculosis* infection. Mucosal Immunol 4(3):261–270. https://doi.org/10.1038/mi.2011.7
44. Domingo-Gonzalez R, Prince O, Cooper A, Khader SA (2016) Cytokines and Chemokines in *Mycobacterium tuberculosis* Infection. Microbiol Spectr. https://doi.org/10.1128/microbiolspec.TBTB2-0018-2016
45. Prendergast KA, Kirman JR (2013) Dendritic cell subsets in mycobacterial infection: control of bacterial growth and T cell responses. Tuberculosis (Edinb) 93(2):115–122. https://doi.org/10.1016/j.tube.2012.10.008
46. Banchereau J, Steinman RM (1998) Dendritic cells and the control of immunity. Nature 392(6673):245–252. https://doi.org/10.1038/32588
47. Swetman CA, Leverrier Y, Garg R, Gan CH, Ridley AJ, Katz DR et al (2002) Extension, retraction and contraction in the formation of a dendritic cell dendrite: distinct roles for Rho GTPases. Eur J Immunol 32(7):2074–2083. https://doi.org/10.1002/1521-4141(200207)32:7%3c2074::AID-IMMU2074%3e3.0.CO;2-S
48. van Vliet SJ, den Dunnen J, Gringhuis SI, Geijtenbeek TB, van Kooyk Y (2007) Innate signaling and regulation of dendritic cell immunity. Curr Opin Immunol 19(4):435–440. https://doi.org/10.1016/j.coi.2007.05.006
49. Daniel J, Maamar H, Deb C, Sirakova TD, Kolattukudy PE (2011) *Mycobacterium tuberculosis* uses host triacylglycerol to accumulate lipid droplets and acquires a dormancy-like phenotype in lipid-loaded macrophages. PLoS Pathog 7(6):e1002093. https://doi.org/10.1371/journal.ppat.1002093
50. Hossain F, Al-Khami AA, Wyczechowska D, Hernandez C, Zheng L, Reiss K et al (2015) Inhibition of fatty acid oxidation modulates immunosuppressive functions of myeloid-derived suppressor cells and enhances cancer therapies. Cancer Immunol Res 3(11):1236–1247. https://doi.org/10.1158/2326-6066.CIR-15-0036
51. Herber DL, Cao W, Nefedova Y, Novitskiy SV, Nagaraj S, Tyurin VA et al (2010) Lipid accumulation and dendritic cell dysfunction in cancer. Nat Med 16(8):880–886. https://doi.org/10.1038/nm.2172
52. Saban DR (2014) The chemokine receptor CCR7 expressed by dendritic cells: a key player in corneal and ocular surface inflammation. Ocul Surf 12(2):87–99. https://doi.org/10.1016/j.jtos.2013.10.007
53. Lenschow DJ, Walunas TL, Bluestone JA (1996) CD28/B7 system of T cell costimulation. Annu Rev Immunol 14:233–258. https://doi.org/10.1146/annurev.immunol.14.1.233
54. Hongo D, Tang X, Baker J, Engleman EG, Strober S (2014) Requirement for interactions of natural killer T cells and myeloid-derived suppressor cells for transplantation tolerance. Am J Transplant 14(11):2467–2477. https://doi.org/10.1111/ajt.12914
55. Cooper AM (2009) Cell-mediated immune responses in tuberculosis. Annu Rev Immunol 27:393–422. https://doi.org/10.1146/annurev.immunol.021908.132703

56. Lyadova IV, Panteleev AV (2015) Th1 and Th17 cells in tuberculosis: protection, pathology, and biomarkers. Mediat Inflamm 2015:854507. https://doi.org/10.1155/2015/854507
57. Cardona P, Cardona PJ (2019) Regulatory T cells in *Mycobacterium tuberculosis* Infection. Front Immunol 10:2139. https://doi.org/10.3389/fimmu.2019.02139
58. McLaughlin TA, Khayumbi J, Ongalo J, Tonui J, Campbell A, Allana S et al (2020) CD4 T cells in *Mycobacterium tuberculosis* and *Schistosoma mansoni* co-infected individuals maintain functional TH1 responses. Front Immunol 11:127. https://doi.org/10.3389/fimmu.2020.00127
59. Shklovskaya E, de St F, Groth B (2007) Balancing tolerance and immunity: the role of dendritic cell and T cell subsets. Methods Mol Biol 380:25–46. https://doi.org/10.1007/978-1-59745-395-0_2
60. Alderton GK (2012) Tumour immunology: TIM3 suppresses antitumour DCs. Nat Rev Immunol 12(9):620–621. https://doi.org/10.1038/nri3288
61. Zoso A, Mazza EM, Bicciato S, Mandruzzato S, Bronte V, Serafini P et al (2014) Human fibrocytic myeloid-derived suppressor cells express IDO and promote tolerance via Treg-cell expansion. Eur J Immunol 44(11):3307–3319. https://doi.org/10.1002/eji.201444522
62. Ahn D, Penaloza H, Wang Z, Wickersham M, Parker D, Patel P et al (2016) Acquired resistance to innate immune clearance promotes Klebsiella pneumoniae ST258 pulmonary infection. JCI Insight 1(17):e89704. https://doi.org/10.1172/jci.insight.89704
63. Agrawal N, Streata I, Pei G, Weiner J, Kotze L, Bandermann S et al (2018) Human monocytic suppressive cells promote replication of *Mycobacterium tuberculosis* and alter stability of in vitro generated granulomas. Front Immunol 9:2417. https://doi.org/10.3389/fimmu.2018.02417
64. Davids M, Pooran A, Smith L, Tomasicchio M, Dheda K (2021) The Frequency and effect of granulocytic myeloid-derived suppressor cells on mycobacterial survival in patients with tuberculosis: a preliminary report. Front Immunol 12:676679. https://doi.org/10.3389/fimmu.2021.676679
65. Vasquez-Dunddel D, Pan F, Zeng Q, Gorbounov M, Albesiano E, Fu J et al (2013) STAT3 regulates arginase-I in myeloid-derived suppressor cells from cancer patients. J Clin Invest 123(4):1580–1589. https://doi.org/10.1172/JCI60083
66. Grzywa TM, Sosnowska A, Matryba P, Rydzynska Z, Jasinski M, Nowis D et al (2020) Myeloid cell-derived arginase in cancer immune response. Front Immunol 11:938. https://doi.org/10.3389/fimmu.2020.00938
67. Kumar V, Patel S, Tcyganov E, Gabrilovich DI (2016) The nature of myeloid-derived suppressor cells in the tumor microenvironment. Trends Immunol 37(3):208–220. https://doi.org/10.1016/j.it.2016.01.004
68. Platten M, Wick W, Van den Eynde BJ (2012) Tryptophan catabolism in cancer: beyond IDO and tryptophan depletion. Cancer Res 72(21):5435–5440. https://doi.org/10.1158/0008-5472.CAN-12-0569
69. Fleming V, Hu X, Weber R, Nagibin V, Groth C, Altevogt P et al (2018) Targeting myeloid-derived suppressor cells to bypass tumor-induced immunosuppression. Front Immunol 9:398. https://doi.org/10.3389/fimmu.2018.00398
70. Montorsi W, Annoni F, Doldi SB, Germiniani R, Longoni F (1975) Letter: plasma concentration of zinc and copper after intestinal shunt. Nouv Presse Med 23:1734
71. Spitzer MH, Carmi Y, Reticker-Flynn NE, Kwek SS, Madhireddy D, Martins MM et al (2017) Systemic immunity is required for effective cancer immunotherapy. Cell 168(3):487–502.e415. https://doi.org/10.1016/j.cell.2016.12.022
72. Al-Khami AA, Rodriguez PC, Ochoa AC (2016) Metabolic reprogramming of myeloid-derived suppressor cells (MDSC) in cancer. Oncoimmunology 5(8):e1200771. https://doi.org/10.1080/2162402X.2016.1200771
73. O'Neill LA, Pearce EJ (2016) Immunometabolism governs dendritic cell and macrophage function. J Exp Med 213(1):15–23. https://doi.org/10.1084/jem.20151570
74. Ganeshan K, Chawla A (2014) Metabolic regulation of immune responses. Annu Rev Immunol 32:609–634. https://doi.org/10.1146/annurev-immunol-032713-120236
75. Rabbani N, Thornalley PJ (2008) The dicarbonyl proteome: proteins susceptible to dicarbonyl glycation at functional sites in health, aging, and disease. Ann NY Acad Sci 1126:124–127. https://doi.org/10.1196/annals.1433.043
76. Phillips SA, Thornalley PJ (1993) The formation of methylglyoxal from triose phosphates. Investigation using a specific assay for methylglyoxal. Eur J Biochem 212(1):101–105. https://doi.org/10.1111/j.1432-1033.1993.tb17638.x
77. Ray S, Ray M (1983) Formation of methylglyoxal from aminoacetone by amine oxidase from goat plasma. J Biol Chem 258(6):3461–3462
78. Lyles GA, Chalmers J (1992) The metabolism of aminoacetone to methylglyoxal by semicarbazide-sensitive amine oxidase in human umbilical artery. Biochem Pharmacol 43(7):1409–1414. https://doi.org/10.1016/0006-2952(92)90196-p
79. Hardy LL, Wick DA, Webb JR (2008) Conversion of tyrosine to the inflammation-associated analog 3'-nitrotyrosine at either TCR- or MHC-contact positions can profoundly affect recognition of the MHC class I-restricted epitope of lymphocytic choriomeningitis virus glycoprotein 33 by CD8 T cells. J Immunol 180(9):5956–5962. https://doi.org/10.4049/jimmunol.180.9.5956
80. Pearce EL, Pearce EJ (2013) Metabolic pathways in immune cell activation and quiescence. Immunity 38(4):633–643. https://doi.org/10.1016/j.immuni.2013.04.005
81. Nagaraj S, Gupta K, Pisarev V, Kinarsky L, Sherman S, Kang L et al (2007) Altered recognition of antigen is a mechanism of CD8+ T cell tolerance in cancer. Nat Med 13(7):828–835. https://doi.org/10.1038/nm1609
82. Mannick JB, Hausladen A, Liu L, Hess DT, Zeng M, Miao QX et al (1999) Fas-induced caspase denitrosylation. Science 284(5414):651–654. https://doi.org/10.1126/science.284.5414.651
83. Zaman K (2010) Tuberculosis: a global health problem. J Health Popul Nutr 28(2):111–113. https://doi.org/10.3329/jhpn.v28i2.4879
84. Collins FM (1997) Tuberculosis research in a cold climate. Tuber Lung Dis 78(2):99–107. https://doi.org/10.1016/s0962-8479(98)80002-6
85. Cohen SB, Gern BH, Delahaye JL, Adams KN, Plumlee CR, Winkler JK et al (2018) Alveolar macrophages provide an early *Mycobacterium tuberculosis* niche and initiate dissemination. Cell Host Microbe 24(3):439–446.e434. https://doi.org/10.1016/j.chom.2018.08.001
86. Aqdas M, Singh S, Amir M, Maurya SK, Pahari S, Agrewala JN (2021) Cumulative signaling through NOD-2 and TLR-4 eliminates the *Mycobacterium tuberculosis* concealed inside the mesenchymal stem cells. Front Cell Infect Microbiol 11:669168. https://doi.org/10.3389/fcimb.2021.669168
87. Jiang Y, Liu H, Wang H, Dou X, Zhao X, Bai Y et al (2013) Polymorphism of antigen MPT64 in *Mycobacterium tuberculosis* strains. J Clin Microbiol 51(5):1558–1562. https://doi.org/10.1128/JCM.02955-12
88. Malen H, Berven FS, Fladmark KE, Wiker HG (2007) Comprehensive analysis of exported proteins from *Mycobacterium*

tuberculosis H37Rv. Proteomics 7(10):1702–1718. https://doi.org/10.1002/pmic.200600853
89. Gaillard T, Fabre M, Martinaud C, Vong R, Brisou P, Soler C (2011) Assessment of the SD Bioline Ag MPT64 Rapid and the MGIT TBc identification tests for the diagnosis of tuberculosis. Diagn Microbiol Infect Dis 70(1):154–156. https://doi.org/10.1016/j.diagmicrobio.2010.12.011
90. Baba K, Dyrhol-Riise AM, Sviland L, Langeland N, Hoosen AA, Wiker HG et al (2008) Rapid and specific diagnosis of tuberculous pleuritis with immunohistochemistry by detecting *Mycobacterium tuberculosis* complex specific antigen MPT64 in patients from a HIV endemic area. Appl Immunohistochem Mol Morphol 16(6):554–561. https://doi.org/10.1097/PAI.0b013e31816c3f79
91. Latchumanan VK, Singh B, Sharma P, Natarajan K (2002) Mycobacterium tuberculosis antigens induce the differentiation of dendritic cells from bone marrow. J Immunol 169(12):6856–6864. https://doi.org/10.4049/jimmunol.169.12.6856
92. Mustafa T, Wiker HG, Morkve O, Sviland L (2008) Differential expression of mycobacterial antigen MPT64, apoptosis and inflammatory markers in multinucleated giant cells and epithelioid cells in granulomas caused by *Mycobacterium tuberculosis*. Virchows Arch 452(4):449–456. https://doi.org/10.1007/s00428-008-0575-z
93. Kato K, Yamamoto K (1982) Suppression of BCG cell wall-induced delayed-type hypersensitivity by BCG pre-treatment. II. Induction of suppressor T cells by heat-killed BCG injection. Immunology 45(4):655–661
94. Bennett JA, Rao VS, Mitchell MS (1978) Systemic bacillus Calmette-Guerin (BCG) activates natural suppressor cells. Proc Natl Acad Sci USA 75(10):5142–5144. https://doi.org/10.1073/pnas.75.10.5142
95. Hassan SS, Akram M, King EC, Dockrell HM, Cliff JM (2015) PD-1, PD-L1 and PD-L2 gene expression on T-cells and natural killer cells declines in conjunction with a reduction in PD-1 protein during the intensive phase of tuberculosis treatment. PLoS ONE 10(9):e0137646. https://doi.org/10.1371/journal.pone.0137646
96. Haist M, Stege H, Grabbe S, Bros M (2021) The functional crosstalk between myeloid-derived suppressor cells and regulatory T cells within the immunosuppressive tumor microenvironment. Cancers (Basel) 13(2):210. https://doi.org/10.3390/cancers13020210
97. Liu J, Zhang X, Cheng Y, Cao X (2021) Dendritic cell migration in inflammation and immunity. Cell Mol Immunol 18(11):2461–2471. https://doi.org/10.1038/s41423-021-00726-4
98. Knight M, Braverman J, Asfaha K, Gronert K, Stanley S (2018) Lipid droplet formation in *Mycobacterium tuberculosis* infected macrophages requires IFN-gamma/HIF-1alpha signaling and supports host defense. PLoS Pathog 14(1):e1006874. https://doi.org/10.1371/journal.ppat.1006874
99. Lei GS, Zhang C, Lee CH (2015) Myeloid-derived suppressor cells impair alveolar macrophages through PD-1 receptor ligation during pneumocystis pneumonia. Infect Immun 83(2):572–582. https://doi.org/10.1128/IAI.02686-14
100. Peyron P, Vaubourgeix J, Poquet Y, Levillain F, Botanch C, Bardou F et al (2008) Foamy macrophages from tuberculous patients' granulomas constitute a nutrient-rich reservoir for *M. tuberculosis* persistence. PLoS Pathog 4(11):e1000204. https://doi.org/10.1371/journal.ppat.1000204
101. Russell DG, Cardona PJ, Kim MJ, Allain S, Altare F (2009) Foamy macrophages and the progression of the human tuberculosis granuloma. Nat Immunol 10(9):943–948. https://doi.org/10.1038/ni.1781
102. Dilek N, Vuillefroy de Silly R, Blancho G, Vanhove B (2012) Myeloid-derived suppressor cells: mechanisms of action and recent advances in their role in transplant tolerance. Front Immunol 3:208. https://doi.org/10.3389/fimmu.2012.00208
103. Huang B, Pan PY, Li Q, Sato AI, Levy DE, Bromberg J et al (2006) Gr-1+CD115+ immature myeloid suppressor cells mediate the development of tumor-induced T regulatory cells and T-cell anergy in tumor-bearing host. Cancer Res 66(2):1123–1131. https://doi.org/10.1158/0008-5472.CAN-05-1299
104. Bronte V, Serafini P, Mazzoni A, Segal DM, Zanovello P (2003) L-arginine metabolism in myeloid cells controls T-lymphocyte functions. Trends Immunol 24(6):302–306. https://doi.org/10.1016/s1471-4906(03)00132-7
105. Comi M, Amodio G, Gregori S (2018) Interleukin-10-producing DC-10 is a unique tool to promote tolerance via antigen-specific t regulatory type 1 cells. Front Immunol 9:682. https://doi.org/10.3389/fimmu.2018.00682
106. Cabezon R, Carrera-Silva EA, Florez-Grau G, Errasti AE, Calderon-Gomez E, Lozano JJ et al (2015) MERTK as negative regulator of human T cell activation. J Leukoc Biol 97(4):751–760. https://doi.org/10.1189/jlb.3A0714-334R
107. Naranjo-Gomez M, Raich-Regue D, Onate C, Grau-Lopez L, Ramo-Tello C, Pujol-Borrell R et al (2011) Comparative study of clinical grade human tolerogenic dendritic cells. J Transl Med 9:89. https://doi.org/10.1186/1479-5876-9-89
108. Rodriguez PC, Ochoa AC (2008) Arginine regulation by myeloid derived suppressor cells and tolerance in cancer: mechanisms and therapeutic perspectives. Immunol Rev 222:180–191. https://doi.org/10.1111/j.1600-065X.2008.00608.x
109. Srivastava MK, Sinha P, Clements VK, Rodriguez P, Ostrand-Rosenberg S (2010) Myeloid-derived suppressor cells inhibit T-cell activation by depleting cystine and cysteine. Cancer Res 70(1):68–77. https://doi.org/10.1158/0008-5472.CAN-09-2587